DEVELOPMENT AND CHARACTERIZATION OF HYBRID GLASS FIBER REINFORCED UNSATURATED POLYESTER/CLAY NANOCOMPOSITE

BY

OMER MOHAMED AHMED MOHAMED

A Thesis Presented to the
DEANSHIP OF GRADUATE STUDIES

KING FAHD UNIVERSITY OF PETROLEUM & MINERALS

DHAHRAN, SAUDI ARABIA

In Partial Fulfillment of the
Requirements for the Degree of

MASTER OF SCIENCE

In

MECHANICAL ENGINEERING

May 2017

KING FAHD UNIVERSITY OF PETROLEUM & MINERALS

DHAHRAN- 31261, SAUDI ARABIA

DEANSHIP OF GRADUATE STUDIES

This thesis, written by **OMER MOHAMED AHMED MOHAMED** under the direction of his thesis advisor and approved by his thesis committee, has been presented and accepted by the Dean of Graduate Studies, in partial fulfillment of the requirements for the degree of **MASTER OF SCIENCE IN MECHANICAL ENGINEERING.**

Dr. Nesar Merah
(Advisor)

Dr. Zuhair M. Gasem
Department Chairman

Dr. Zafarullah Khan
(Member)

Dr. Salam A. Zummo
Dean of Graduate Studies

Dr. Asif Matin
(Member)

9/11/17
Date

To my parents, without their support, the work could not be done

ACKNOWLEDGMENTS

I acknowledge King Fahd University of Petroleum and Minerals (**KFUPM**) for offering me this chance to pursue master degree. Many thanks to my advisor Dr. Nesar Merah for his great support toward the thesis, his precious guidance and encouragement eased the difficulties. His fatherhood attitude is unforgettable, I learnt many things from him.

I extend my thanks to the committee members: Dr. Zafarullah Khan and Dr. Asif Matin for their guidance and help. Thanks also to Dr. Mazin Khaled and Dr. Musa for their help in securing fume-hood and working area to complete the experimental work. Never forgetting to thank Mr. Lateef and Mr. Kamal for their help on the experimental work in advanced materials science lab and mechanical workshop. Thanks also go to Gulf Chemicals and Industrial Oils Co. (**GCIR**) for providing the uP resin besides the curing agents, their help is highly appreciated. To the friends: Majeed, Musa, M. Elhadi, M. Khalaf, and M. Faisal thanks for being there. Last but not least great thanks to Sudanese community inside KFUPM campus, for making life very easy by their support and continuous encouragement.

TABLE OF CONTENTS

ACKNOWLEDGMENTS ..... **V**

TABLE OF CONTENTS ..... **VI**

LIST OF TABLES ..... **XI**

LIST OF FIGURES ..... **XIII**

LIST OF ABBREVIATIONS ..... **XVII**

ABSTRACT ..... **XIX**

ملخص الرسالة ..... **XXI**

CHAPTER 1 INTRODUCTION **1**

1.1 Background **1**

1.2 Polymers Classifications **2**

1.2.1 Thermoplastics 2

1.2.2 Thermosets 2

1.3 Motivation **5**

1.4 Objectives **6**

1.5 Research Methodology **7**

1.5.1 Literature Review 7
1.5.2 Synthesizing of the uP/c Nanocomposites 7
1.5.3 Material Characterization 8
1.5.4 Development of Hybrid GFRuP/c Nanocomposite 8
1.5.5 Water Absorption Test 8
1.5.6 Mechanical Testing 8

CHAPTER 2 LITERATURE REVIEW 9

2.1 Synthesizing Techniques of uP/c Nanocomposites 9
2.1.1 In-situ Polymerization 9
2.1.2 Melt Compounding (Blending) 10
2.1.3 Solution Blending (Intercalation) 10

2.2 Mechanical Properties of uP/c and GFRuP/c Nanocomposites 11

2.3 Effect of Water Uptake on Mechanical Behavior of uP Composites 15

2.4 Materials Characterization Techniques 16
2.4.1 XRD 16
2.4.2 SEM 18
2.4.3 DSC 18

2.5 Manufacturing of uP/c Nanocomposites 20

CHAPTER 3 EXPERIMENTAL PROCEDURE 22

3.1 Materials 22

3.1.1 The uP Resin 22

3.1.2 Curing Agents 23

3.1.3 Clays 24

3.1.4 Glass Fiber (GF) 26

3.2 Molds Assembly 27

3.3 Development of GFRuP/c Nanocomposites 29

3.3.1 Synthesis of Neat uP 29

3.3.2 Synthesis of uP/c Nanocomposite 30

3.3.3 Synthesis of GFRuP/c Nanocomposite 32

3.4 Material Characterization 33

3.4.1 X-ray Diffraction (XRD) 33

3.4.2 Scanning Electron Microscopy (SEM) 34

3.4.3 Differential Scanning Calorimetry (DSC) 34

3.5 Water Absorption Test 35

3.6 Mechanical Testing 36

3.6.1 Flexural Test 36

3.6.2 Tensile Test 37

CHAPTER 4 RESULTS AND DISCUSSION 40

4.1 Optimization of Curing Parameters 40

4.1.1 Pre-Curing Optimization 42

4.1.2 Post-Curing Optimization Parameters 45

4.2 Effect of HSM Speed..... 48

4.3 Effect of nc Type on the Dispersion State of uP/c Nanocomposites 57

4.4 Effect of nc Type and Loading on Tensile Properties of uP/c Nanocomposites.. 58

4.5 Effect of nc Type and Loading on Flexural properties of the uP/c Nanocomposites..... 63

4.6 Mechanical Properties of Hybrid GFRuP/c Nanocomposite 66

4.7 Fractographic Analysis of The Tensile Fractured surfaces 69

4.8 Water Uptake of uP, uP/c and Hybrid GFRuP/c Nanocomposites 75

4.8.1 Weight Gain Percentage Over Time 75

4.8.2 Diffusion Coefficient of uP, uP/c and GFRuP/c Nanocomposites 78

4.9 The Effect of Water Uptake on The Flexural Properties uP, uP/c and Hybrid GFRuP/c Nanocomposites..... 80

CHAPTER 5 CONCLUSIONS AND RECOMMENDATIONS 82

5.1 Conclusions..... 82

5.2 Recommendations..... 84

REFERENCES..... 86

VITAE 94

LIST OF TABLES

Table 2.1 The averaged values of Hardness and Elastic modulus for GFRuP/c nanocomposites 12

Table 2.2 Flexural properties of GFRuP/c laminates..... 13

Table 2.3 Mechanical properties of VE/c nanocomposites containing (1 wt%, 3wt% and 5wt%) of nc loading 14

Table 3.1 Typical physical properties of the uP resin..... 23

Table 3.2 Curing characteristics of the uP resin 23

Table 3.3 Nanomer I.30E physical properties 25

Table 3.4 Cloisite 10A physical properties..... 25

Table 3.5 Cloisite 20A physical properties..... 26

Table 4.1 Pre-curing optimization 42

Table 4.2 Post-curing optimization..... 46

Table 4.3 Glass transition temperature of post-cured specimens 47

Table 4.4 Elemental composition of the spectrum 1, 2 and 4..... 56

Table 4.5 Average tensile strength for uP/c nanocomposites prepared by (10A,20A and I.30E) with optimized 3wt%..... 59

Table 4.6 Average tensile strength for neat uP and uP/c nanocomposites prepared with different clay loadings 61

Table 4.7 Flexural strength measurements for neat uP and uP/c nanocomposites 65

Table 4.8 Mechanical properties of GFRuP/c nanocomposite compared to neat uP and uP/c (3wt%) 68

Table 4.9 The improvement in water uptake resistance of uP/c compared to uP 78

Table 4.10 The effect of nc loading on diffusion coefficient 79

LIST OF FIGURES

Figure 1.1 Nanocomposite's structures formed after dispersion of silicate layers 4

Figure 2.1 XRD of neat polyester and polyester/clay nanocomposite containing 17

Figure 2.2 Typical DSC graph 19

Figure 2.3 Typical glass transition temperature measurement 19

Figure 2.4 Manufacturing processes of polymer/ composites 20

Figure 3.1 The chemical structure of the montmorillonite clays 24

Figure 3.2 E-CR glass chopped strand mat 27

Figure 3.3 Small mold drawing 27

Figure 3.4 The Large mold assembly drawing 28

Figure 3.5 Exploded view of the large mold 29

Figure 3.6 L5M-A high shear mixer 31

Figure 3.7 Sonic vc-33 ultrasonicator 31

Figure 3.8 uP/c fabrication process layout 32

Figure 3.9 Bruker D8 XRD equipment 33

Figure 3.10 MERA3 TESCAN FESEM equipment 34

Figure 3.11: METTLER TOLEDO DSC equipment 35

Figure 3.12 UTM equipped with flexural test head 37

Figure 3.13 UTM equipped with tensile test head 38

Figure 3.14 CNC machining layout for test specimens 39

Figure 4.1 Representation of how glass transition temperture could be measured from DSC curve 41

Figure 4.2 DSC curves for pre-cured uP specimens at different curing temperature while curing time fixed at 2 hours 42
Figure 4.3 Zoomed in DSC curves for the uP specimens pre-cured for 2 hours at different curing temperature..... 43
Figure 4.4 Variation of glass transition temperature as a function of pre-curing temperature 44
Figure 4.5 DSC curves for pre-cured specimen at 120 ℃, for different curing time 45
Figure 4.6 Variation of glass transition temperature as a function of pre-curing time..... 45
Figure 4.7 DSC curves of post-cured specimens at different curing temperature..... 46
Figure 4.8 DSC curves for post-cured specimen at 120 ℃ curing temperature, for different curing time 48
Figure 4.9 XRD full spectra for neat uP, I.30E nanoclay, and uP/c nanocomposites synthesized at 1000 mixing speed..... 49
Figure 4.10 XRD pattern for synthesized polyester 50
Figure 4.11 XRD spectra for uP/c (3wt%) nanocomposites synthesized at different mixing speeds..... 50
Figure 4.12 (a – d) SEM micrographs for neat uP and uP/c nanocomposites syntheized at differnet speeds (1000, 3000, 5000 and 7000 rpm) while the clay loading kept at 3wt% 53
Figure 4.13 Energy dispersive spectra for spots 1, spot 2 and spot 4..... 55
Figure 4.14 XRD spectra for uP/c nanocomposites containing 3wt% of different nanoclay types 57

Figure 4.15 Typical stress-strain curves for uP/c prepared from the different clay types 58
Figure 4.16 Effect of clay type on the tensile strength of uP/c nanocomposites 59
Figure 4.17 Representative Stress-strain curves for neat uP and uP/c Nanocomposites containing different loadings of I.30E nc 60
Figure 4.18 The effect of clay loading on the tensile strength of the neat uP and uP/c nanocomposites 61
Figure 4.19 Variation of Young's modulus with clay loadings 63
Figure 4.20 The effect of clay type on the flexural strength of the uP/c nanocomposites containing 3 wt% of nc 64
Figure 4.21 The effect of clay loading on the flexural strength of the uP/c nanocomposites prepared by I.30E 65
Figure 4.22 Variation of Flexural modulus respect with clay loading 66
Figure 4.23 Variation of tensile strength with addition of nc and GF 67
Figure 4.24 Variation of flexural strength with addition of nc and GF 68
Figure 4.25 SEM fractographs of the fractured surfaces for: (a) neat uP, and uP/c nanocomposites containing nanoclay loading of (b) 1wt% (c) 2wt% (d) 3wt% (e) 4wt% and (f) GFRuP/c nanocomposites containing 3wt% of nc. All fractographs taken at fixed magnification (50X) 70
Figure 4.26 Fractographic analysis mapping for the uP/c nanocomposite containing 3wt% of nc 71
Figure 4.27 SEM fractographs of the neat uP at diffrent magnifications: (a) 200X (b) 500X (c) 1000X (d) 2000X 72

Figure 4.28 SEM fractographs at fixed magnification (2000X) of uP/c nanocomposites containing: nanoclay loading of (a) 1wt% (b) 2wt% (c) wt3% (d) 4wt% 73

Figure 4.29 SEM fractographs of GFRuP/c nanocomposite containing 3wt% nc loading at different magnifications: (a) 200 X (b) 500 X (c) 1000 X (d) 2000 X 75

Figure 4.30 The difference in weight gain percentage with square root of immersion time for uP, uP/c and GFRuP/c (3wt%)..... 76

Figure 4.31 The effect of nc loading on the diffusion coefficient 79

Figure 4.32 Effect of water uptake on the flexural strength of neat uP, uP/c and hybrid GFRuP/c nanocomposites 80

LIST OF ABBREVIATIONS

uP: Unsaturated Polyester

nc: Nanoclay

uP/c: Unsaturated Polyester Nanoclay

GF: Glass fiber

GFRP: Glass Fiber Reinforced Plastic

GFRuP/c: Glass Fiber Reinforced Unsaturated Polyester Nanoclay

MEKP: Methyl Ethyl Ketone Peroxide

Co: Cobalt

Wt%: Weight Percentage

RTM: Resin Transfer Molding

VARTM: Vacuum Assisted Resin Transfer Molding

VI: Vacuum infusion

SEM: Scanning Electron Microscope

XRD: X-ray Diffraction

DSC: Differential Scanning Calorimetry

d-spacing: Interlayer distance

FRP: Fiber Reinforced Polyester

T_g: Glass Transition Temperature

ABSTRACT

Full Name : Omer Mohamed Ahmed Mohamed

Thesis Title : Development and Characterization of Hybrid Glass Fiber Reinforced Unsaturated Polyester/Clay Nanocomposite

Major Field : Mechanical Engineering

Date of Degree : May 2017

In this work, hybrid glass fiber reinforced unsaturated polyester/nanoclay (GFRuP/c) nanocomposites are developed using an optimized process which combines high shear mixing (HSM), ultrasonication and hand layup techniques. Different nanoclay loadings (0, 1, 2, 3 and 4wt%) and different nanoclay types (C10A, C20A and I.30E) are used to fabricate the unsaturated polyester/clay (uP/c) nanocomposites. The developed nanocomposites are found to have higher resistance to water uptake and better mechanical and physical properties than the neat uP. Differential scanning calorimetry (DSC) is used to estimate the glass transition temperature (T_g) and to optimize curing parameters. Post-curing at 120 ℃ for 6 hours, was found to yield the best T_g of about 178ºC. X-ray diffraction (XRD) analysis showed that, most developed nanocomposites had reasonably exfoliated/disorder-intercalated structures, which are known to enhance the overall performance of polymer nanocomposites. Moreover, nanocomposites prepared by I.30E nanoclay (nc) yielding better dispersion state among that prepared by C10A and C20A.

Both tensile and flexural tests are revealing that I.30E nanoclay is contributing to better performance when compared to the other nanoclay types. Tensile test results are showing that, similar to the resin all nanocomposites failed in a brittle manner. Addition of 3wt% nc is resulting in significant improvement of tensile and flexural strengths, 76% and 56%,

respectively. Nanoclay filling did not have an appreciable effect on the stiffness of the material. As expected, the reinforcement of the uP/c nanocomposite by E-CR chopped fiberglass is resulting in dramatic enhancement in both flexural and tensile strength. The tensile strength of hybrid GFRuP/c containing 3wt% of nc yielded a 165% improvement over that of neat uP and 70% improvement when compared to uP/c nanocomposite. The flexural test of GFRuP/c nanocomposite showed 419% enhancement in flexural strength over neat uP besides 232% improvement of strength over uP/c nanocomposite containing the same nc loading (3wt%). The water uptake test was performed at ambient conditions (25°C and atmospheric pressure). The maximum water uptake is found to be about 1.6%, in case of neat uP. Meanwhile, addition of nc resulted in linear improvement of the water uptake resistance until reaching a maximum improvement of 39% in case of 4wt% of nc loading. Flexural test revealed degradation in the flexural strength due to moisture uptake. However, the reduction was found to be minimum at higher nc loading (3 and 4wt%), meaning that nc improved water uptake resistance.

ملخص الرسالة

الاسم الكامل: عمر محمد أحمد محمد

عنوان الرسالة: تطوير وتشخيص مركبات هجين من البوليستر غير المشبع والمواد النانوطينية مدعمة بالألياف الزجاجية

التخصص: الهندسة الميكانيكية

تاريخ الدرجة العلمية: مايو 2017 م

في هذا العمل تم تطوير مركبات هجين من البوليستر غير المشبع مدعمة بالألياف الزجاجية بإستخدام عملية مثلى متمثلة في إستخدام تقنية الخلط ذو القص العالي، الصوتنة، ومن ثم الطريقة اليدوية لتدعيم المواد المستحدثة بالألياف الزجاجية. استخدمت في تصنيع المركبات حشوات نانوطينية ذات نسب وزنية مختلفة (من 0 الى 4%)، كذلك استخدمت أنواع مختلفة من المواد النانوطينية (C10A و C20A و I.30E). المواد المطورة ذات خصائص ميكانيكة وفيزيائية محسنة بالمقارنة مع مادة البوليستر الخام. استخدمت تقنية المسح التفاضلي لقياس الكالوري لإيجاد العوامل المثلى لمعالجة البوليستر، وأظهرت النتائج أن المعالجة عند درجة حرارة 120 مئوية لمدة 6 ساعات تمثل العوامل المثلى في معالجة البوليستر، حيث وجد عند هذه الظروف أن درجة حرارة التحول الزجاجي هي 177.8 درجة مئوية. أظهر تحليل حيود الأشعة السينية أن جميع المركبات النانوطينية تحتوي على البنية مقشورة بشكل معقول والتي من المعروف أنها تعزز الأداء العام للمركبات النانوطينية. وعلاوة على ذلك، المركبات المصنعة من النوع I.30E ظهرت بحالة تشتت أفضل مقارنة مع C10A و C20A.

أظهر كل من اختباري الشد والثني أن المواد المصنعة من النانوطين I.30E ساهمت في إيجاد خصائص ميكانيكية أفضل بالمقارنة مع الأنواع الأخرى. أظهر اختبار الشد أن جميع المركبات النانوطينية إنهارت بطريقة هشة. إضافة المواد النانوطينية أدت إلى تحسن كبير في مقاومة الشد والثني مع زيادة أقصاها 76% و 56% على التوالي في حالة استخدام حشوة تحتوي على نسبة وزنية 3% من المواد النانوطينية. كما بينت نتائج إختبار الشد أن المواد النانوطينية ليست ذات تأثير كبير على مرونة المواد المصنعة. وكما هو متوقع، أدى تدعيم المواد المركبة بالألياف الزجاجية المقطعة من النوع E-CR إلى تحسن كبير في كل من مقاومة الشد ومقاومة الثني. مقاومة الشد في حالة

المركب الهجين الذي يحتوي على حشوة نانوطينية ذات نسبة وزنية 3% تحسنت بنسبة 165% مقارنة مع البوليستر الخام، وتحسنت بنسبة 70% بالمقارنة مع المركب النانوطيني. في حين أظهر إختبار الثني تحسناً بنسبة 419% في مقاومة الثني مقارنة بالبوليستر الخام. بالإضافة إلى ذلك تحسنت مقاومة الثني بمقدار 232% مقارنةً مع المركبات التي تحتوي على نفس نسبة المواد النانوطينية.

أجري إختبار إمتصاص الماء عند الظروف الجوية (درجة حرارة 25 مئوية وضغط جوي 1 جو). أظهرت النتائج أن إمتصاص الماء الأقصى وصل إلى 1.602% في حالة البوليستر الخام. وفي الوقت نفسه، وجد أن استخدام المواد الناونطينية أدى إلى تحسن خطي في مقاومة إمتصاص الماء، بحيث زاد التحسن بزيادة المواد النانوطينية. تم الوصول إلى أقصى قدر من التحسن بنسبة 39% عند استخدام حشوة تحتوي على 4% من المواد النانوطينية. أظهر إختبار الثني تدني في مقاومة الثني نسبة لإمتصاص الرطوبة، مع ذلك وجد أن التدني عند أدنى قيمه في حالة استخدام حشوات نانونطينية (3% وزنا)، مما يعني أن الحشوات النانوطينية أدت الى تحسين مقاومة امتصاص الماء.

CHAPTER 1

INTRODUCTION

1.1 Background

Nowadays, polymers are being extensively used in the industry due to their lightweight, great resistance to chemicals and their good properties as electrical and thermal insulators. Polymers are the type of materials whose molecules have high molar masses (are called macromolecules). These macromolecules are formed by combining a larger number of small molecules, or small repeated units called monomers, in chain. Monomer units can be repeated linearly, in branched fashion, or in interconnected network. The broad forms of polymers are Homopolymer, composed of single repeating monomer, and Heteropolymers [1]. Polymers can exist naturally like proteins, cellulose, starches, and latex, or can be synthesized. Synthetic polymers are usually manufactured on large scale with a wide spectrum of properties like plastics. Polymers are used extensively in everyday life, such as in housing materials, clothing, automotive parts, aerospace industry, oil industry and communication. Beside their low processing cost, polymers have low weight, high resistance to chemicals and good optical properties such as transparency, which in some applications, give them the advantage over metals and ceramics [1], [2]

1.2 Polymers Classifications

Polymers are categorized into several classifications. The most familiar classification could be made based on chains type, reaction mode of polymerization and reaction to heating. The most commonly used category is reaction to heating, in which the classification is based on the behavior or response of polymers to heating. Within this scheme, the following classifications are discussed:

1.2.1 Thermoplastics

Thermoplastics are the class of polymers that become soft when heated, and hard when cooled. As the temperature is raised, molecular motion increases, resulting in a consequent diminishing in the forces of the secondary bonding which facilitate the relative movement of adjacent chains when a stress is applied. Thermoplastics are usually found with linear or branched chains. These materials are usually manufactured by concurrent application of pressure and heat. There are various thermoplastic polymers such as: polyethylene, polyethylene terephthalate and polystyrene.

1.2.2 Thermosets

These polymers become permanently hard after formation and do not soften when heated. The structure of thermosets is usually three-dimensional networks with chains that are cross-linked with each other. Most of the time, bonding between these chains is covalent. When the polymer is subjected to a high temperature, these bonds tend to prevent both rotational and vibrational motion of the chains, and therefore, softening of the material is prevented. Thermoset polymers are stronger and harder than thermoplastics. Epoxies, vulcanized rubbers, phenolic, and unsaturated polyester are good examples of thermoset

polymers. Thermosets have good thermal and dimension stability, highly flexible design and good mechanical properties over the thermoplastics.

Recently, polyester/clay nanocomposites attracted a lot of attention due to their enhanced properties and performance when compared with conventional polyester. These improvements are resulting from dispersion of clay nanoparticles into polyester matrix as discovered by Toyota research group [3], [4]. Nanoclays are basically inorganic layered mineral silicates that have at least one of their dimensions in the range of (1-100) nanometer, usually layer thickness is estimated to be as 1 nm while the width and depth have a dimension starting from 30 nm. They are classified according to their chemical composition and morphology into: montmorillonite, bentonite, kaolinite, hectorite, and halloysite. The most commonly used class in materials industry is montmorillonite [5] since it has high aspect ratio, great surface area, good surface reactivity [6] and enhanced flame retardancy. Nanoclays have been intensively used as reinforcement in polymers, resulting in development of novel, better and light weight composite materials with improved mechanical properties (tensile strength, impact properties and flexural strength), thermal properties (thermal stability and flammability resistance) and barrier properties (permeability and water absorption). The developed polyester/clay nanocomposites are widely used in automobile industry, aerospace, coating applications, infrastructures, adhesives, etc.

The mixing technique of nc and polyester resin besides the clay content and clay type affect the microstructure and the performance of polyester/clay nanocomposites, so depending on the above parameters three different microstructures could be formed. The first one is immiscible structure, wherein polymer chains are not penetrating into nc layers, the

intercalated structure formed when polymer chains intercalate between reinforcement layers with full penetration while silicate layers' structure is kept in the same order. The last structure is exfoliated (delaminated) structure wherein silicate layers dispersed fully in the polymer's resin [5], [7]. The exfoliated structure is the important factor to obtain better mechanical properties [8], [9]. However, there is a real challenge to get perfect exfoliated structure during synthesizing and preparation of polymer/nanoclay nanocomposites [10]. Fig 1.1 shows the possible microstructures which could be obtained after dispersion of nc into resin systems.

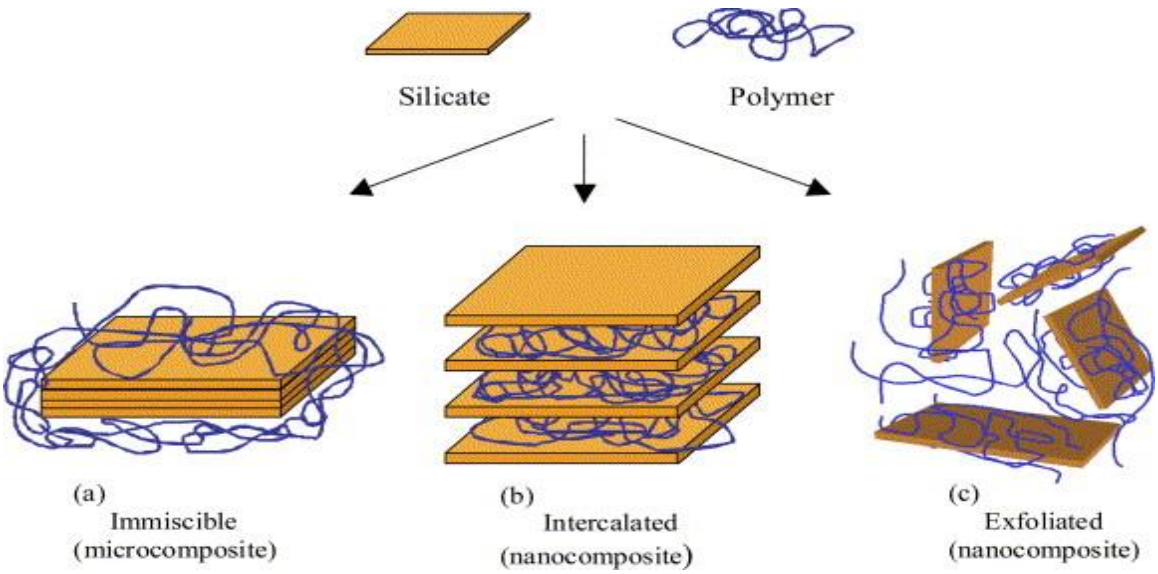

Figure 1.1 Nanocomposite's structures formed after dispersion of silicate layers [7]

Thermoset polyester is becoming widely used as casting material. Nowadays polyester is considered to be the most common polymer used in composite materials industry [11], because it is much cheaper than other alternatives. Thermoset polyester can be produced either from unsaturated dicarboxylic acid, saturated dicarboxylic acid or their anhydrides, i.e., maleic anhydride or phthalic anhydride. Therefore, according to the synthesizing

technique polyester is classified into saturated and unsaturated polyester. Unsaturated polyester is prepared by chemical reaction of dicarboxylic acid along with di-alcohols, i.e., propylene glycol or ethylene glycol, in order to formulate the ester groups, which will be crossed linked later with help of curing agents to the harden the resin, hence, to produce the solid polyester. Nowadays, uP resins are in high demand due to their low density, good mechanical properties, and low cost as well [12].

1.3 Motivation

Metallic pipes in industry field and water transportation have always been a critical issue due to their corrosive properties, less chemical resistance, difficulties in handling and transporting metallic pipes because of heavy weight, metallic pipes also exhibit relatively rough surface which result in increase in coefficient of friction. For all these reasons, the general trend now is replacing those metallic pipes by polymeric composites. The replacement led to manufacturing of lightweight pipes with minimum friction and improved chemical resistance properties. However, mechanical properties of polymer pipes are a big concern because polymers have much less strength when compared to metals. Many polymer composites have been developed to overcome this concern, various classes of GF have been used as reinforcements to improve the mechanical properties of polymer composite, accordingly GF has led to an improvement in the strength of many polymer matrices including: epoxy, polyester, vinyl ester, etc. Moreover, exposure of GFRP to harsh weather environment and immersion of those GFRP into water remains a big concern due to deterioration of the mechanical properties with time as a result of moisture uptake. The degradation in mechanical properties reduces the overall performance of GFRP as well as minimizing the life time. Incorporation of nanoclay into GFRP

compensates the deterioration and minimizes water uptake due to its good barrier properties. The focus of this work is directed to uP resin, since it is economically feasible when compared to other resins. The global market of uP resins is growing rapidly, it is expected to worth 12.15 Billion USD by the year 2021[13]. However, the development of GFRuP/c nanocomposites is still under research, because till now there is no well-established technique to fabricate these GFRuP/c nanocomposites, so contradicting results are expected regarding their mechanical properties and performance as well. Hopefully, this work may be a contribution in this field, leading to further improvement in the develop material, which will be used in wide range applications including: naval industry, automobile, infrastructure and most interestingly piping industry.

1.4 Objectives

The main objective of this work is to fabricate hybrid GFRuP/c composites having enhanced mechanical properties as well as improved water absorption resistance. The developed material is intended for structural and piping applications in harsh water laden environments.

The specific objectives are:

1) Synthesizing and characterizing uP/c composite.
2) Investigating the effect of different processing parameters, clay types and clay loadings on the physical and mechanical properties of uP.
3) Developing a hybrid GFRuP/c nanocomposite using optimized parameters.
4) Studying the effect of clay loading and processing on mechanical properties of GFRuP/c.

5) Investigating water uptake effect on the developed nanocomposites and hybrid GFRuP/c.

1.5 Research Methodology

In this work, the above mentioned objectives are addressed according to the following approach: 1) literature review of current status of research, 2) synthesizing of the uP/c nanocomposites, 3) materials characterization, 4) development of hybrid GFRuP/c nanocomposites. 5) water absorption tests, 6) mechanical testing.

1.5.1 Literature Review

Literature was surveyed to review the current status of research about uP/c and GFRuP/c nanocomposites including process parameters, mixing techniques, characterization techniques as well as mechanical properties of the uP/c nanocomposites. Literature review will be described vividly in chapter 2.

1.5.2 Synthesizing of the uP/c Nanocomposites

Specific amount of the uP resin was weighed by mass balance and poured into a beaker, followed by addition of different clay loadings (0, 1, 2, 3 and 4wt%) into the resin. The mixing process was performed by HSM with the optimized parameters, followed by sonication to enhance mixing and remove gaseous bubbles and micro voids within the mixture. Afterwards, the curing agents were added to the nanocomposite and hand-mixed for about 5 minutes. The resulting uP/c nanocomposites were then then poured into a rectangular mold in order let the resin cure.

1.5.3 Material Characterization

Several characterization techniques were used to examine the structure and the properties of the developed materials. These included: X-ray diffraction (XRD), Scanning electron microscopy (SEM), differential scanning calorimetry (DSC)

XRD was used to evaluate the degree of intercalation or exfoliation of nc in uP matrix. SEM was utilized to examine the topography of the nanocomposites as well as for fractography analysis. The glass transition temperature T_g was measured by DSC.

1.5.4 Development of Hybrid GFRuP/c Nanocomposite

The development of hybrid GFRuP/c nanocomposites started after finding the optimized processing parameters as well as clay content and type. Hand lay-up method was utilized to fabricate the developed hybrid GFRuP/c nanocomposites.

1.5.5 Water Absorption Test

Water absorption test was conducted according to ASTM D570 standard [14].

1.5.6 Mechanical Testing

Flexural and tensile tests were performed following ASTM D790-02 standard [15] and ASTM D638-02a standard [16], respectively. Both of the mechanical tests were conducted on the Universal Testing Machine (UTM).

CHAPTER 2

LITERATURE REVIEW

This chapter reviews synthesizing and preparation techniques for polymer composites and nanocomposites and their performance. The review is focused on the latest studies related to the previously defined objectives.

2.1 Synthesizing Techniques of uP/c Nanocomposites

A lot of challenges faced researchers and scientists who worked on nc nanocomposites field. Because till now there is no well-established standard, or procedure to synthesize these nanomaterials. However, literature contains various techniques utilized to synthesize and develop polymer nc and hybrid composites

2.1.1 In-situ Polymerization

First attempt to synthesize nc nanocomposites was done by simple melt mixing of clay and nylon-6 [17].resulting in inhomogeneous composite material. Later, Kawasumi introduced in-situ polymerization method to disperse nanoclay reinforcement into nylon-6; the dispersion method successfully generated an exfoliated nanocomposite structure [18]. Since it is simple and has less environmental impact because of the absence of solvent during process, manufacturers utilized this method and produced commercialized polymer/clay nanocomposites with uniform distribution of nc. However, in-situ polymerization has some limitations represented in lowering grafting density [19] and requiring a well-controlled polymerization reaction. Finally, in-situ polymerization method is suitable only for epoxy based and polyamides composite materials [20], [21].

2.1.2 Melt Compounding (Blending)

Melt compounding known also as melt blending technique, in which polymer pellets are melted then nanoparticles (reinforcements) are dispersed into polymer by high temperature diffusion [5], [22]. This technique, which brought improvement of nanoclay dispersion, opened the gate to a remarkable progress in the nanoclay nanocomposite materials. Cho et al. [23] conducted many experiments on the effect of melt blending conditions on the properties and the performance of Nylon 6 nanocomposites, they used a single screw and a twin screw extruder to synthesize polyamide/clay nanocomposite. Their findings showed that with a single screw extruder there was a poor exfoliation, while the twin screw extruder yielded considerable improvements in the properties (especially stiffness and yield strength). Albdiry et al. [24] showed that melt blending method gives the best dispersion quality among other techniques, however it was found that this technique is compatible only with polar polymers whereas not completely compatible with non-polar polymers like polyolefin [25].

2.1.3 Solution Blending (Intercalation)

In this technique, nc is dispersed into polyester resins by using different mixing techniques such as: HSM, hand mixing and ultrasonication. The ultrasonication process is used as mixing and degassing technique at the same time. Solution blending technique involves using of special kind of catalysts, initiators and promoters to cure the resins.

Based on the literature, HSM and ultrasonication techniques lead to good dispersion of nc into uP resin due to the generation of fluctuating pressure waves within the resin, resulting in the formation of slight vacuum bubbles, those small bubbles collapse and cause heavy hydrodynamic shear forces that cause deagglomeration of clay clusters. Many studies

reported that one hour of sonication at 50°C are the best sonication parameters [26], [27]. On the other side, there is a consensus that HSM for 1 hour is good enough to obtain adequate exfoliated structure for polyester resins [28]. However, contradictory findings have been reported regarding the mixing speed [29], [30].

2.2 Mechanical Properties of uP/c and GFRuP/c Nanocomposites

Bashir [31] studied the influence of synthesizing techniques on the processing of uP/c nanocomposite. In his study, uP (R580-ZPE-14) and nc (Cloisite 20A) reinforcement were mixed via ultrasonication technique, dynamic mechanical analyzer was utilized to measure storage modulus and results showed enhancement in storage modulus by 16% in case of 5wt% of nanoclay. The study also demonstrated that three roll milling is not appropriate for uP resins containing styrene because it increases the viscosity dramatically therefore, decreasing the degree of exfoliation.

Dalir et al. [32] prepared uP/c nanocomposites using Cloisite 15A with different clay loadings (2, 4 and 6wt%). They found that, the addition of nc enhanced Young's Modulus by 51% in case of 4wt% of nc.

Contrary to the previous study, Bensadoun et al.[33] showed that, for nanocomposites prepared by three types of nc (C11B, C30B and C15A), there is no enhancement in Elastic Modulus. Additionally, degradation in the modulus has been observed in case of C15 nc. This behavior was attributed to the increase in the viscosity of the polyester resin.

Dhakal et al. [34] carried out nanoindentation tests on uP/c nanocomposites, showing that for clay loadings of 1, 3 and 5wt%. there is enhancement of hardness by 29%, 24% and 14%, respectively. Besides that, Young's modulus also increased by15%, 13% and 23% accordingly, as shown in Table 2.1.

Table 2.1 The averaged values of Hardness and Elastic modulus for GFRuP/c nanocomposites [34]

Specimen	Hardness (MPa)	Elastic Modulus (GPa)
Neat uP	301	5.39
uP+1 % wt. of Nc	387	6.19
uP+3 % wt. of Nc	372	6.07
uP+ 5 % wt. of Nc	343	6.65
uP+E-glass 38 wt% fiber	330	5.97

Esfahani et al. [35] examined the effects of nanoclay loading (1.5wt% and 3wt%) on the flexural properties and hardness of GFRuP/c nanocomposites. Four layers of E-GR were used as reinforcement. All nanocomposites were prepared by hand lay-up technique. They were cured initially at room temperature for 24 hours, then post-cured at 80 ℃ for 20 hours. Hardness tests conducted by Barcol impressor revealed that, the hardness is independent of nanoclay content. These results are inconsistent with Dhakal's results as reported above [34]. However, flexural tests indicated an enhancement in flexural strength by 14% and improvement in flexural modulus by 20% in case of 1.5wt% of nanoclay loading as illustrated in Table 2.2.

Table 2.2 Flexural properties of GFRuP/c laminates [35]

nc content (wt%)	Flexural strength (MPa)	Elastic at break (%)
0	9571.3	3.34
1.5	11383	2.76
3	10761.5	2.96

Chaeichian et al. [36] studied the flexural properties and fracture toughness of the uP/c nanocomposites. They found that nc had negative impact on flexural strength. They attributed the degradation of flexural strength to imperfect adhesion between nc and uP. Kchit et al. [37] studied the effect of clay loading on the mechanical properties and the flammability resistance of GFRuP/c nanocomposites. Mechanical tests showed that, adding 3 wt% of nanoclay does not seem to enhance Young's modulus. However, addition of nc improved the impact resistance by 9%.

Bensadoun et al. [38] performed comprehensive analysis of the effect of clay type on the flexural modulus of GFRuP/c nanocomposites. The authors used (C 11B, C 15A and C 30B) and found that 2 wt% of C 11B and 4wt% of C 30B resulted in the highest flexural modulus.

Vinyl ester (VE) is a subclass of uP, which is formed by esterification of epoxy resin and unsaturated carboxylic acid. Due to lower content of hydrolytically unstable ester bonds, VE shows better chemical resistance and less water absorption than uP resin [39]. It also exhibits superior cross bonding and better tolerance to stretching when compared to

unsaturated polyester. VE composites demonstrate good impact strength and less delamination behavior.

Razavi et al.[40] prepared VE/nc nanocomposites with different nanoclay loading (1 , 3 and 5wt%). Tensile testing showed great enhancement in both of tensile strength and Young's modulus. Table 2.2 shows that 1wt% of nc yields 100% improvement in the tensile strength, 2wt% of loading resulted in 161 % improvement. Even though, many researchers agreed that clay loading below 3wt% is reasonable for the maximum enhancement in the mechanical properties of clay/nanocomposites, Razavi et. al [34] found that, in case of 5wt% loading, the tensile strength jumped dramatically, almost 3 times greater than the neat VE, as illustrated in Table 2.3. The improvement was rationalized due to high interaction between VE chains and Cloisite 30B nc which was modified by alkyl ammonium ions.

Table 2.3 Mechanical properties of VE/c nanocomposites containing (1 wt%, 3wt% and 5wt%) of nc loading [40]

Sample	Tensile Strength (MPa)	Modulus (GPa)
VE	13	0.9
VE1	25	1.7
VE3	34	2.3
VE5	41	2.0

Nanoclays also have considerable role in the enhancement of thermal properties of uP/c nanocomposites. Chieruzzi et al. [41] found that incorporation of nc decreased the coefficient of thermal expansion of polyester resins.

Laski et al. [42] showed that as nanoclay percentage increases the thermal conductivity rises because the thermal conductivity of montmorillonite is higher three times than neat polymer.

2.3 Effect of Water Uptake on Mechanical Behavior of uP Composites

Immersion of polymer composites into saline or even fresh water degrades their tensile strength, flexural strength and impact strength. The degradation takes place because of water absorption due to moisture diffusion into material structure, which boosts growth of damages inside polymeric composites.

Pandian et al. [43] have studied water absorption of woven and short basalt fiber reinforced polyester (FRP) composites, when immersed into normal water (NW) for 100 days. Tensile test showed that, immersion in NW reduced the tensile strength dramatically, causing 27% and 55% reduction in case of woven and short basalt FRP, respectively.

The flexural strength of the short basalt FRP was not affected by water uptake while that of the woven FRP has decreased by 46%.

Razavi et al. [40] conducted 24 hour water uptake test on VE/c nanocomposites containing (1, 3 and 5wt%) of nc showing reduction in weight gain from 0.5 % to 0.38 % in case of 1wt% loading, while for 3wt% and 5wt% of nc, the water uptake decreased down to 0.34%.

Despite the fact that polyester is hydrophobic; it has been observed that water absorption in polyester composites containing fiber as reinforcement is significant because fiber is hydrophilic, which means it absorbs water more than the matrix. Also, due to weak bonded

area between the matrix and the reinforcement, polyester composites absorb a small quantity of water which will result in the reduction in the performance of polyester composites [44]. It was reported that water absorption depends on interfacial linkage between the matrix and fiber, presence of voids in the composite as well as reinforcement type [45]. So, nanoclay was introduced as a key solution to improve barrier properties of GFRP composites.

2.4 Materials Characterization Techniques

Characterization is a concept of studying structure/property relationship of materials using some of experimental techniques such as: Differential Scanning Calorimetry (DSC), X-ray Diffraction (XRD) and Scanning Electron Microscopy (SEM). The developed uP/c nanocomposites are characterized to: check the uniformity and status of nanoclay dispersion into the polymer matrix, estimate the degree of exfoliation or intercalation, measure glass transition temperature as well as evaluate thermal stability of the developed materials.

2.4.1 XRD

The degree of intercalation or exfoliation of nc into polymer matrix determines the overall performance of polymer nanoclay nanocomposite. XRD is the most common characterization technique used to examine and identify nanocomposites structure [46], [47].The XRD peaks are obtained only if constructive interference occurs which means that Bragg's law has been satisfied as shown in equation 2.1.

$$2 \quad n\lambda = 2d\,sin\theta \qquad (2.1)$$

Where n is an integer constant, considered to be 1 in case of principal reflection, λ is wavelength of incident X-ray, θ is scattering angle and d is planar or interlayer spacing. By knowing diffraction angle in which diffraction peak appears, interlayer spacing could be measured thus the exfoliated and the intercalated structures could be distinguished by their interlayer spacing. In exfoliated structure polymer chains fully penetrate between clay layers resulting in increase of interlayer (basal) distance. It is reported that the exfoliated structure is obtained when interlayer spacing is greater than 8.8 nm [48], while intercalated structure occurs when interlayer spacing is in the range of 1.5 to 8 nm.

Laske et al. [42] demonstrated that as interlayer distance increases, the exfoliation degree increases accordingly. Their work introduced a new method to estimate the degree of exfoliation based on the area under the peak intensity, which states that smaller area under the curve means better exfoliation due to the low probability of X-rays to hit the particles.

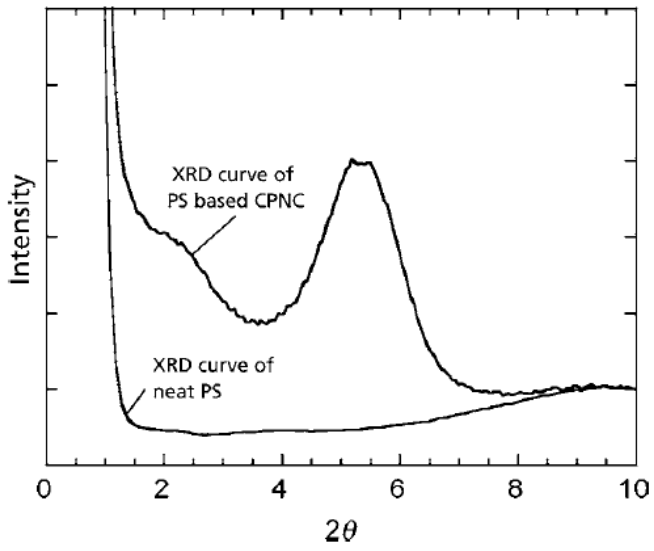

Figure 2.1 XRD pattern of neat polyester and polyester/clay nanocomposite containing 4wt% clay loading [49]

Fig 2.1 shows diffraction patterns of neat polyester and polyester/clay nanocomposite containing 4wt% clay loading. It is obvious that XRD pattern for neat polyester is

featureless due to its amorphous structure, so incorporating nanoclay produced semi crystalline structure, for that reason a peak appeared at $2\theta \approx 5.5º$ due to diffraction.

2.4.2 SEM

SEM is an indirect imaging technique used to study the structure of materials, defects within the materials as well as obtaining the elemental analysis of different kinds of materials. The information is obtained when high energy beam radiates and scans the specimen surface. Therefore, the sample should be conductive in a way to allow the motion of electrons throughout the specimen. Most of polymers are non-conductive so a lot of preparation techniques are needed including: coating, conductive paint, sectioning, cutting, grinding, polishing and etching. Polymers, when being imaged by electron microcopy, exhibit a very low contrast between the structural details because polymers consist of the same elements, carbon, hydrogen and oxygen. These elements are light and they weakly interact with the incident electron beam, giving rise to slightly degraded contrast. In addition to that, in case of polymer nanocomposites containing dispersed nanoparticle such as polyester nanoclay nanocomposite, it is difficult to show the state of the dispersion of nanoclay even if a high-resolution SEM is used. Even so SEM is utilized to examine the topography of uP/c nanocomposites as well as for the fractographic analysis.

2.4.3 DSC

DSC is characterization technique used to study polymerization reaction, crystallization of amorphous polymer and thermal behavior of nanocomposites. DSC observes heat effects on polymers at a given temperature by monitoring heat flow difference between the

specimen to be characterized and reference sample which is usually aluminum. Then the heat flow is plotted as a function of temperature.

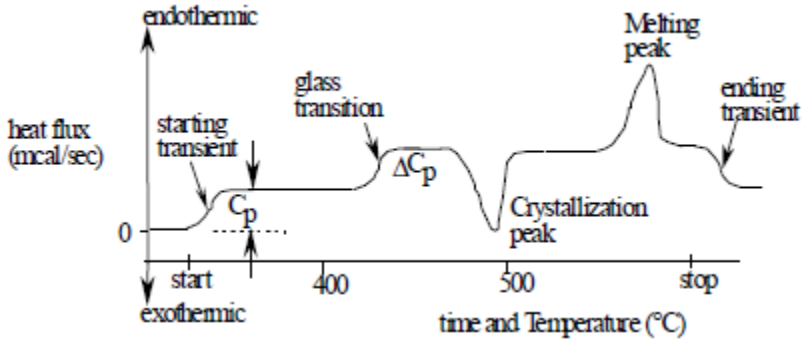

Figure 2.2 Typical DSC graph

From Fig 2.2, a lot of information could be obtained, such as heat capacity C_p, melting temperature and most interestingly glass transition temperature T_g, which is an important property of any polymer because polymer's properties change significantly and transit from glassy phase to rubbery phase beyond it.

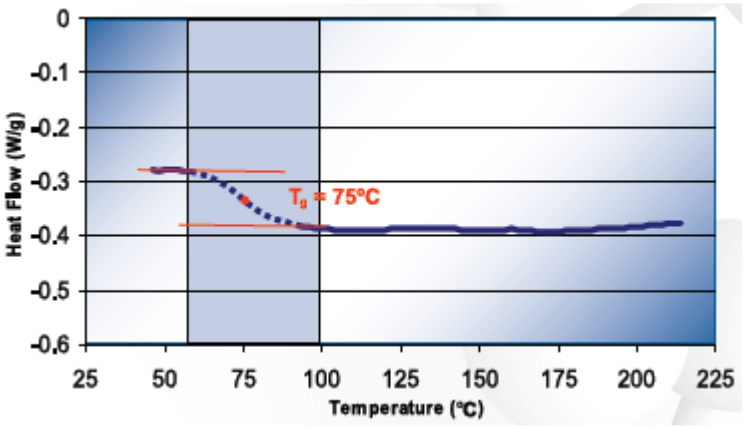

Figure 2.3 Typical glass transition temperature measurement [47]

Fig 2.3 shows the approach by which T_g could be estimated from DSC curve, as recommended by ASTM D3418-99 standard [50].

2.5 Manufacturing of uP/c Nanocomposites

Nowadays, the challenge is how to reflect the rapid development of research in uP/c nanocomposite into industry in order to produce commercialized uP/c nanocomposite effectively and accurately with minimum voids and porosity levels, relatively low production cost and minimum production time.

Several fabrication processes were used to produce polyester/nanocomposites, the most common processes are shown in Fig 2.4.

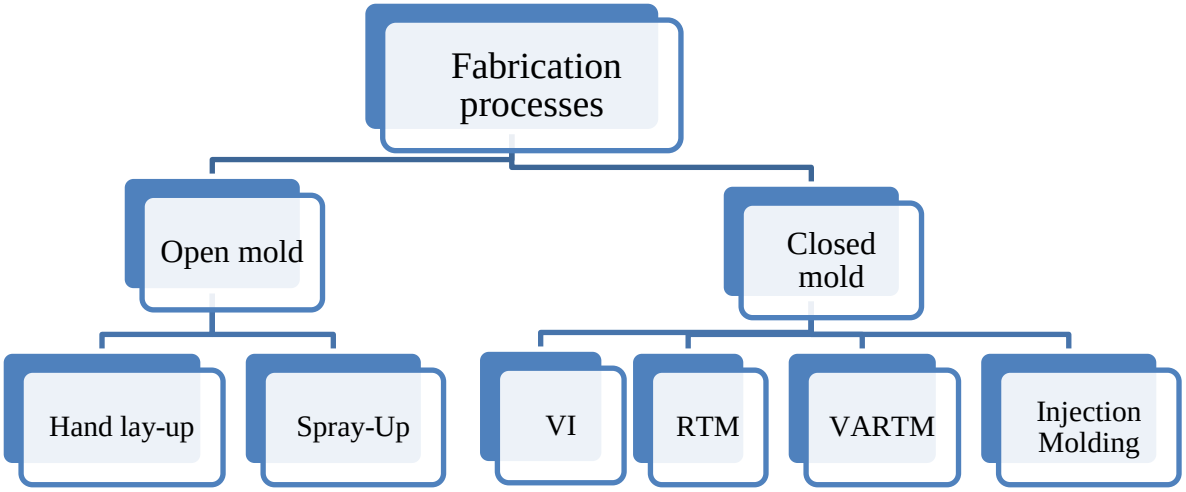

3

Figure 2.4 Polymer/ composite manufacturing processes

Hand lay-up technique is the oldest and the simplest open molding fabrication process, in which the reinforcement material is applied into the mold then resin fill the mold's space using: pouring, spraying or brush coating. Air molecules are removed by consolidation rollers to the form laminated structure, then composites have to be cured using some catalysts to harden polyester/nanocomposite. Hand lay-up manufacturing technique is simple, low cost tooling; however it is labor intensive, requires restrict health and safety regulations, low volume production rate and gives poor mechanical properties due to voids

and non-uniform distribution of the reinforcement [51], [52]. Vacuum Infusion (VI) is a closed mold production process, wherein the filler is placed into the mold, then the resin infused and the vacuum pulls it through the reinforcement and eliminates the air. It is suitable for low viscosity resins, it also minimizes voids level and so resulting in products which have good mechanical properties. However, it has moderate production rates. Another fabrication process is Injection Molding, which is commonly used for thermoset polymers having low viscosity, it uses a ram or screw plunger to squeeze and inject resins under high pressure into a mold cavity. Mold design should be considered carefully to produce an accurate and complex parts, but still used for the production of low quantity parts.[53]

A modern technique known as resin Transfer Molding (RTM), also a closed-mold process, uses a flexible counter tool to transfer resin into closed mold cavity under low pressure. RTM has many advantages over the other processes, since it produces complex shapes with high tolerance, less finishing processes are needed, it also minimizes the porosity of manufactured parts. RTM solved the limitation coming from some reinforcement types such as fibers and braids. It however, has high tooling costs. Vacuum Assisted Resin Transfer Molding (VARTM) is a modification of the RTM, it has a similar concept as RTM, but the main difference is the top portion of the mold that was replaced by a vacuum bag to enhance resin flow. The main advantages of VARTM are: reduction of voids, high volume production rates with relatively lower costs and minimum environmental impact.
In the present work, hand-layup technique utilized, since the mold that is used to synthesize the material is very simple. The curing process is done at room temperature while the post curing is performed in the oven.

CHAPTER 3

EXPERIMENTAL PROCEDURE

In this chapter, the materials and the experimental procedure utilized to synthesize uP/c nanocomposite and its hybrid GFRuP/c nanocomposite is firstly described in details. Then, it is followed by the presentation of the techniques and procedures employed to characterize and test the developed nanocomposite and its hybrid composite as well.

3.1 Materials

3.1.1 The uP Resin

Isophthalic acid based uP is used in this study, since it exhibits better mechanical properties when compared to orthopthalic. The resin was provided by Gulf Chemicals and Industrial Oils Co. (GCIR) under the commercial name: SAUDPOL SP-351-BV13. Table 3.1 illustrates the physical properties of the uP resin as provided by the manufacturer, while Table 3.2 presents the curing characteristics of the uP.

Table 3.1 Typical physical properties of the uP resin

Monomer contents @ 105 ℃ for 1 hour	**38**%
Acid value	**15 – 20 mg KOH / g**
Color	**Clear yellow APHA max.**
Density (20 ℃)	**1.12 g/ml**
Stability @ 20 ℃ in dark	**6 months**

Table 3.2 Curing characteristics of the uP resin

Gel time (100g resin, 0.25g Co.6%, 1g M60) @ 25 ℃	**13.55 minutes**
Total curing time	**25.14 minutes**
Peak exotherm	**165.4 ℃**
Viscosity (Brookfield RV DV-E @ 25 ℃, Sp.02, 60 rpm)	**355 mPa.s**

3.1.2 Curing Agents

Methyl ethyl ketone peroxide (MEKP), supplied by AkzoNobel under the product name: Butanox-M60, was used as a hardener,

Butanox-M60 is a colorless liquid having a density of 1.17 g/cm^3, and a viscosity of 25 mPa.s (measured @ 20 ℃)

In order to increase curing reaction rate cobalt ethyl hexanoate, 6% Co, was used as an accelerator besides MEKP. The accelerator was provided by AkzoNobel**,** under the commercial name: NL-51P and Co 6%.

NL-51P accelerator has a blue violet color, with a density of 0.963 g/cm^3, and a viscosity of 16 mPa.s (measured @ 20 ℃).

3.1.3 Clays

Organically modified montmorillonite clays are used in this work, all nc are 2:1 smectite clays, meaning that each octahedral sheet of alumina sandwiched between two tetrahedral sheets of silica as shown in Fig 3.1. The montmorillonite clays are naturally inorganic hydrophilic materials, so they were modified by lengthy alkyl chains such as phosphonium cations or quaternized ammonium, in order to become organophilic.

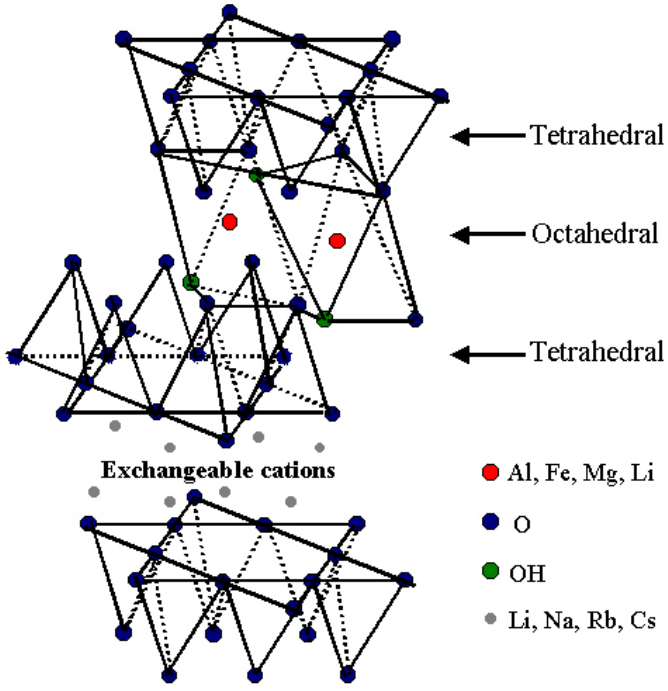

Figure 3.1 The chemical structure of the montmorillonite clays [53]

Different types of montmorillonite clays are utilized, namely: Nanomer I.30E, Cloisite 10A and Cloisite 20A. The Nanomer I.30E was supplied by Nanocor Inc, USA while the Cloisite 10A and 20A were acquired from Southern Clay Product, USA.

The physical properties of the different nc types are described in Table 3.3, Table 3.4 and Table 3.5.

Table 3.3 Nanomer I.30E physical properties

Appearance	White Powder
Mean Dry Particle Size (microns)	18-23
+ 325 Mesh Residue (percent)	0.1
Specific Gravity	1.90
Moisture (percent)	3.0 max
Bulk Density (pounds/ft3) (gms/cc)	(34)- (0.55)
Purity(percent)	98.5

Table 3.4 Cloisite 10A physical properties

Appearance	Off White
Mean Dry Particle Size (microns)	<10
Specific Gravity	1.90
Moisture (percent)	<3.0
Bulk Density (g/l)	265

Table 3.5 Cloisite 20A physical properties

Appearance	Off White
Mean Dry Particle Size (microns)	<10
Specific Gravity	1.77
Moisture (percent)	<3.0
Bulk Density (g/l)	177

3.1.4 Glass Fiber (GF)

Polyester is commonly reinforced by GF to improve its overall performance. GF are classified according to the application and usage into: A-glass (alkali soda lime glass) which is sensitive to alkali environment, E-CR glass which has a good electrical and chemical resistance, S-glass is used for high strength applications, wherein high value of tensile strength is required. C-glass is a modified class of E-class to enhance chemical resistance to some acids which deteriorate E-CR. GF exists in many forms such as: woven, stitched and chopped.

In this study, E-CR glass chopped strand mat (Fig 3.2) was used, which was supplied by Amiantit Fiberglass Industries Limited. E-CR glass chopped strand mat has a density of 2.66 g/cm^3 and a weigh of 600 g/cm^2.

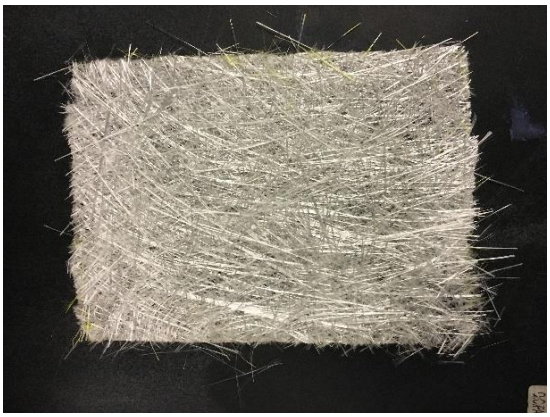

Figure 3.2 E-CR glass chopped strand mat

3.2 Molds Assembly

Two rectangular aluminum molds were used to fabricate the neat uP, its nanocomposite and GFRuP/c nanocomposites. In order to minimize polyester wastages, a small open mold (Fig 3.3) was employed for optimizing the curing parameters. The second mold was a closed one. It was used mainly to fabricate the plates from the synthesized nanocomposites. This mold consists of three parts: bottom plate, middle hollow plate and upper plate, as shown in Fig 3.4 and Fig 3.5. The mold was designed and manufactured by Ahmad Rafiq [54]. All dimensions are in mm.

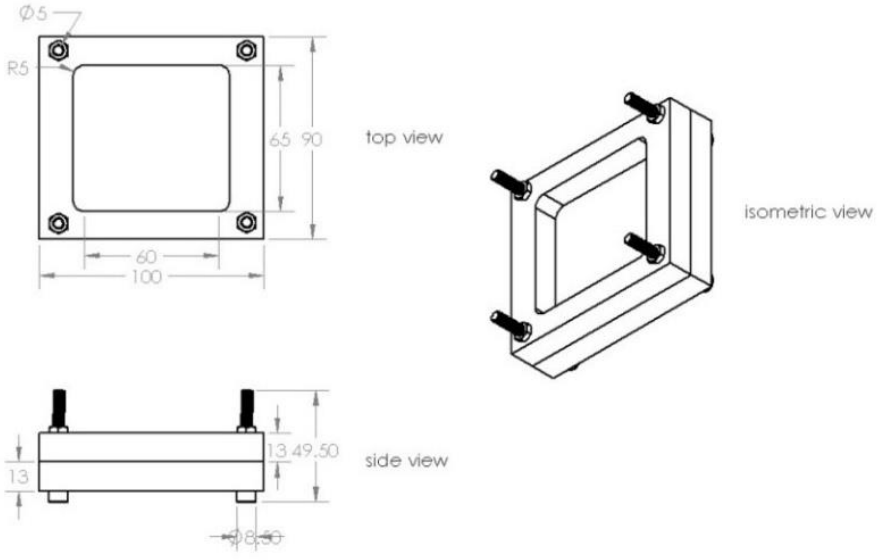

Figure 3.3 Small mold drawing

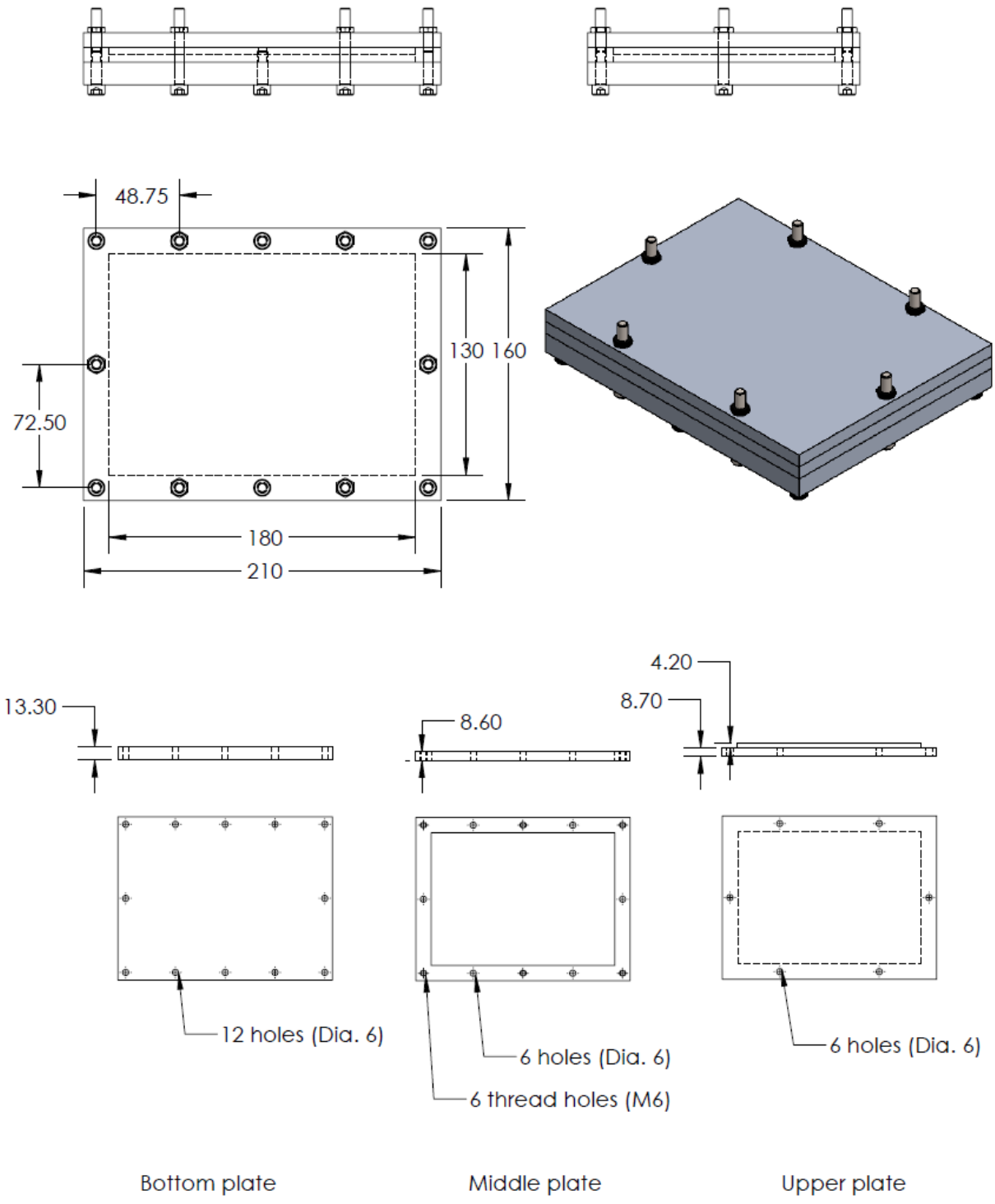

Figure 3.4 The Large mold assembly drawing [54]

Figure 3.5 Exploded view of the large mold

3.3 Development of GFRuP/c Nanocomposites

3.3.1 Synthesis of Neat uP

The amount of uP resin to produce (126 ×178×4) mm bulk sample was estimated to be 120 g. The quantity of resin was weighed by mass balance, and poured into a beaker. A 0.25wt% of cobalt promoter was added to the beaker to initiate the reaction, and gently hand mixed for about 3 minutes using a stirring rod. This is followed pouring a 1wt% of MEKP and mixing it with the resin for 5 minutes. The mixture is then transferred to the mold which was coated by mold release agent (Honey Wax) to ease removal of the hardened materials. The prepared mixture was poured inside the mold. Then, the mold was held initially at atmospheric conditions for 24 hours to avoid shrinking of the uP. Furthermore, post-curing at 120 ℃ for 6 hours was Performed at oven.

3.3.2 Synthesis of uP/c Nanocomposite

120 g of uP resin was weighed and poured into a beaker. Then different clay loadings (1, 2, 3 and 4) wt% were weighed and added separately to the resin, and mixed manually using a stirring rod for 5 minutes, to prevent outpouring of nanoclay at the beginning of HSM. The model L5M-A HSM (Fig 3.6) supplied by Silverson, UK, was used to disperse the nc into the uP resin at different mixing speeds. Starting from 1000 rpm up to 7000 rpm with a constant increase rate of 1000 rpm. Since there is almost an agreement that HSM for 1 hour is good enough to obtain adequate mixing. So, this mixing time was maintained. The nc loading was also maintained at (3wt%) for optimization purpose. Sonic vc-33 Ultrasonicator (Fig 3.7) was used in impulse mode (20s on, 20s off) for 1 hour to remove gaseous bubbles as well to improve the dispersion of nc into uP. Both of HSM and Ultrasonication were held under water bath to avoid extreme temperatures from being induced into the resin, that would affect the mixture viscosity. The final mixture was degassed using a vacuum chamber for 30 minutes to remove the remaining bubbles. After that the curing agents were added to the mixture and the final mixture poured into the mold to cure initially at room temperature for 24 hours. Then post-curing was conducted on the oven under 120 ℃ for 6 hours. Fig 3.8 illustrates the hierarchy of the whole synthesize process.

Figure 3.6 L5M-A high shear mixer

Figure 3.7 Sonic vc-33 ultrasonicator

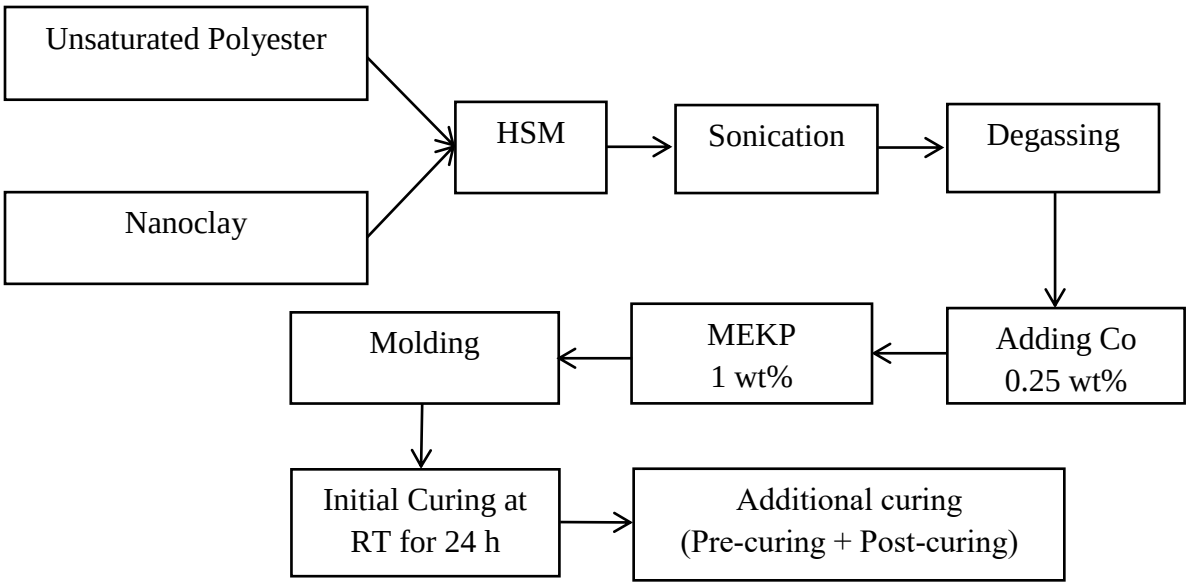

Figure 3.8 uP/c fabrication process layout

3.3.3 Synthesis of GFRuP/c Nanocomposite

The same procedure which was followed to develop uP/c nanocomposites is repeated again to fabricate GFRuP/c nanocomposite with help of Hand-layup technique. Firstly, 4 layers of E-CR chopped strand mat were cut by scissor to the dimensions of (176 mm ×125mm). the mold is coated by mold release agent (Honey Wax), then specific amount of prepared mixture of uP/c (3wt%) was poured to the mold's bottom. First stand mat was introduced into the mold, then it rolled by metallic roller until the mat became fully wetted by uP resin, then immediately the second mat was applied, and so forth until all 4 layers of GF are fully wetted, representing 40% of fiber to matrix ratio. Instantly, after all Mats were fully wetted, the mold was closed and tightened by screw sets, to apply necessary pressure to the mixture in the mold. The mold was held at room temperature for 24 hours, then post-curing was done at 120 ℃ for 6 hours.

3.4 Material Characterization

To study the structure/property relationships of the developed materials, several characterization techniques were used.

3.4.1 X-ray Diffraction (XRD)

XRD was used to examine and identify the structure of the developed composites. More specifically, to evaluate the degree of intercalation or exfoliation of nc in polymer matrix, which alters the overall performance of uP/c nanocomposite. Bruker D8 Advance XRD equipment was used (Fig 3.9), the equipment has 9 specimen's holder with auto-positioning feature, and the source of radiation is copper (Cu Kα), with a wavelength of 1.5406 Å. XRD analysis was conducted on neat uP, nc powder, and uP/c nanocomposites, over the range of 2 theta ($2^{\circ} - 90^{\circ}$).

Figure 3.9 Bruker D8 XRD equipment

3.4.2 Scanning Electron Microscopy (SEM)

SEM was used to study the morphology of uP/c nanocomposites as well as for fractography analysis of the fractured surfaces. SEM analysis was done by FESEM MERA3 TESCAN (Fig 3.10). All specimens were cut into small pieces to fit into SEM sample holder and then they were coated by gold sputter coating to avoid charging effect.

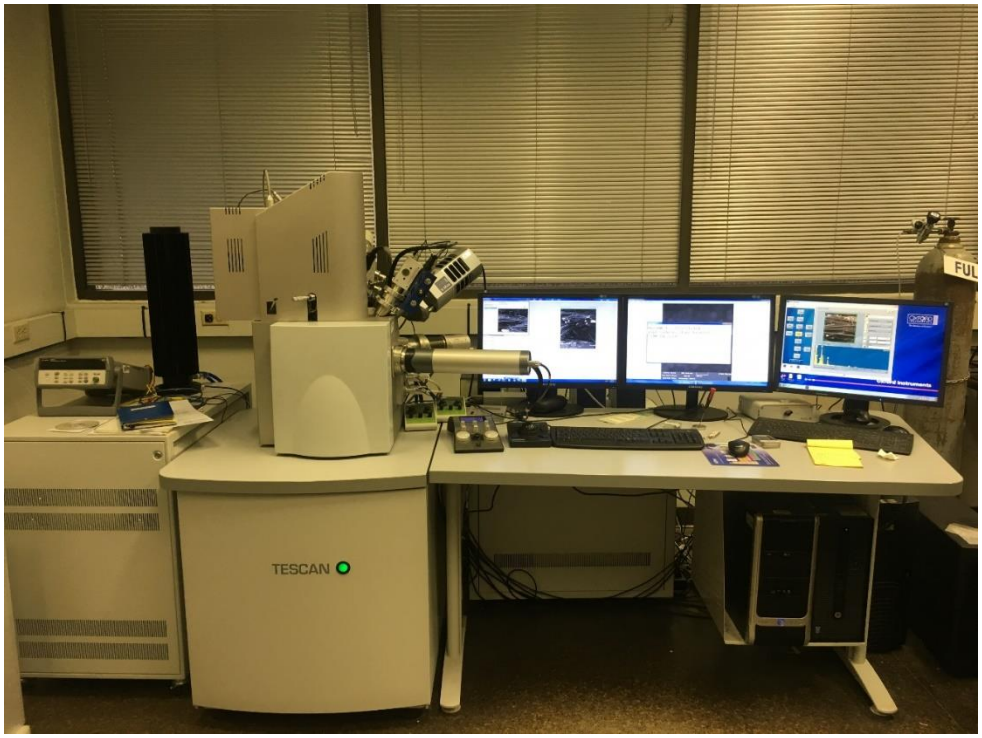

Figure 3.10 MERA3 TESCAN FESEM equipment

3.4.3 Differential Scanning Calorimetry (DSC)

Polymerization reaction is studied through DSC. The thermal behavior of nanocomposites could be observed by monitoring the heat flow difference between the specimen to be characterized and a reference sample which is usually aluminum. In this study, METTLER TOLEDO - DSC822e (Fig 3.11) model was utilized to measure glass transition

temperature T_g according to ASTM D3418-99 standard [50], with a heat flow of $10℃/min$, and using thermal cycle in the range of (50-250℃).

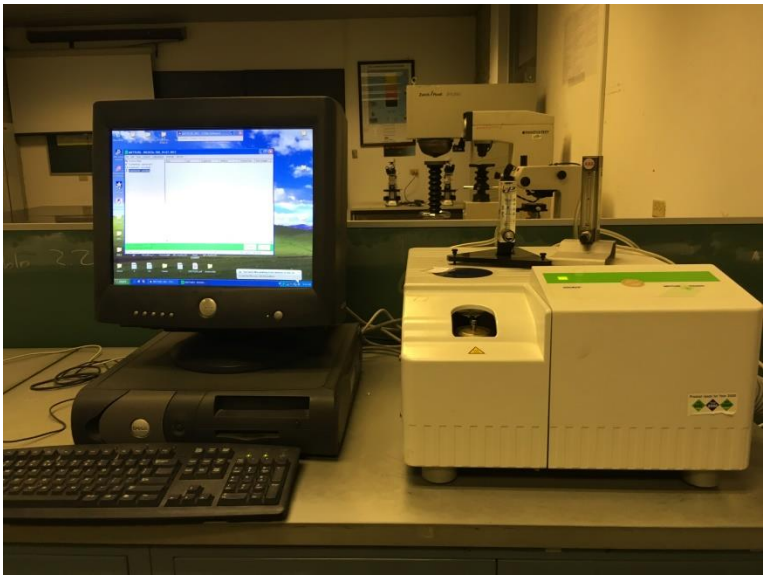

Figure 3.11: METTLER TOLEDO DSC equipment

3.5 Water Absorption Test

Water absorption test was conducted according to ASTM D570-98 standard [14], in order to know how water uptake affects the performance of neat up, uP/c and the developed GFRuP/c nanocomposite. For each sample, three specimens were cut using CNC milling machine to the following dimensions (76.2 mm×25.4 mm×4 mm). Initially, weight measurements of dry specimens were taken by mass balance, then the specimens were fully immersed into tap water at room temperature and atmospheric pressure. After 24 hours of immersion, all specimens were removed from the container, then dried by a cloth and weighs were measured immediately. The same procedure was repeated by the end of the first week, then by the end of every two weeks until specimens reached or approached the saturation. These immersion durations are recommended by ASTM D570-98 standard,

following long-term immersion procedure. The percentage weight gain was calculated accordingly using equation 3.1.

$$M_t = \frac{W_i - W_o}{W_o} \times 100 \qquad (3.1)$$

Where: M_t is the percentage weight gain after specific immersion time t, W_i is instantaneous weight of the specimen and W_o is original weight of the specimen before the exposure to water.

3.6 Mechanical Testing

3.6.1 Flexural Test

Three point-bending test was performed, according to ASTM-D790-02 standard [15]. For each sample, three specimens were cut by CNC milling machine to the dimensions of (127 mm×12.7 mm×4 mm). Instron 3367 testing machine was employed to determine the flexural properties of the specimens. The machine equipped with flexural test head, which has a variable span length as seen in Fig 3.12. The span length is adjusted at 60 mm then loading was applied at a rate of 1.15 mm/min.

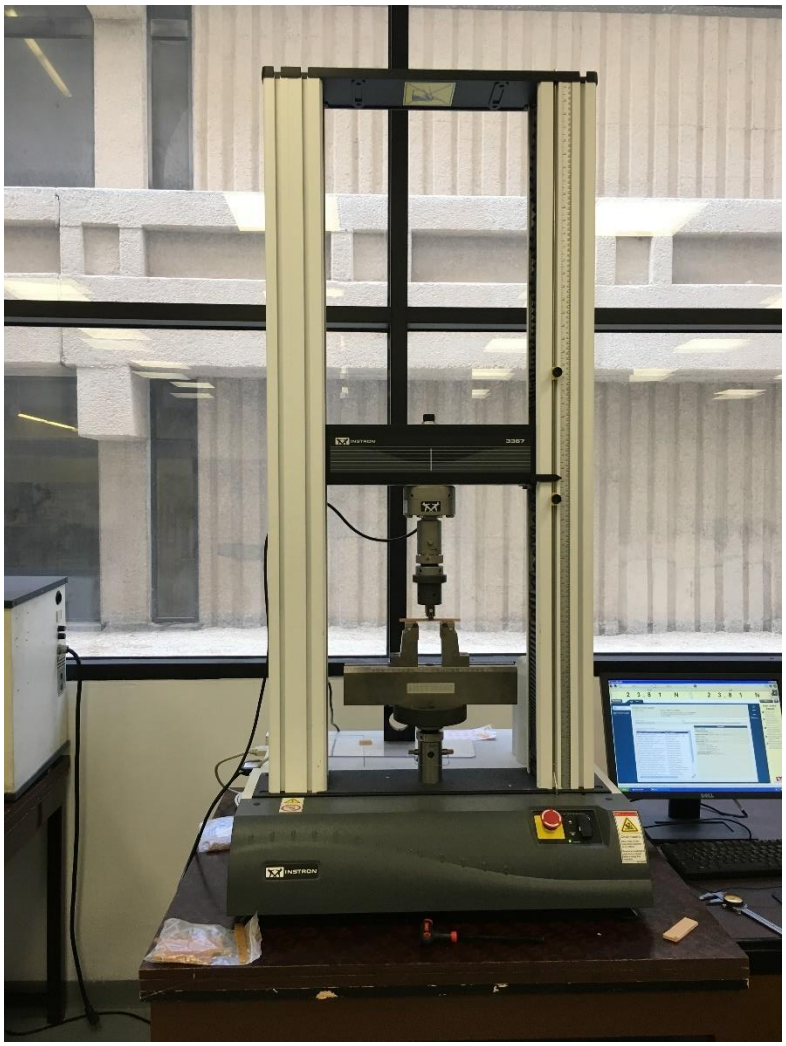

Figure 3.12 UTM equipped with flexural test head

3.6.2 Tensile Test

The tensile test was conducted on universal testing machine (UTM) shown in Fig 3.13. The test was done according to ASTM D638-02a standard [16]. For each sample, three specimens were machined to dumbbell-like shape, using CNC milling machine, and then the rough surfaces were smoothed by grinding, with help of carbide abrasive papers. The crosshead motion was adjusted to 1 mm/min. Specimen's dimensions for all tests are illustrated in Fig 3.14, wherein, all the dimensions are in mm.

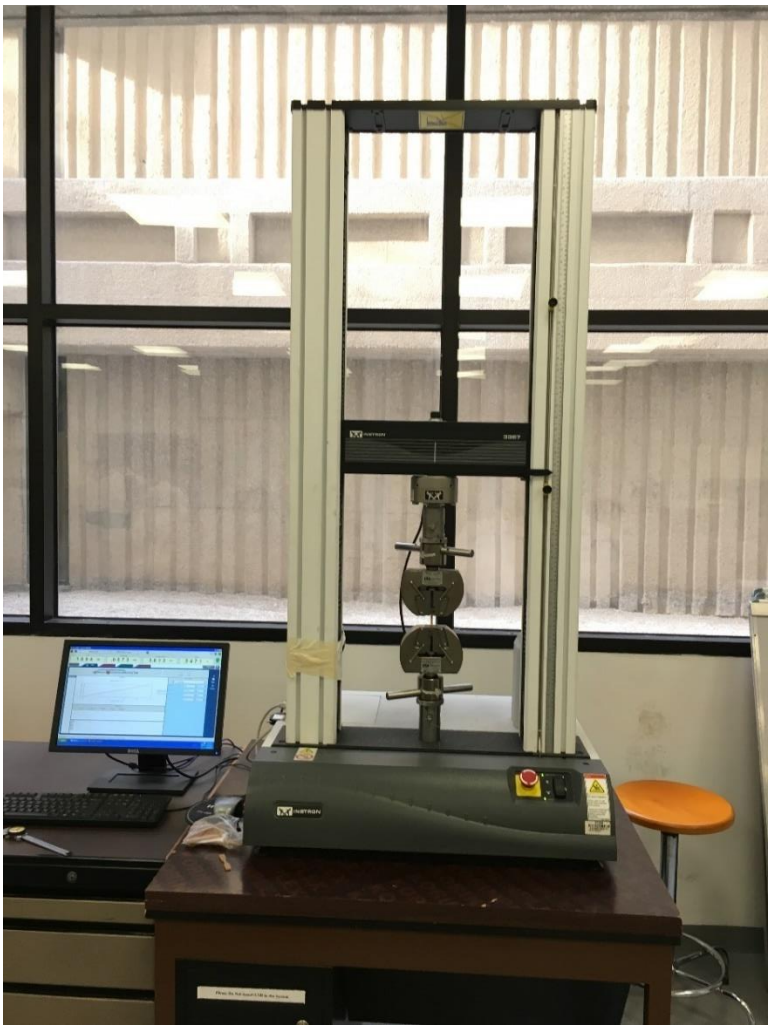

Figure 3.13 UTM equipped with tensile test head

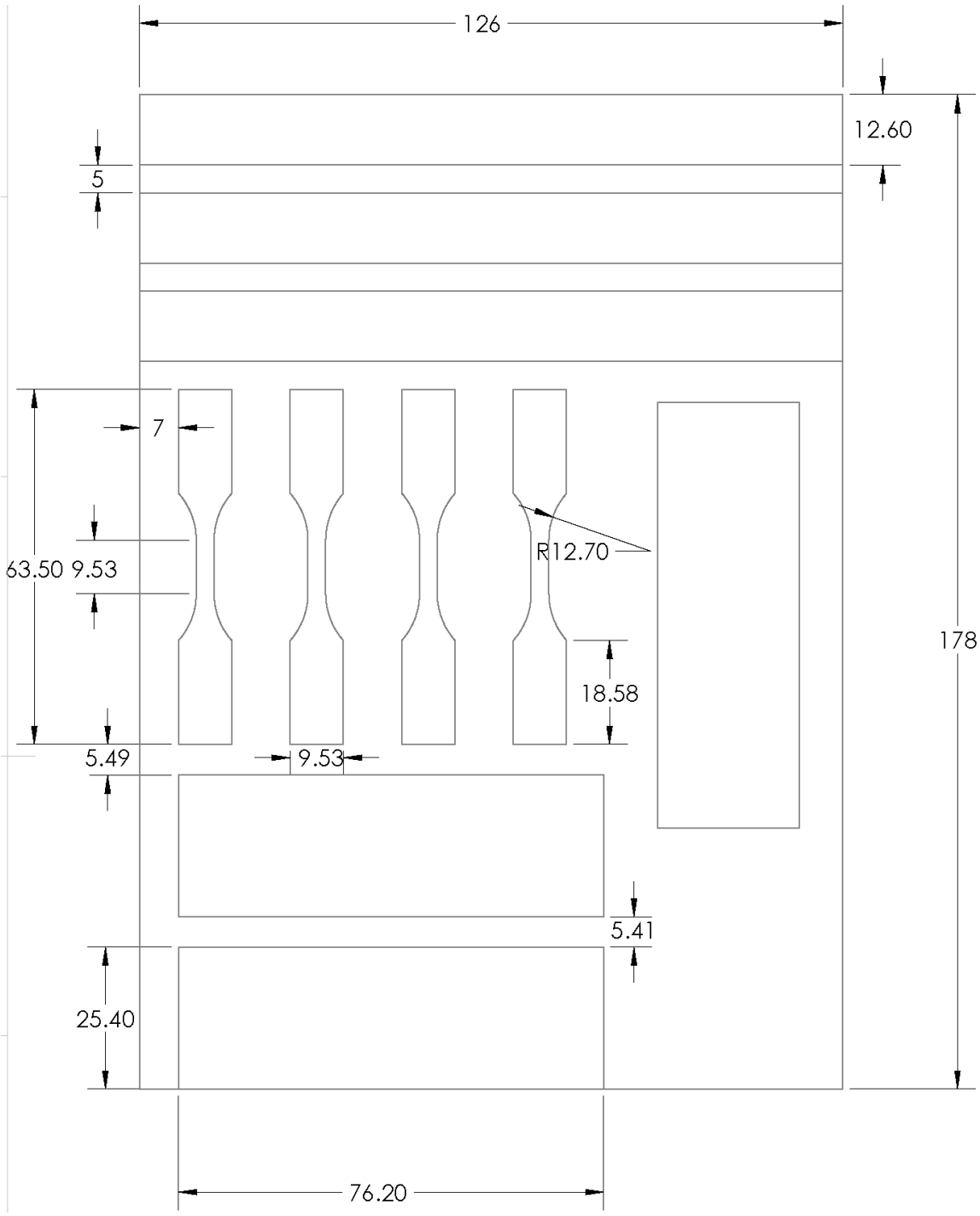

Figure 3.14 CNC machining layout for test specimens

CHAPTER 4

RESULTS AND DISCUSSION

4.1 Optimization of Curing Parameters

The study of cure kinetics gives a clear vision of the curing mechanism which affects the mechanical properties of synthesized polyester. DSC is a commonly used method to study cure kinetics of polymers by the following either isothermal or dynamic method. In case of thermosets polymers, it is difficult to study curing kinetics using isothermal method due to the lower sensitivity of the DSC to the total reaction heat measurements in case of temperature rise during the process [55]. Isothermal method is tedious to analyze and the obtained results are difficult to interpret. Glass transition temperature (T_g) represents a good indication of the cross linking of the uP. As T_g increases, better mechanical properties could be obtained. By this concept, the dynamic method was used in this study to measure T_g according to ASTM D3418-99 standard [50]. Argon gas has been introduced as inert environment for the cooling cycle. Specimens were weighed to be in the range of (5-20) mg. Furthermore, midpoint method was adopted to determine $T_g$directly from the curve, from the region where there is baseline shift or drop (Fig 4.1).

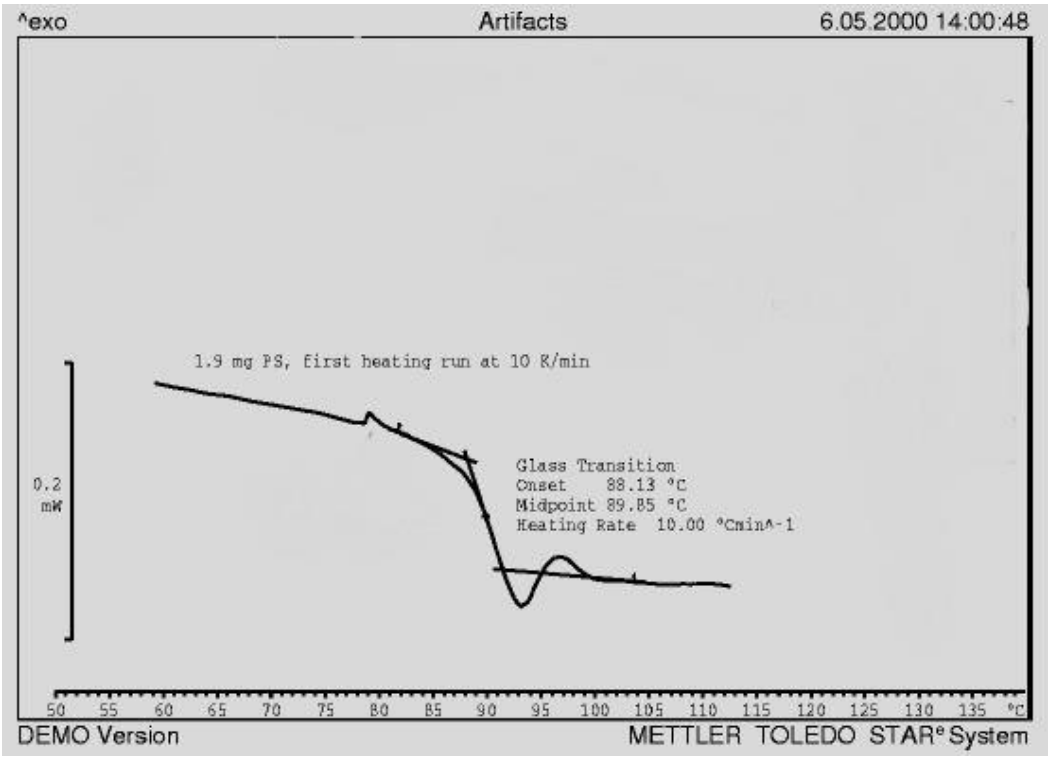

Figure 4.1 Representation of how glass transition temperture could be measured from DSC curve [56]

Fig 4.1 represent the approach by which T_g is estimated. Actually, the transition occurs over a temperature range rather than a single point. At beginning of the transition, a specimen absorbs heat to transit from hard or glassy state to soft one. Consequently, drop in the heat flow is observed over wide temperature ranges. Hence, to estimate the value of, two lines tangent to the baselines of heat flow curve are drawn, another line tangent to the decline region of the curve is also drawn. The midpoint of the line that connects the interference of these three tangent lines is believed to estimate T_g accordingly.

4.1.1 Pre-Curing Optimization

Two factors affect the curing process of the uP, which are curing time and curing temperature. So, to optimize the pre-curing process, curing time was maintained at 2 hours, while pre-curing temperatures were taken as 60, 120 and 160ºC. Then the pre-curing temperature which gives better $\boldsymbol{T_g}$ was kept to optimize pre-curing time. Table 4.1 shows the pre-curing optimization steps.

Table 4.1 Pre-curing optimization

Temperature optimization		Time optimization	
Pre-curing temperature (℃)	Pre-curing time (h)	Pre-curing temperature (℃)	Pre-curing time (h)
80	2	Optimized temperature	2
120			3
160			4

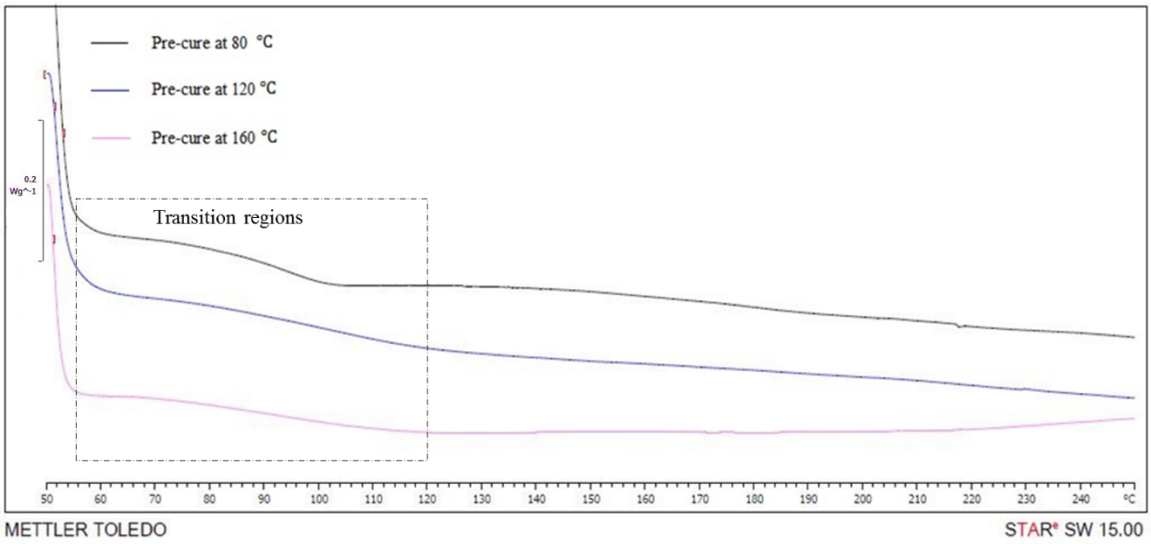

Figure 4.2 DSC curves for pre-cured uP specimens at different curing temperature while curing time fixed at 2 hours

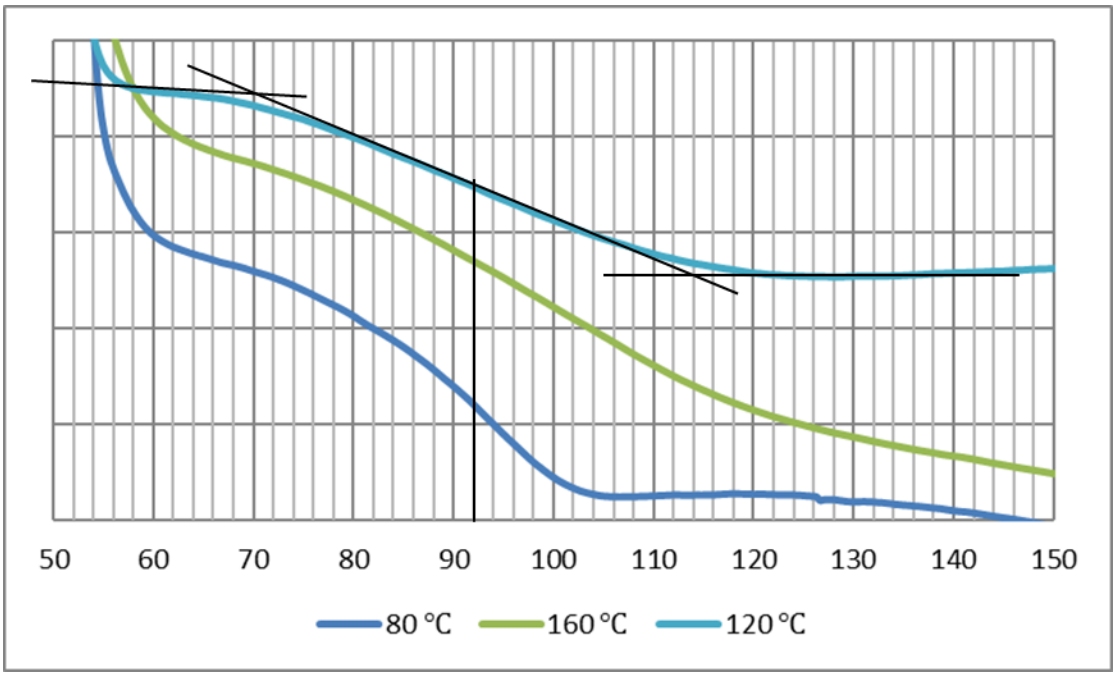

Figure 4.3 Zoomed in DSC curves for the uP specimens pre-cured for 2 hours at different curing temperature

Fig 4.2 shows the curve of heat flow vs. temperature, which was obtained from DSC. Fig 4.3 is a reproduction of the heat flow-temperature curves in the area of interest, through it T_g were measured for all specimens with help of midpoint method which was described previously in Fig 4.1. For all pre-cured specimens, T_g were relatively low due to the inadequate curing of the resin, this was obvious in the presence of very wide transitions, which occurred over an extended range of temperature. However, as curing temperature increased from 80 ℃ to 120 ℃, observable improvement in glass transition was detected due to the improvement in the degree of the cross linking. Moreover, at 160 ℃ glass transition temperature declined to 87 ℃, this reduction may be characterized by degradation of the uP due to excessive pre-curing temperature.

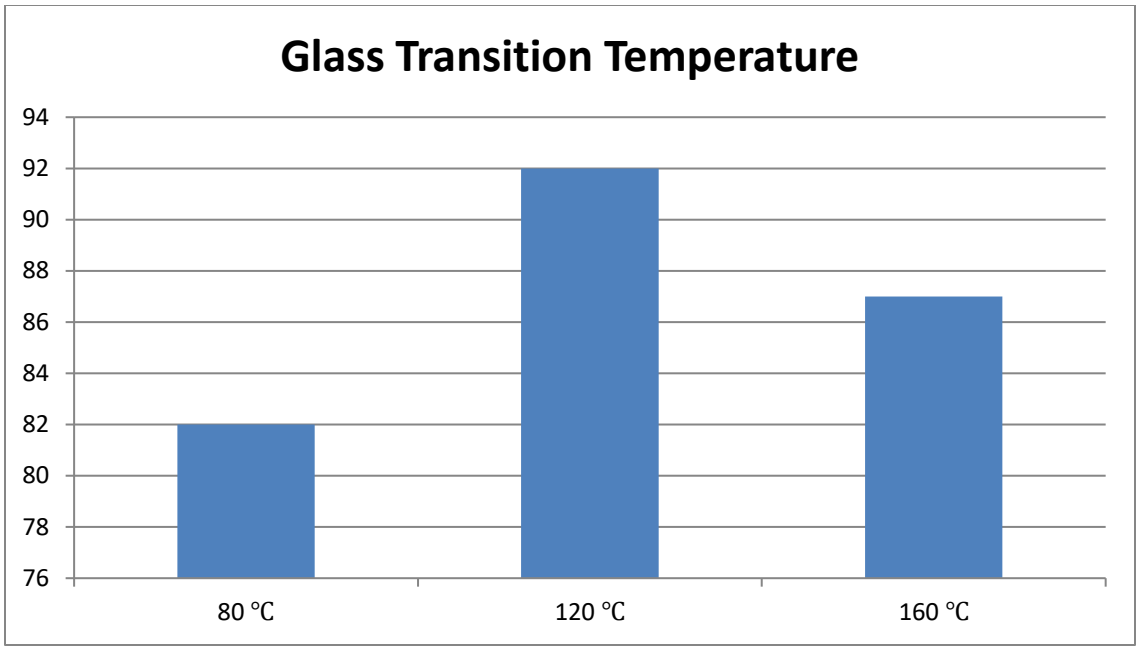

Figure 4.4 Variation of glass transition temperature as a function of pre-curing temperature

Fig 4.4 shows T_g for the specimens cured at different pre-curing temperature: 80, 120 and 160 ℃. While the pre-curing time was maintained at 2 hours. It has been found that pre-curing at 120 ℃ gave better T_g, which was 92 ℃. Accordingly, the effect of pre-curing time is studied to optimize pre-curing time which gives the better T_g. Fig 4.5 demonstrates the effect of pre-curing time on the T_g for different pre-curing time periods as mentioned in Table 4.1. It has been found that, increasing curing time from 2 hours to 3 hours has slight effect on glass transition temperature as indicated in Fig 4.6. However, in case of curing for 4 hours, noticeable improvement in T_g has been observed, represented by the presence of sudden drop in heat flux.

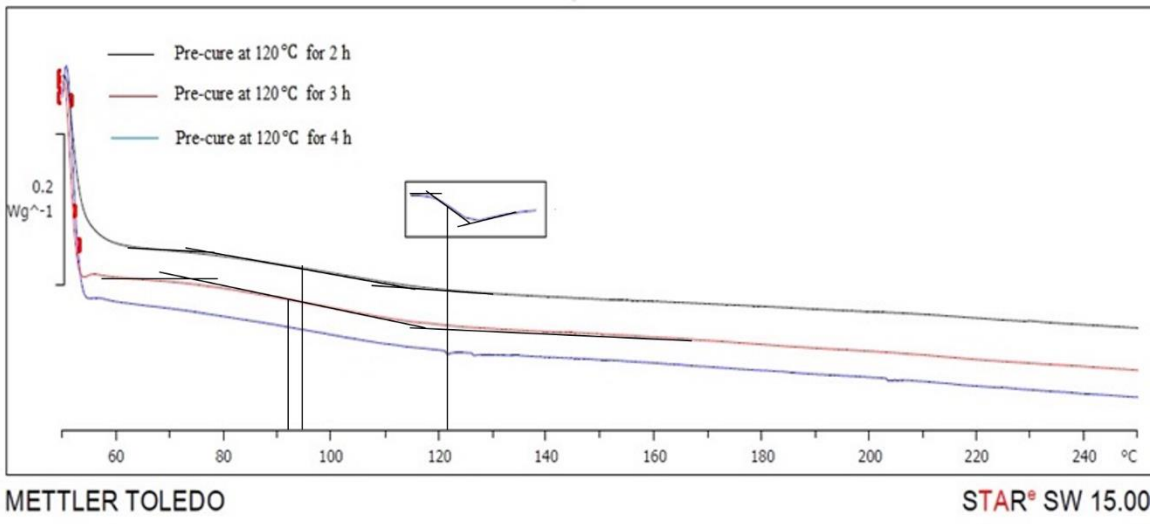

Figure 4.5 DSC curves for pre-cured specimen at 120 ℃, for different curing time (2 h, 3h, and 4 h)

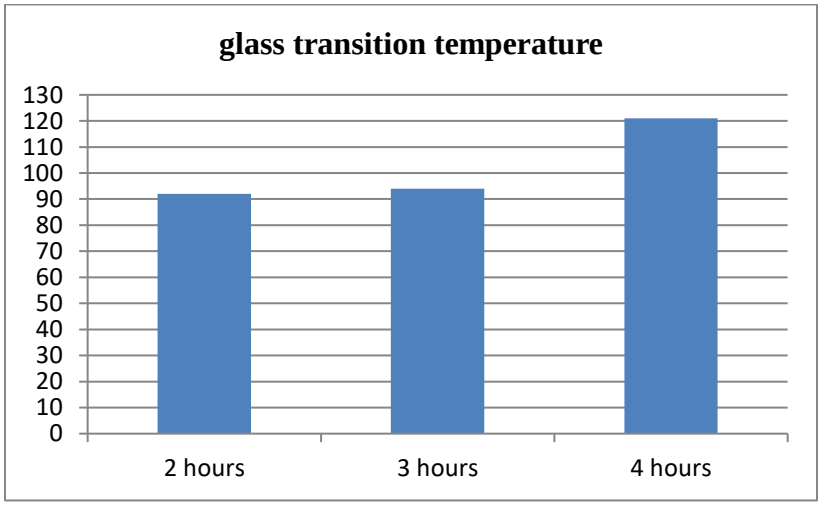

Figure 4.6 Variation of glass transition temperature as a function of pre-curing time

4.1.2 Post-Curing Optimization Parameters

In the previous section, it was found that curing at 120 ℃ for 4 hours gave an improved T_g, having a value of 121 ℃. Moreover, in order to examine how additional curing affects the

T_g of the uP, post-curing was conducted. The optimization parameters of post-curing are shown in Table 4.2.

Table 4.2 Post-curing optimization

Temperature optimization		Time optimization	
Post-curing temperature (℃)	Post-curing time (h)	Post-curing temperature (℃)	Post-Curing time (h)
120	2	Optimized temperature	2
140			3
160			4
180			

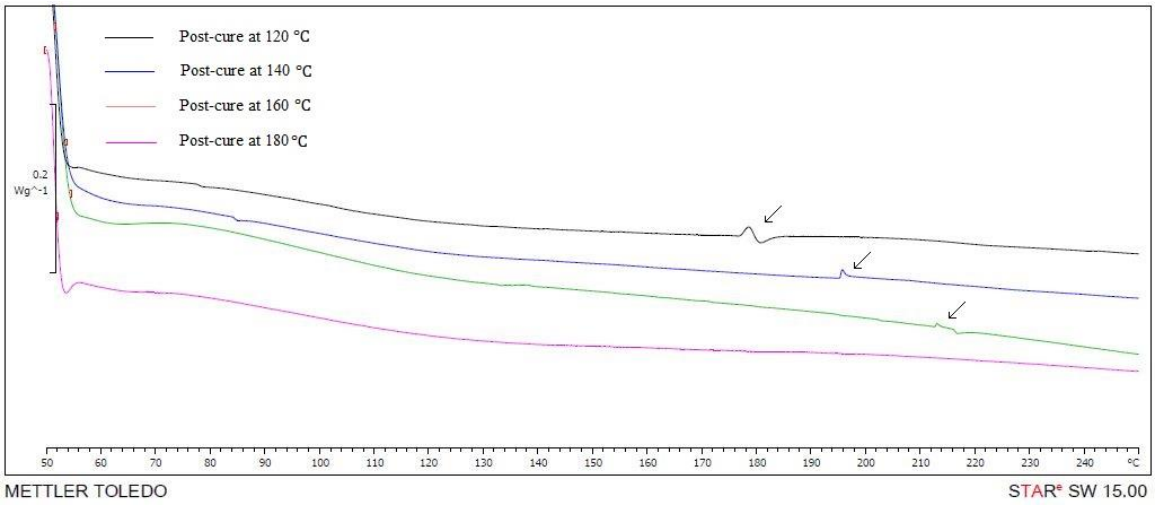

Figure 4.7 DSC curves of post-cured specimens at different curing temperature, curing time fixed at 2 hours

Fig 4.7 shows the effect of post-curing on the $\boldsymbol{T_g}$of uP. It is obvious that, due to the additional curing, uP showed some degree of crystallinity, which was proven by the presence of exothermic and endothermic peaks consequently. Meanwhile, rising of post-curing temperature above 120 ℃ showed a shift in exothermic and endothermic peaks to the right, while the peak size decreased subsequently until they disappeared at 180℃. These thermal events were rationalized by the decomposition of the uP due to curing at high

temperature as suggested by With et. al [57], this explanation is supported by the change in the specimen's color to brown, hence the glass transition temperature was reported for all post-cured specimens in Table 4.3.

Table 4.3 Glass transition temperature of post-cured specimens

Pre-curing temperature (℃)	Pre-curing time (hour)	Post-curing temperature (℃)	Post-curing time (hour)	T_g (℃)
120	4	120	2	177.8
		140		195.4
		160		212.8
		180		-

To compromise between degradation of uP and obtaining higher values of T_g, post-curing at 120 ℃ for 2 hours is considered to be good enough for further analysis, since $T_g$was found to be about 177.8 ℃. Accordingly, post-curing time, certainly additional 2 and 3 hours are studied as a final step to optimize the whole curing process. Fig 4.8 confirmed that post-curing at 120 ℃ resulted in improved T_g which was found to be 177.8 ℃, while increasing post-curing time above 2 hours confirmed the decomposition of the uP represented in the absence of exothermic and endothermic peaks as mentioned previously.

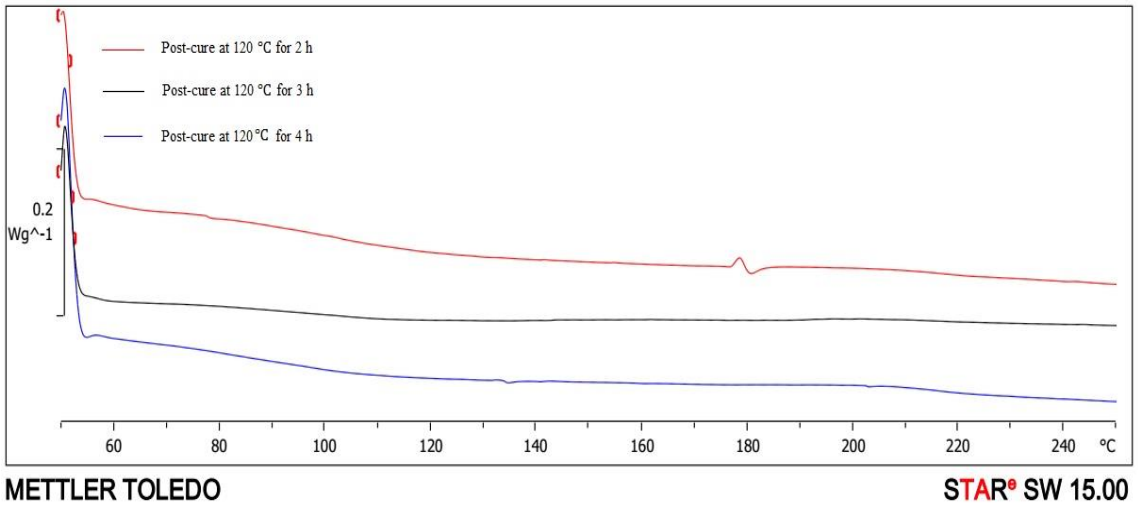

Figure 4.8 DSC curves for post-cured specimen at 120 ℃ curing temperature, for different curing time (2 h, 3h, and 4 h)

To conclude the curing optimization, it has been found as curing temperature and time increased, the value of T_g has improved. However, at elevated curing temperature and extended post curing time the decomposition of the uP is noticeable. So, pre-curing at 120 ℃ for 4 hours followed by post-curing at the same temperature for additional 2 hours yielded the optimized T_g, which was 177.8 ℃.

4.2 Effect of HSM Speed

HSM is considered to be one of the best techniques to disperse nc into uP resin, hence through it, the exfoliated structure could be obtained adequately [33]. It has been mentioned that there is a consensus regarding mixing time. It was reported that 1 hour is good enough for the mixing process, while contradictory reports were found regarding the mixing speed [29], [30]. So, for the purpose of the study, to optimize mixing speed, different speeds were used, and so XRD technique was utilized to measure the state of dispersion by observing the interlayer spacing (d-spacing).

The shear force generated from HSM during mixing process is proportional to mixing speed. The induced force is splitting nc, and forcing uP monomers to disperse into nanoclay's d-spacing. Hence, there is dependency between d-spacing and mixing speed. Therefore, XRD analysis was conducted on the neat uP, I.30E nc powder, and seven uP/c nanocomposites samples, which were synthesized at different mixing speed: 1000, 2000, 3000, 4000, 5000, 6000, and 7000 rpm.

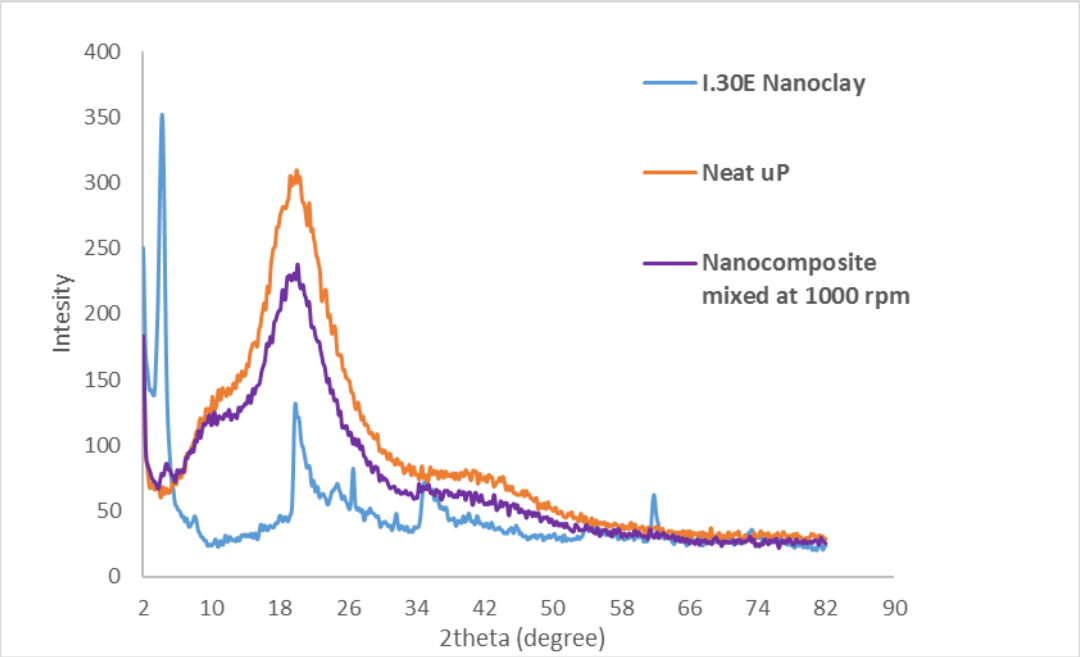

Figure 4.9 XRD full spectra for neat uP, I.30E nanoclay, and uP/c nanocomposites synthesized at 1000 mixing speed

Fig 4.9 illustrates the full XRD spectra of neat uP, I.30E nc, and uP/c nanocomposites mixed at 1000 rpm. I.30E nanoclay's spectrum showed a sharp peak, which means high order stacking of nc. The characteristic diffraction peak for I.30E nanoclay powder was detected at Bragg's angle of 4.22°, then Bragg's law (equation 2.1) was applied to calculate d-spacing, which was found to be 2.10 nm. Confirming to what was found in the literature [10], [58], [59]. Neat uP exhibited broad hump-like peak at Bragg's angle of 20°, showing

that uP has a certain degree of crystallinity as suggested by Farahat [60]. Farag et al. have found similar XRD pattern of the neat polyester wherein Bragg's angle was found to be around 21° as shown in Fig 4.10. In case of nanocomposites, no sharp peaks of nanoclay's were observed, which could be a demonstration of formation of exfoliated structure [58].

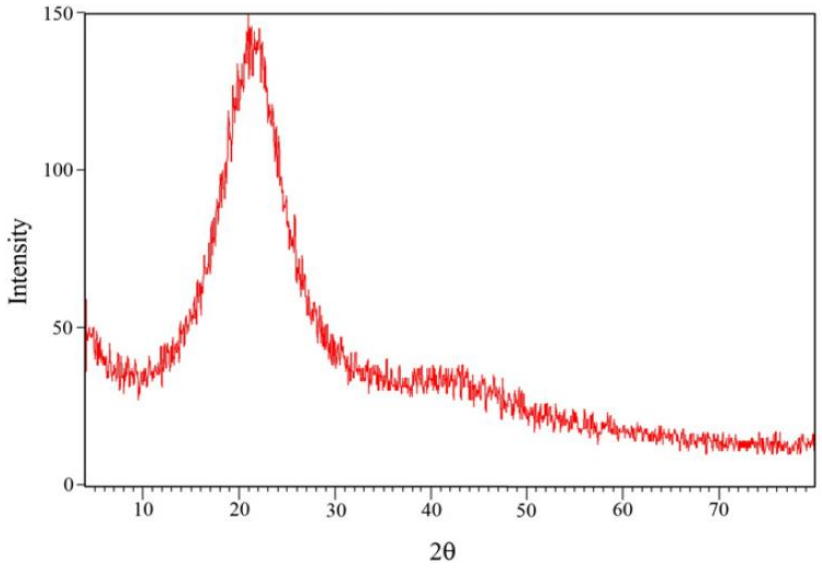

Figure 4.10 XRD pattern for synthesized polyester [61]

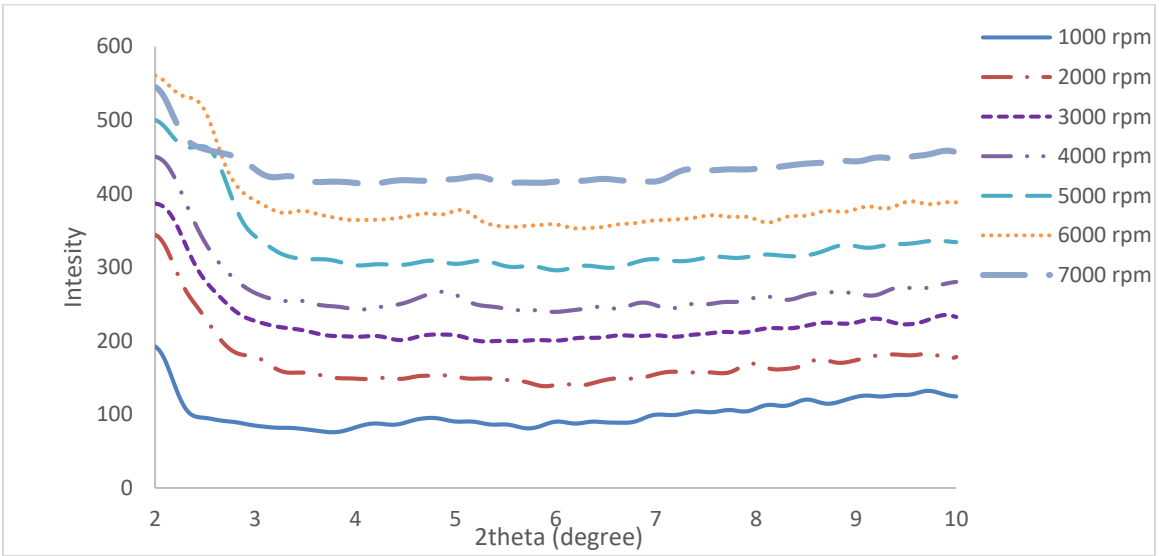

Figure 4.11 XRD spectra for uP/c (3wt%) nanocomposites synthesized at different mixing speeds

Many authors confirmed that the diffraction peaks of uP/c (3wt%) nanocomposites could be detected at Bragg's angle between $2^{\circ}$and 10°[30], [31], so for the purpose of the study, Fig 4.11 shows the effect of mixing speed on the state of dispersion. It is clear that, there were no peaks for all nanocomposites, which could be rationalized due to formation of exfoliation structure or disordered intercalation structure [30], [62] Also, it is observed that as the mixing speed increases the XRD spectrum becomes smoother, which may indicates better dispersion of uP chains into clay interlayer galleries. Nonetheless, increasing mixing speed promotes bubbles formation and heat generation into uP resin, the latter affects the viscosity of the resin accordingly, while the former promotes voids and flaws formation which affects the mechanical properties. Moreover, to have a vivid image on the effect of mixing speed on the microstructure of uP/c nanocomposites, SEM analysis is conducted.

The effect of mixing speed on the microstructure of the nanocomposites is shown in Fig 4.12 (a - d). The micrographs reveal the microstructure uP/c nanocomposites, containing 3 wt% loading of I.30E nanoclay, and syntheized at differnet high shear mixing speeds (1000, 3000, 5000 and 7000 rpm). The micrographs were taken at three different magnifications (200, 2000 and 6000×)

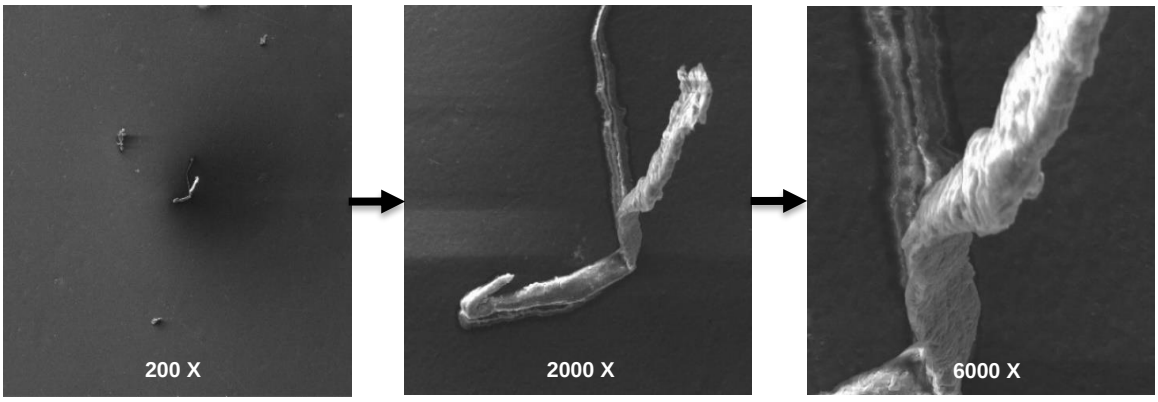

Figure 4.12.a uP/c nanocomposite mixed at 1000 rpm

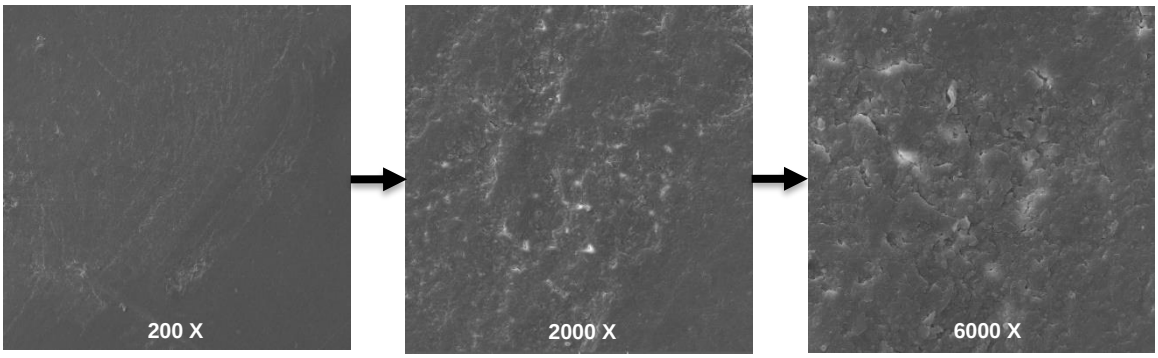

Figure 4.12.b uP/c nanocomposite mixed at 3000 rpm

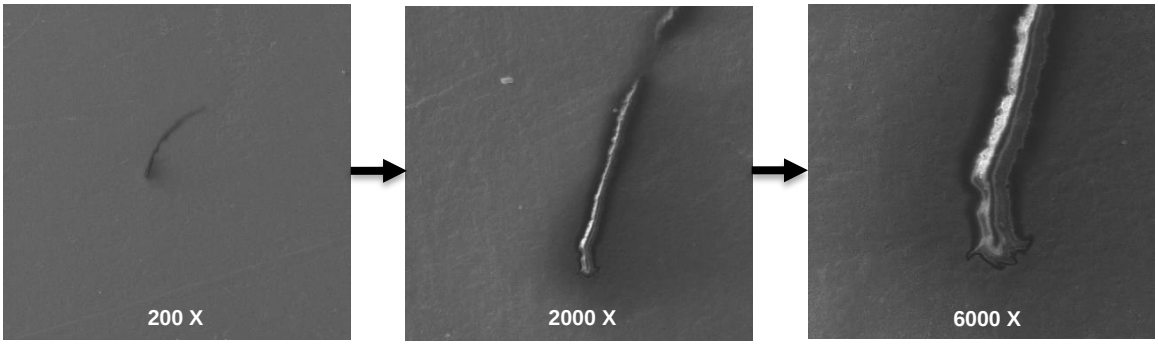

Figure 4.12.c uP/c nanocomposite mixed at 5000 rpm

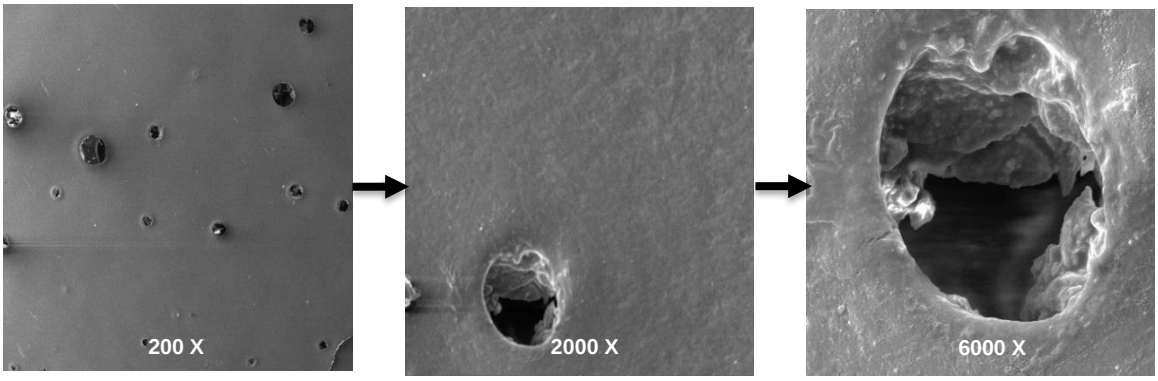

Figure 4.12.d uP/c nanocomposite mixed at 7000 rpm

Figure 4.12 (a – d) SEM micrographs for neat uP and uP/c nanocomposites syntheized at differnet speeds (1000, 3000, 5000 and 7000 rpm) while the clay loading kept at 3wt%

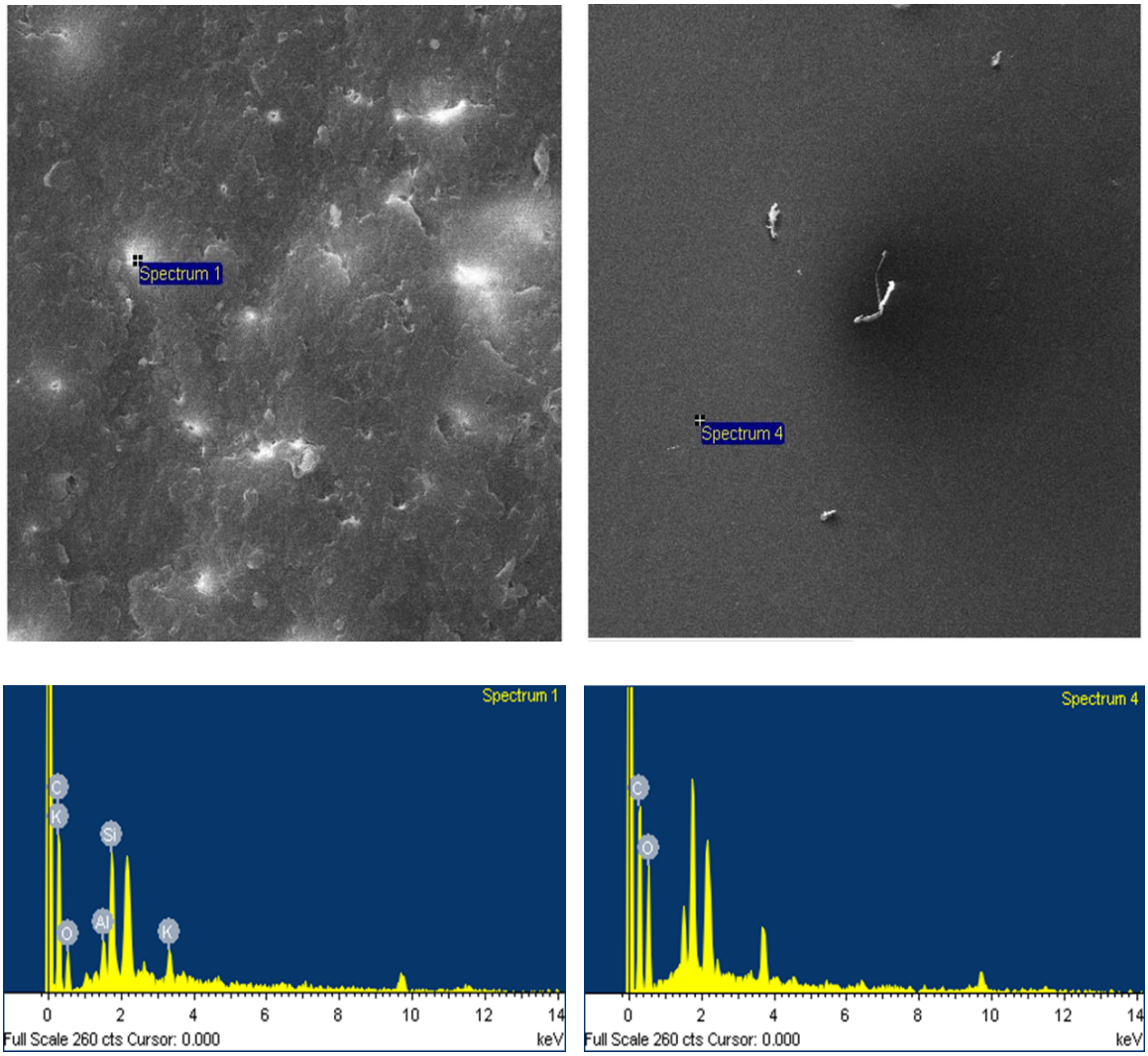

Figure 4.13.a Energy dispersive spectra for spots 1 and 4

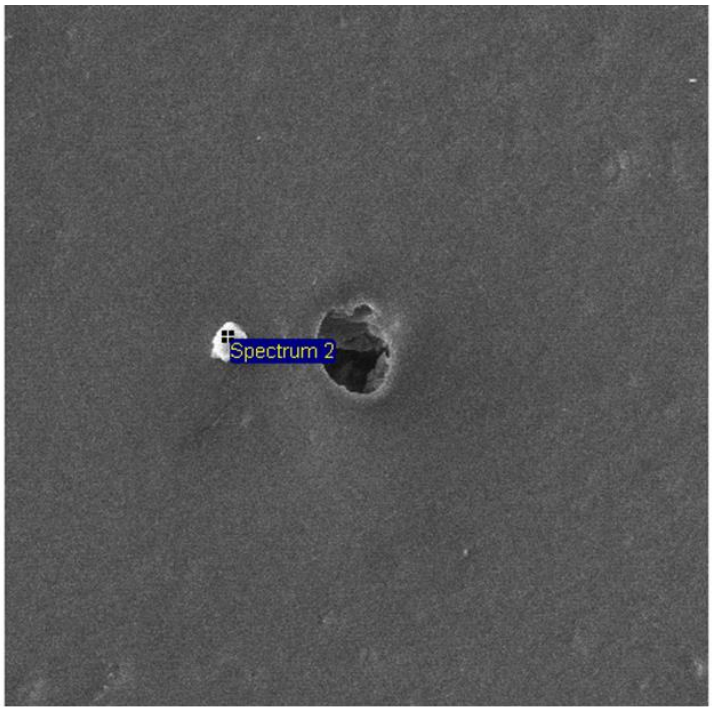

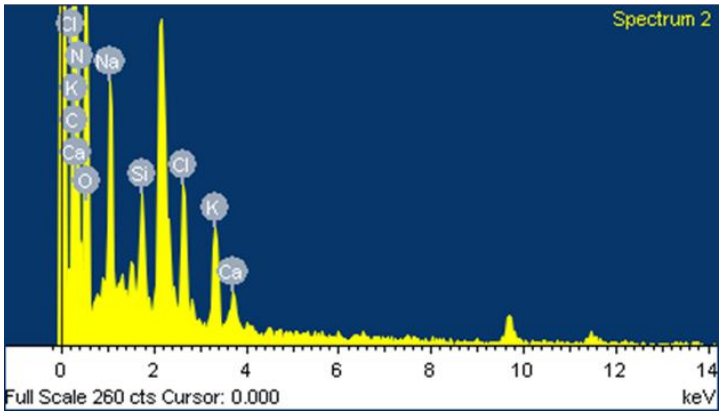

Figure 4.13.b Energy dispersive spectrum for spot 2

Figure 4.13 Energy dispersive spectra for spots 1, spot 2 and spot 4

Table 4.4 Elemental composition of the spectrum 1, 2 and 4

Element	Spectrum 1 (wt%)	Spectrum 2 (wt%)	Spectrum 4 (wt%)
C	65.50	55.07	49.15
O	24.22	26.63	50.85
Al	2.03	0	0
Si	5.98	0.38	0
K	2.28	0.63	0
Na	0	1.67	0
Cl	0	0.73	0
Ca	0	0.22	0
N	0	14.67	0
Totals	100.00	100.00	100.00

The white dots may represent the agglomeration of nc while the dark dots indicate flaws and defects within the nanocomposites. To support the claim, energy dispersive analysis (EDX) was conducted by FESEM to examine the elemental compositions within the selected spots. The elemental analysis is shown in Fig 4.13.a and Fig 4.13.b, confirming that the white dots are representing clusters of nanoclay, since both of these figures and Table 4.4 are showing that the EDX spectrum for the selected spot 1 is rich in elements which refers to clay minerals, while spectrum 4 is constituted only of C and O elements. Fig 4.13.a and Fig 4.13.b are showing that at high mixing speed (7000 rpm), the microcracks are observable due to breakage of nanoclay platelets besides the defects formation resulted from the high shear force. Based on the above observations, moderate

speed of 3000 rpm is considered to be the optimum mixing speed at which all the nanocomposite specimens were prepared.

4.3 Effect of nc Type on the Dispersion State of uP/c Nanocomposites

Three different nc types were chosen to study the effect of clay type on the dispersion state, namely: Nanomer I.30E, Cloisite 10A, and Cloisite 20A. All uP/c nanocomposites were prepared by the optimized mixing speed of 3000 rpm, while clay loading kept at 3wt%. Therefore, XRD analysis was performed to study the effect of clay type on the microstructure of the developed materials.

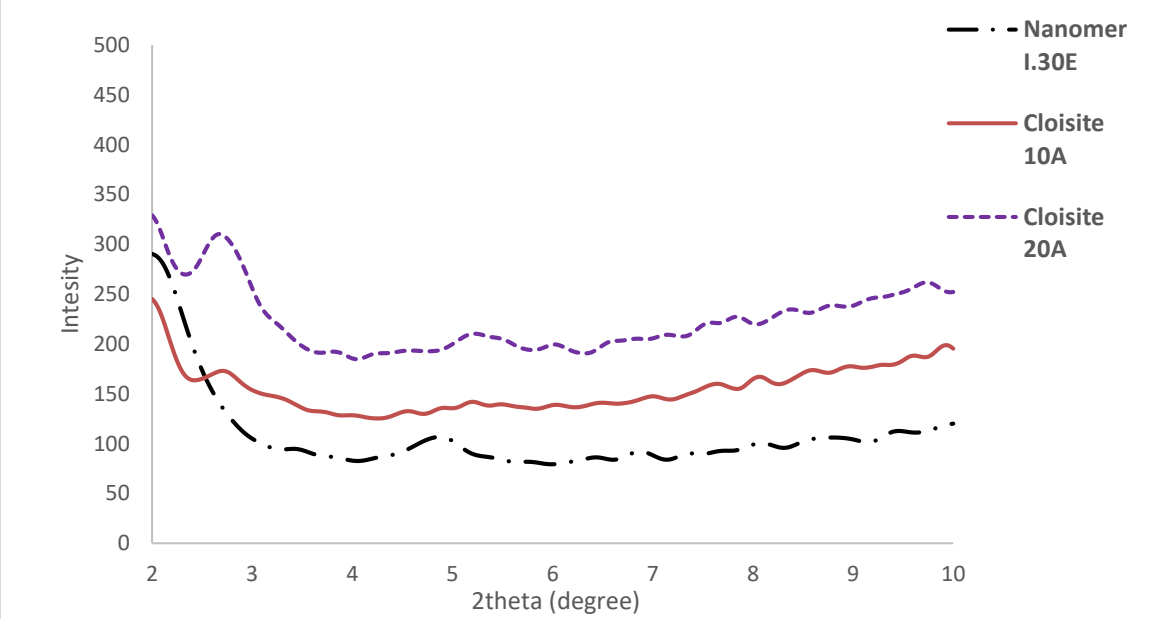

Figure 4.14 XRD spectra for uP/c nanocomposites containing 3 wt% of different nanoclay types

Fig 4.14 represents the XRD spectra for uP/c nanocomposites prepared by different clay types: I.30E, Cloisite 10 A, and Cloisite 20 A respectively. Cloisite 20 showed relatively large hump-like peak, while Cloisite 20 presented lower one, whereas in case of I.30E no peaks were noticed, which may indicate that I.30E has high surface interaction, resulted in high d-spacing, accordingly this will ease the diffusion of uP chains between nc platelets

[38]. Hence, uP/c nanocomposites were prepared by I.30E nanoclay may reveals better exfoliation state among the others.

4.4 Effect of nc Type and Loading on Tensile Properties of uP/c Nanocomposites

To investigate the effect of clay type on the tensile properties of uP/c nanocomposites, three uP/c nanocomposites were prepared by different clay types: Nanomer I.30E, Cloisite 10A and Cloisite 20A. While the clay loading maintained at 3wt%. Hence, tensile test was conducted on three samples for each of the developed nanocomposite.

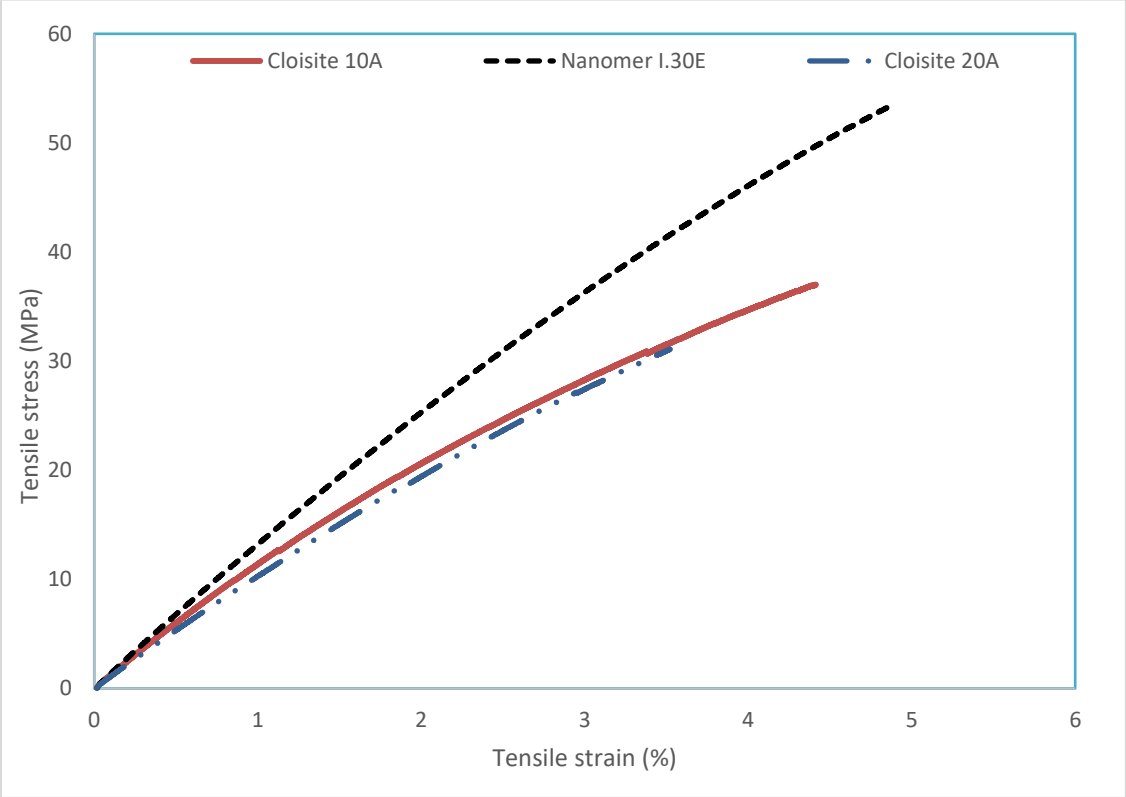

Figure 4.15 Typical stress-strain curves for uP/c prepared from the different clay types

Fig 4.15 shows the representative stress strain curve for uP/c nanocomposites which were prepared by: 10A, 20A and I.30E. Bearing in mind that the curves were plotted for one

sample for each of nc type. However, the tensile strength was measured for three samples for each uP/c nanocomposite. Then, the average values of tensile strength were calculated besides the standard deviation as listed in Table 4.5.

Table 4.5 Average tensile strength for uP/c nanocomposites prepared by: 10A, 20A and I.30E

Nanoclay type	10A	20A	I.30E
Sample 1	31.12	37.35	48.60
Sample 2	37.00	31.10	55.85
Sample 3	31.31	43.06	53.44
Average tensile strength(MPa)	33.14	37.17	52.63
Standard deviation	3.34	5.98	3.69

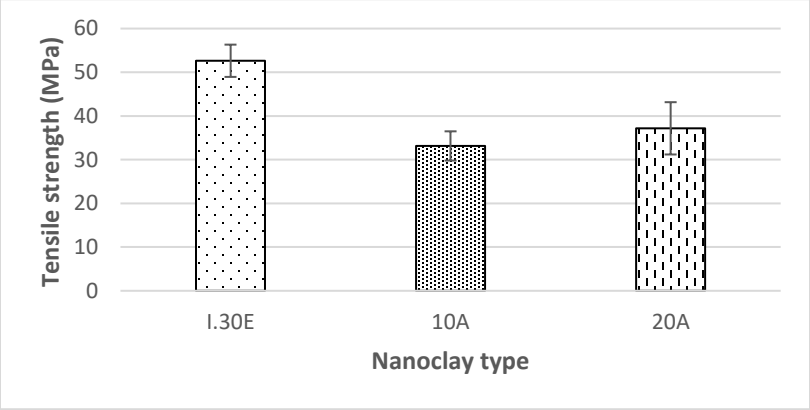

Figure 4.16 Effect of clay type on the tensile strength of uP/c nanocomposites

Fig 4.16 shows that among the three types of nc, Nanomer I.30E was presented the highest average tensile strength, had an average value of 52.63 MP. While Cloisite 10A and Cloisite 20A had strength of 33.1 MPa and 37.1 MPa respectively. uP/c nanocomposites prepared by I.30E account for 59% and 42% improvement in tensile strength over that prepared by 20A, and 10A respectively.

Al-Qadhi [30] prepared epoxy/clay nanocomposites, using different kinds of nc: I.28E, I.30E, C10A and C20A. Similar to what was found, I.30E yielded the best tensile strength over the others. The enhancement in the tensile strength can be attributed to the high aspect ratio of I.30E nanoclay. It may also be attributed to formation of exfoliated structure [8], [9] as observed in XRD analysis. Nanomer I.30E indicated a good compatibility between clay interlayer galleries and uP chains, so it was chosen to prepare uP/c and the hybrid GFRuP/c nanocomposites.

Furthermore, to study the effect of clay loading on the tensile strength of uP/c nanocomposites, tensile test was conducted on neat uP and uP/c nanocomposites, prepared by different clay loading: 1, 2, 3 and 4 wt% of I.30E nanoclay.

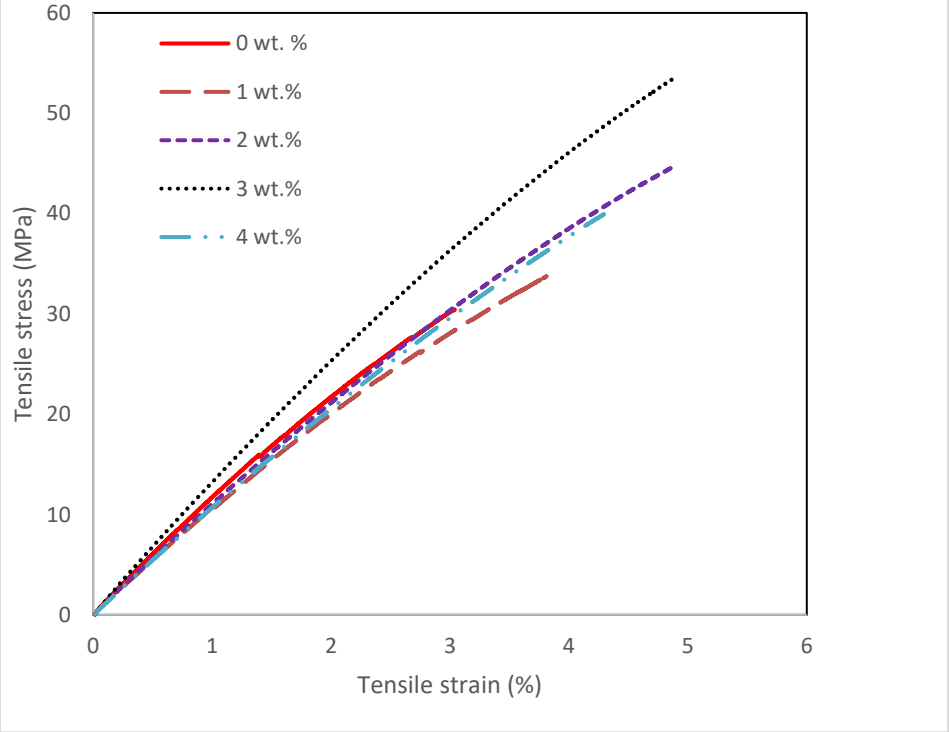

Figure 4.17 Representative Stress-strain curves for neat uP and uP/c Nanocomposites containing different loadings of I.30E nc

Fig 4.17 depicts stress–strain curves for neat uP and uP/c nanocomposites. The graph is showing relatively low values of tensile strength due to the brittle behavior of uP. Similar to above, the curves were plotted for one representative sample for each nc loading. Moreover, the tabulated values of average tensile strength for each sample are shown in Table 4.6.

Table 4.6 Average tensile strength for neat uP and uP/c nanocomposites prepared with different clay loadings

Nanoclay loading wt%	0	1	2	3	4
Sample 1	25.28	32.82	41.48	48.60	37.68
Sample 2	30.44	33.75	45.29	55.85	42.19
Sample 3	33.76	34.74	44.53	53.44	39.95
Average tensile strength (MPa)	29.82	33.77	43.76	52.63	39.94
Standard deviation	4.27	0.96	2.01	3.69	2.25

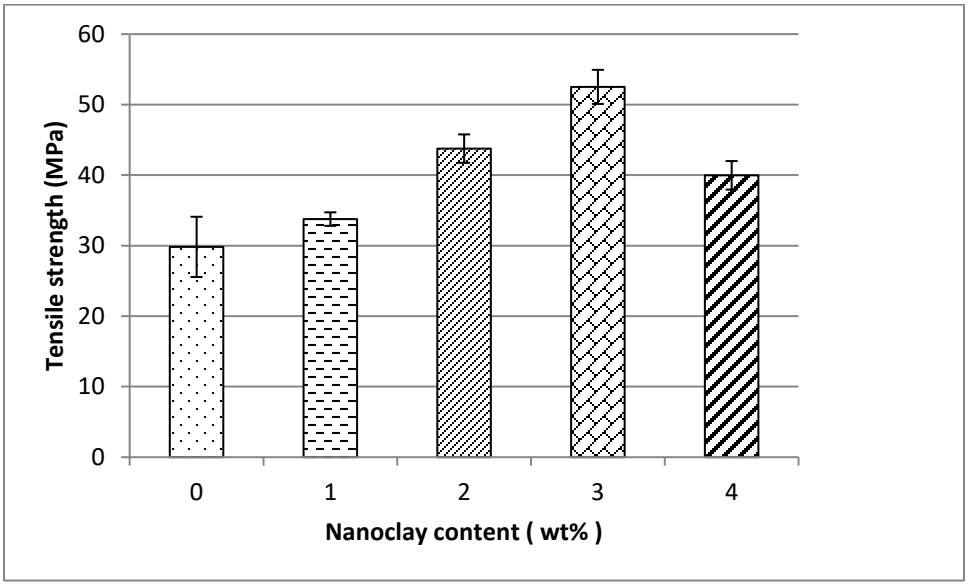

Figure 4.18 The effect of clay loading on the tensile strength of the neat uP and uP/c nanocomposites

Fig 4.18 shows that, as the clay loading increases, the tensile strength of uP/c rises until reaching the peak in case of 3wt% of clay loading, which had an average value of 52.6 MPa. The enhancement is attributed to the good adherence between clays and uP matrix,

leading to improvement of load transfer mechanism between the matrix and nc. Moreover, going beyond 3wt% led to loss in the improvement of tensile strength, because at higher clay loading, the probability of clay particles agglomeration becomes high. These agglomerated particles act as stress concentrations, hence causing the decrease in the tensile strength[54], [63]. Alamri et al. [64] suggested that the reduction basically due to increase of the resin's viscosity, thereby the mixing and degassing processes become much difficult, due to presence of micro voids and air gaps, consequently the diffusion of uP chains between nc platelet will become a difficult task. Some studies showed an agreement on 3wt% of nc loading, which is responsible for the maximum improvement in the tensile strength of uP/c nanocomposite [28], [29]. On another hand, and contrary to what was found, Saharudin et al. [65] reported that just 0.7wt% of halloysite nanoclay responsible for 46% improvement in the tensile strength of neat polyester. In addition, going beyond this loading will reduce the mechanical properties of polyester/nanoclay composite accordingly.

Furthermore, results showed relatively low modulus of elasticity for all uP/c nanocomposites. Fig 4.19 shows that nc slightly decreased elastic modulus in the case of 1wt% loading. However, it was recovered at 3wt% loading. Therefore, it could be stated that nanoclay has no considerable effect on the stiffness of the composites. This behavior is similar to what has been found by Bensadoun et al.[33].

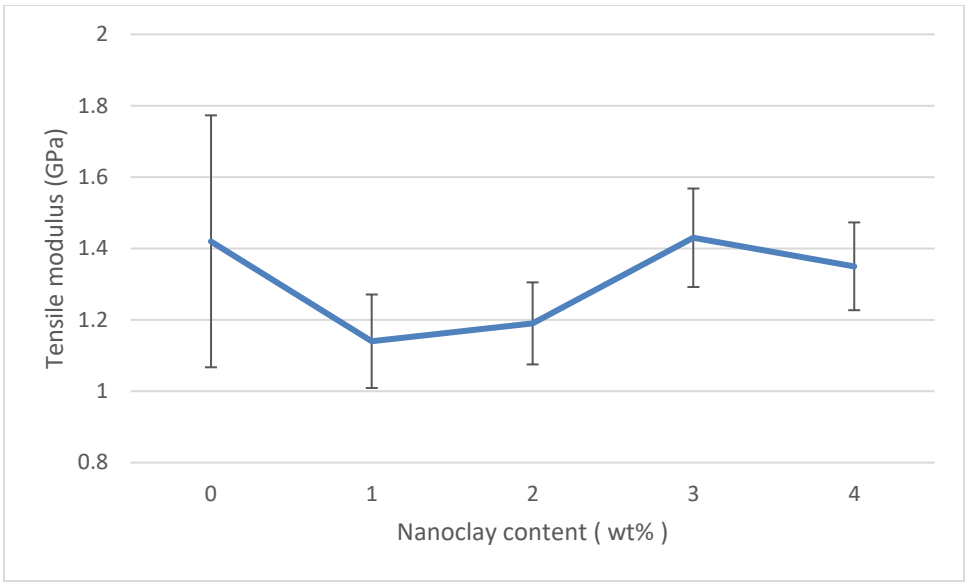

Figure 4.19 Variation of Young's modulus with clay loadings

4.5 Effect of nc Type and Loading on Flexural properties of the uP/c Nanocomposites

In this section, the study of the effect of nc type and loading on flexural properties of the developed materials is highlighted. Similar to the tensile test, the same test procedure was followed.

Fig 4.20 shows the average flexural strength for the three types of nanoclay: I.30E Nanomer, 10A Cloisite and 20A Cloisite; prepared by 3wt% of nc loading. In the same way as the tensile test, the maximum flexural strength was in the case of I.30E nanoclay, attaining a value of 61.8 MPa, confirming that I.30E nanoclay is the best one over the other clay types.

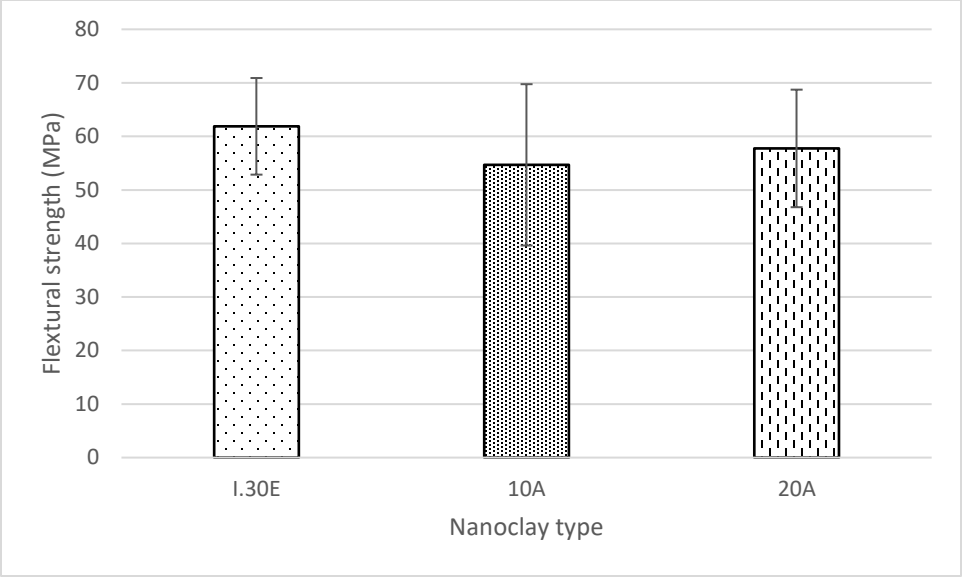

Figure 4.20 The effect of clay type on the flexural strength of the uP/c nanocomposites containing 3 wt% of nc

Fig 4.21 illustrates that; the flexural strength increases as clay loadings increase. This trend is similar to that seen for tensile strength. Furthermore, noticeable improvements of flexural strength with a maximum of 56% increase was observed at 3wt%. However, beyond 3wt% of clay loading, the degradation of the flexural strength was observed, yielding 27 % reduction in the strength of uP. The rationalization of this trend can be attributed to low reinforcement-matrix interaction [66], which reduces stress transfer mechanism between the matrix and nc. Also mentioning that, at higher clay loading uP resin becomes viscous; therefore, the elevated viscosity deteriorates the diffusion of uP chains into nc platelets [64], [67]. Also, at high clay loading the agglomeration of nanoclay tends to weaken the boundaries between nc and uP

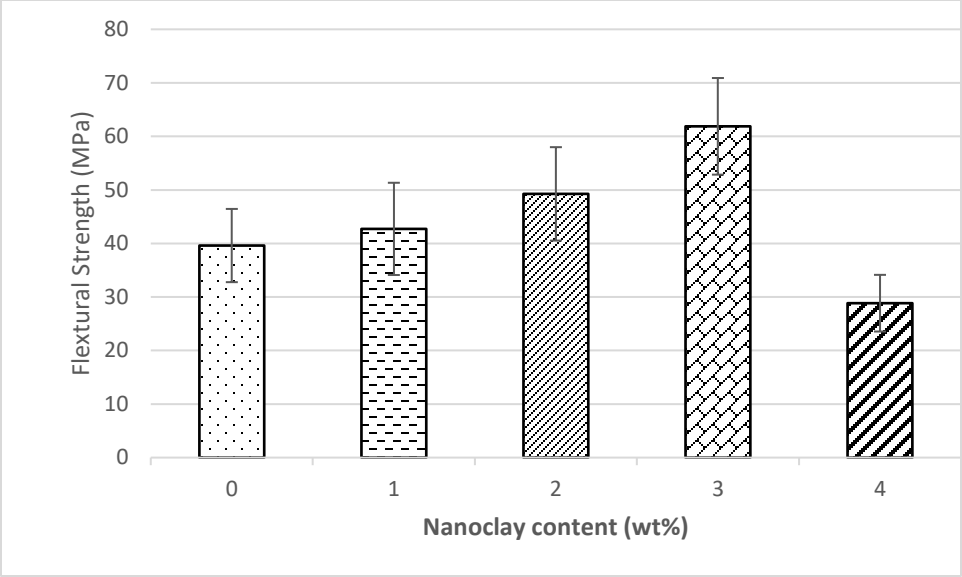

Figure 4.21 The effect of clay loading on the flexural strength of the uP/c nanocomposites prepared by I.30E

The flexural strength was measured for each sample, average values besides standard deviations were also calculated and reported in Table 4.7.

Table 4.7 Tabulated flexural strength measurements for neat uP and uP/c nanocomposites

Samples	nc Loading (wt%)					nc Type (3wt%)		
	0	1	2	3	4	I.30E	10A	20A
Sample 1	32.07	32.85	43.32	61.43	23.65	61.43	66.92	45.41
Sample 2	45.41	48.73	59.28	53.09	28.65	53.09	59.28	66.42
Sample 3	41.35	46.58	45.19	71.12	34.23	71.12	37.86	61.43
Average Flexural Strength (MPa)	39.61	42.72	49.26	61.88	28.84	61.88	54.69	57.75
Standard deviation	6.84	8.62	8.72	9.02	5.29	9.02	15.06	10.98

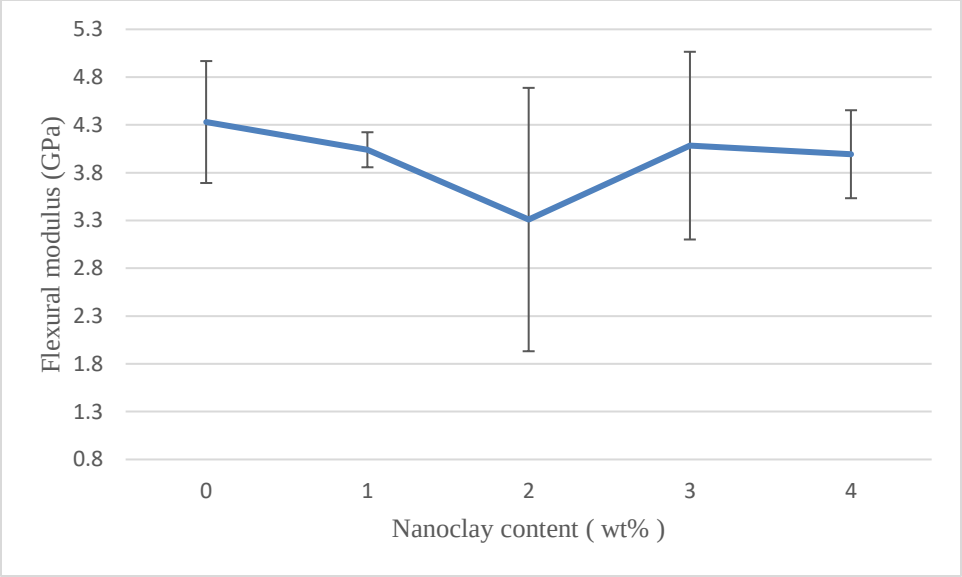

Figure 4.22 Variation of Flexural modulus respect with clay loading

Fig 4.22 illustrates the effect of clay loading on the flexural modulus of uP/c nanocomposites. Though the margin of error regarding flexural modulus is relatively large for uP/c nanocomposites containing 2wt% and 3wt% of nc, the percentage change in the average flexural moduli of the neat uP and uP/c (4wt%) is only 7 %. It seems that, similar to what was found for Young's modulus, nc has no significant effect of the stiffness of the developed uP/c nanocomposites. Similar to what has been reported by Kchit et. al and Bensadoun et al. [33], [37].

4.6 Mechanical Properties of Hybrid GFRuP/c Nanocomposite

In fact, due to superior mechanical properties of GF, reinforcing uP/c by GF has led to significant enhancement in the tensile strength of the hybrid GFRuP/c as expected. Fig 4.23 shows that the tensile strength of hybrid GFRuP/c containing 3wt% of nc has reached 105 MPa, yielding 165% improvement compared to the neat uP, with only 70% improvement when compared to uP/c nanocomposite.

Regarding the flexural test, Fig 4.24 depicts the effect of GF and nc on the flexural strength of uP. It was found that, introducing GF into uP resulted in great improvement of the flexural strength of GFRuP/c nanocomposites, yielding 419% enhancement when compared to the neat uP. Besides, 232% improvement when compared to uP/c nanocomposite contains similar clay loading (3wt%). The improvement attributed to the good interfacial bonding between GF and uP/c matrix as well as the good mechanical properties of E-CR chopped GF.

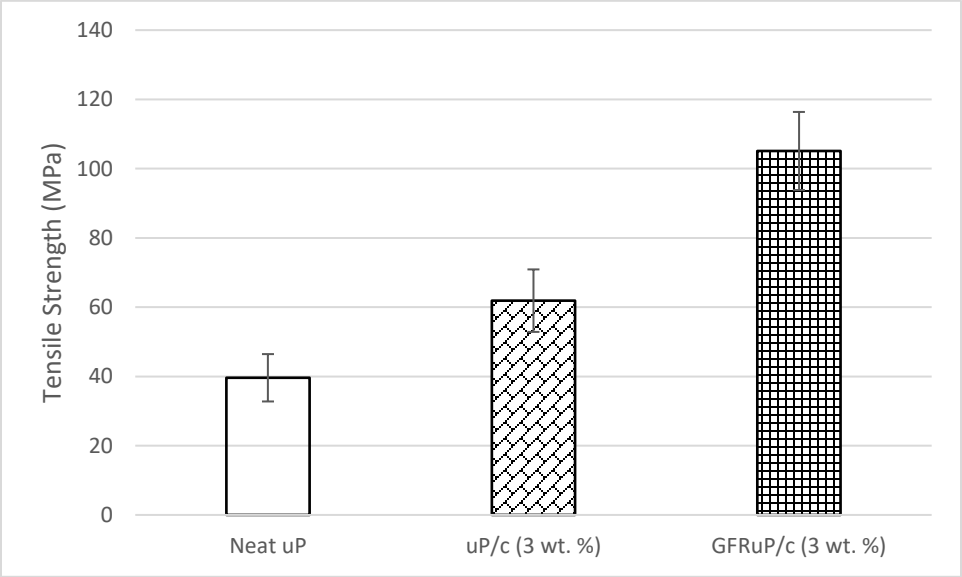

Figure 4.23 Variation of tensile strength with addition of nc and GF

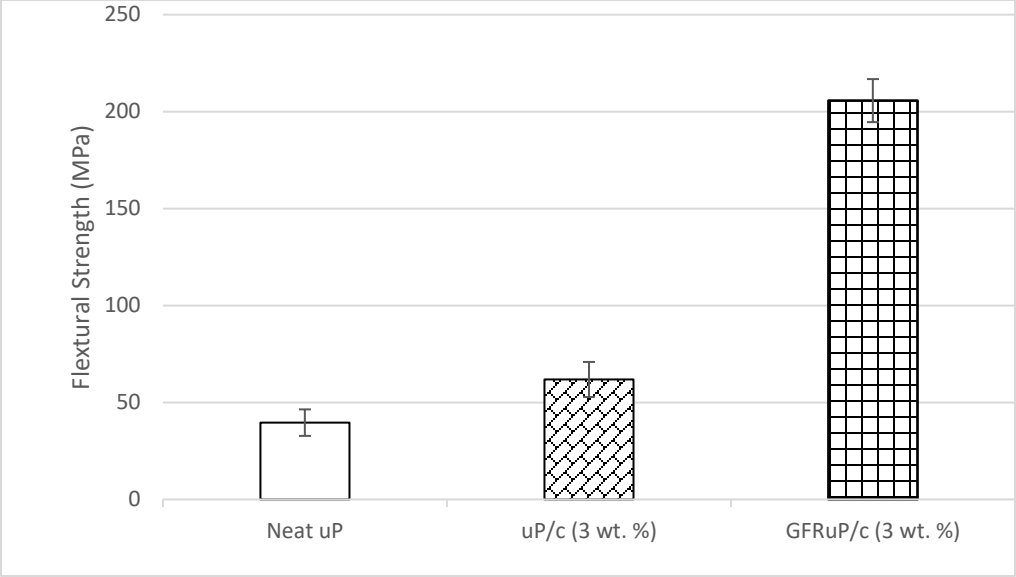

Figure 4.24 Variation of flexural strength with addition of nc and GF

Table 4.8 depicts both of flexural and tensile strengths measurements for GFRuP/c along with neat uP and uP/c nanocomposites.

Table 4.8 Tabulated mechanical properties of GFRuP/c nanocomposite compared to neat uP and uP/c (3wt.%)

	Flexural Strength (MPa)			Tensile Strength (MPa)		
	Neat uP	**uP/c (3wt%)**	**GFRuP/c (3wt%)**	**Neat uP**	**uP/c (3wt%)**	**GFRuP/c (3wt%)**
Sample 1	32.07	61.43	200.72	25.28	48.60	117.33
Sample 2	45.41	53.09	218.38	30.44	55.85	95.12
Sample 3	41.35	71.12	197.90	33.76	53.44	102.84
Average measurement	39.61	61.88	205.66	29.82	52.63	105.09
Standard deviation	6.83	9.02	11.09	4.27	3.69	11.27

4.7 Fractographic Analysis of The Tensile Fractured surfaces

The fractured surfaces of failed tensile specimens were examined by FESEM to study the fracture mechanisms and explain how the nanoclay and glass fibers affect the failure of the matrix. In addition to that, crack initiation and propagation regions also are examined.

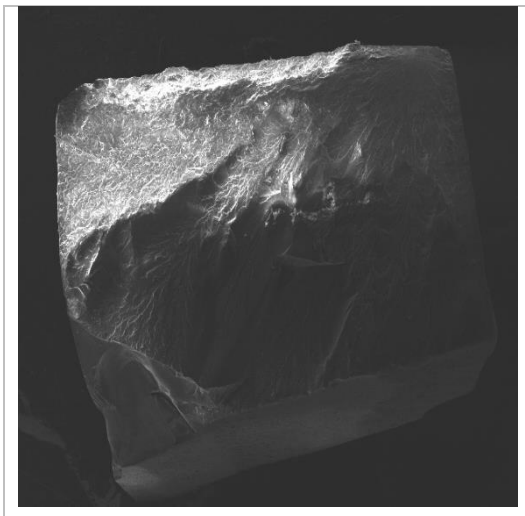

(a)

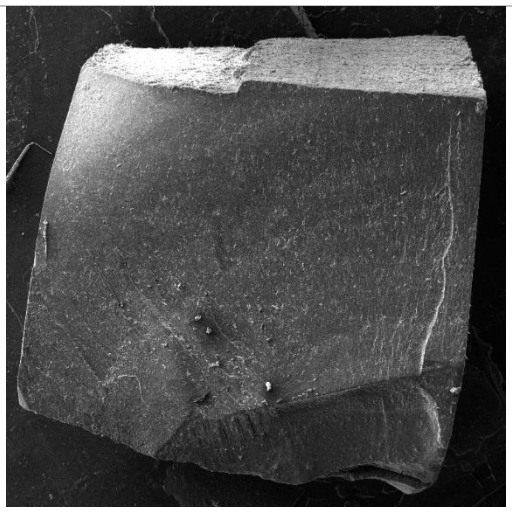

(b)

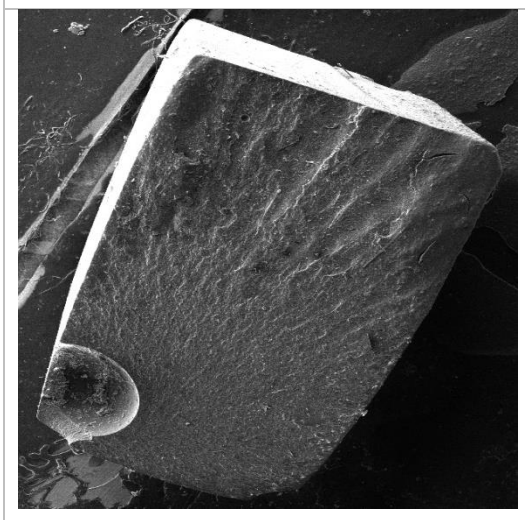

(c)

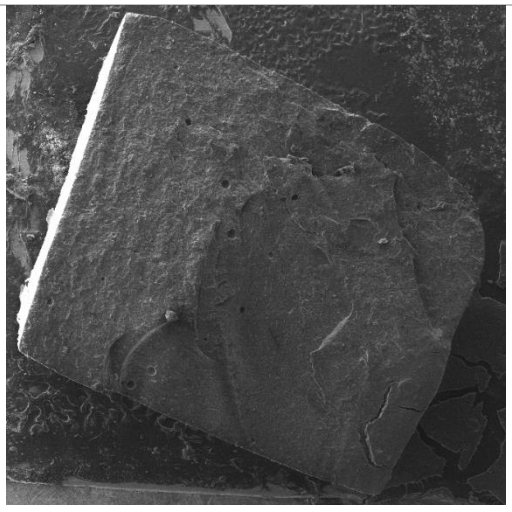

(d)

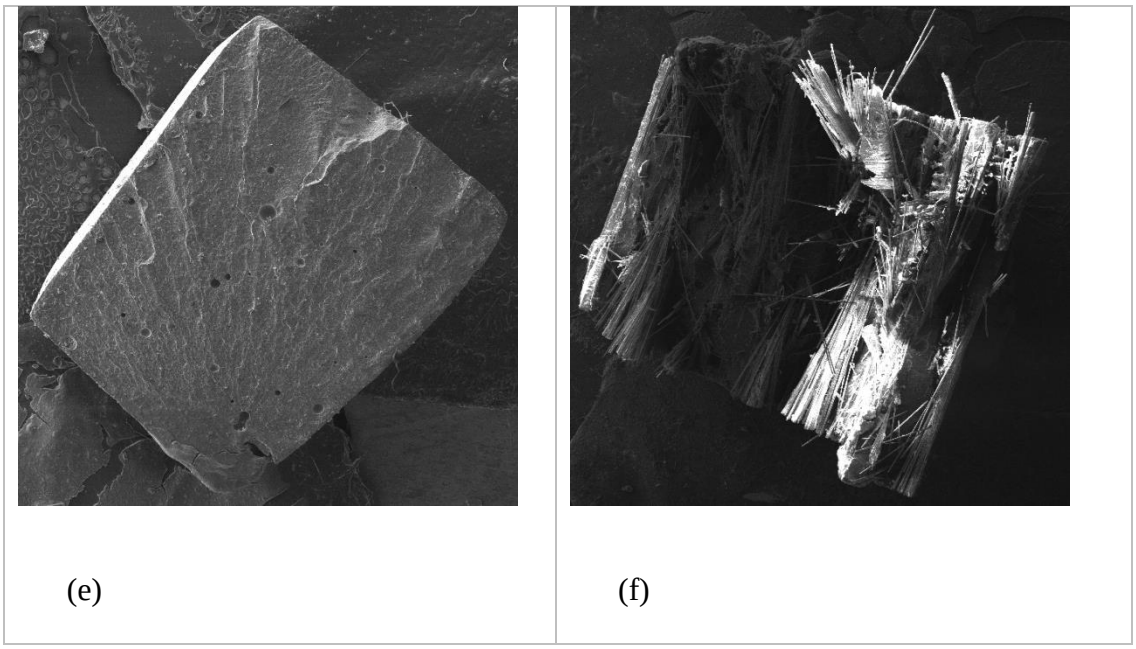

(e) (f)

Figure 4.25 SEM fractographs of the fractured surfaces for: (a) neat uP, and uP/c nanocomposites containing nanoclay loading of (b) 1wt% (c) 2wt% (d) 3wt% (e) 4wt% and (f) GFRuP/c nanocomposites containing 3 wt% of nc. All fractographs taken at fixed magnification (50X)

Fig 4.25 shows the fractured surfaces for all specimens at low magnification (50 X).

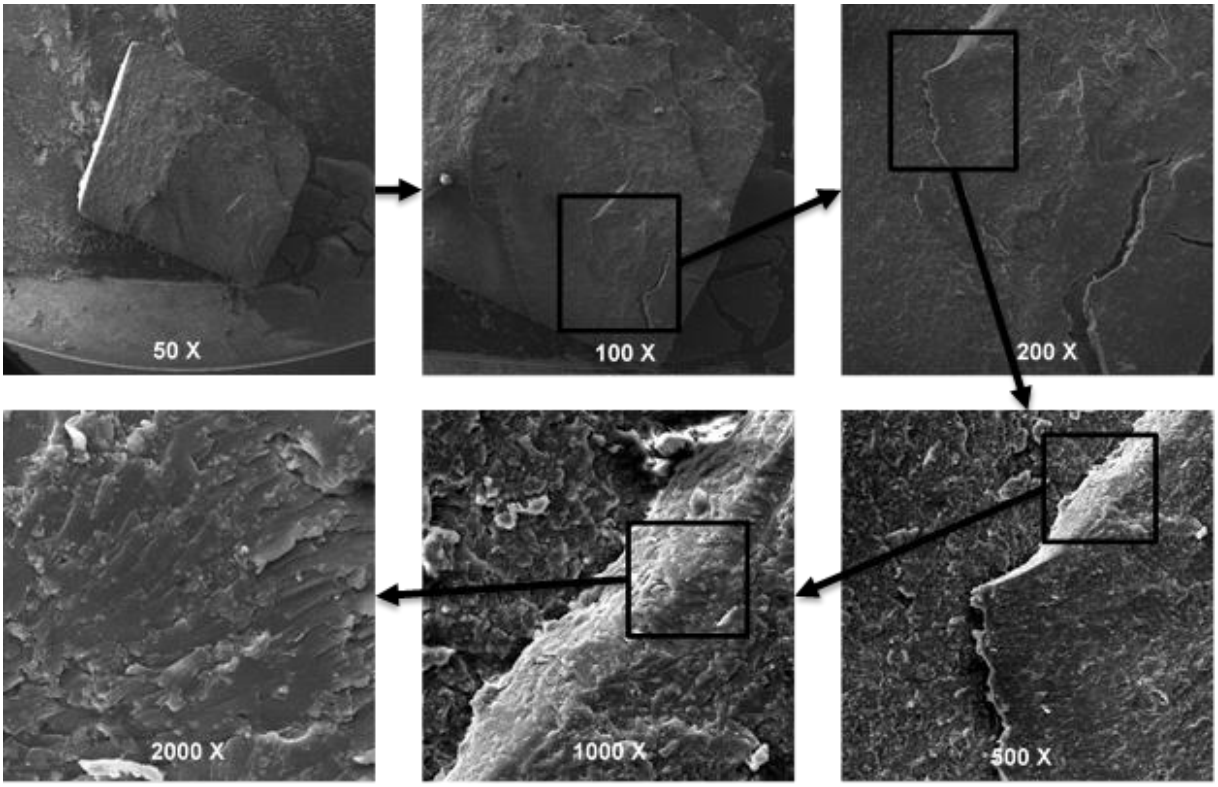

Figure 4.26 Fractographic analysis mapping for the uP/c nanocomposite containing 3wt% of nc.

Fig 4.26 illustrates the fractographic analysis mapping for uP/c nanocomposite containing 3wt% of nc.

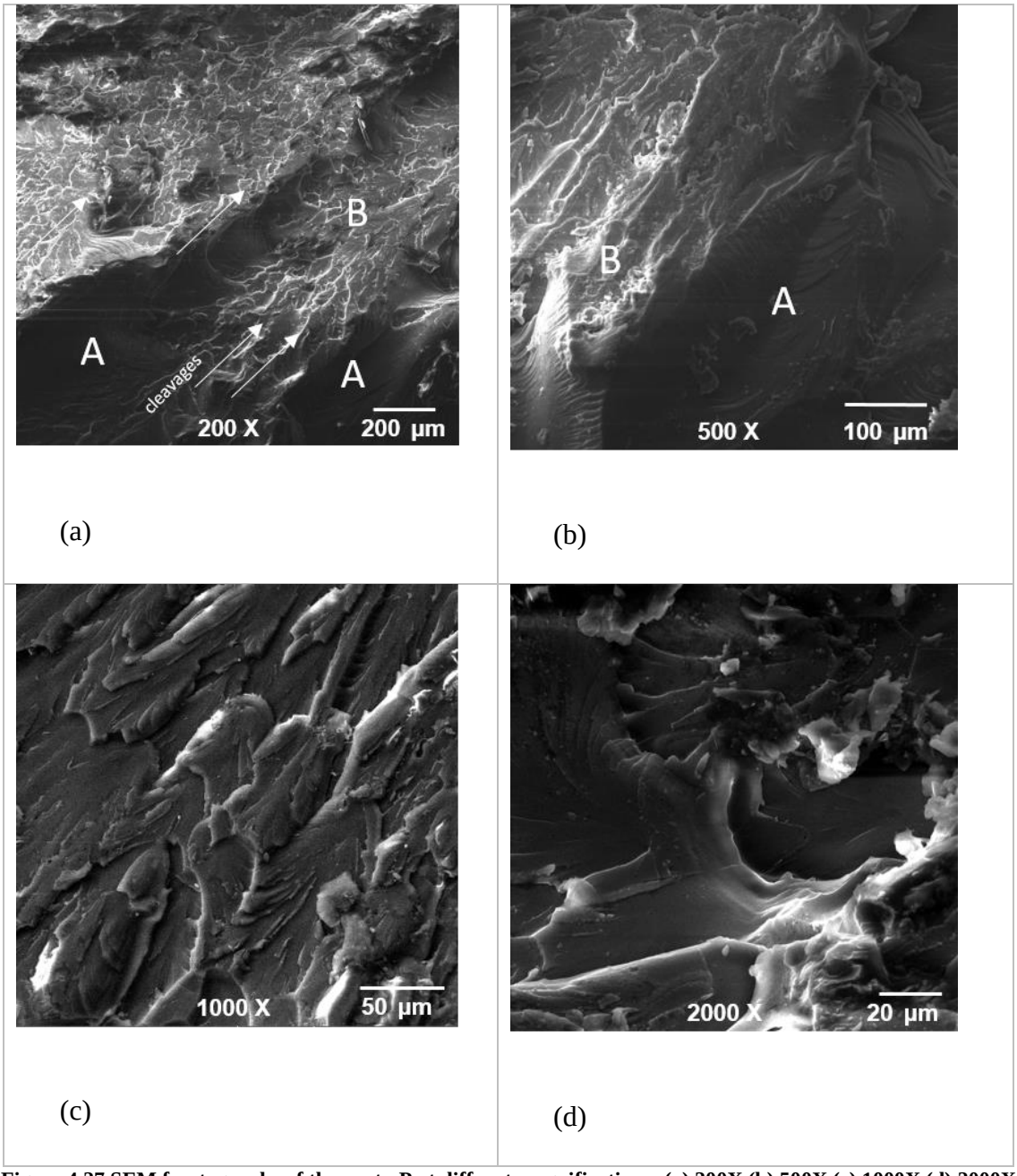

Figure 4.27 SEM fractographs of the neat uP at diffrent magnifications: (a) 200X (b) 500X (c) 1000X (d) 2000X

Fig 4.27:(a-d) shows the FESEM fractographs of the neat uP at different spots taken at different magnifications. From Fig (4.27-a) two regions could be observed, namely A and B. Region A is identified by its softness, wherein cracks initiate, and propagate in region B by higher rate. Region B has coarse surfaces due to secondary cracks represented by

arrows (Fig 4.27-a), these arrows show that the cracks planes perpendicular to direction of the applied force are responsible for the transgranular fracture.

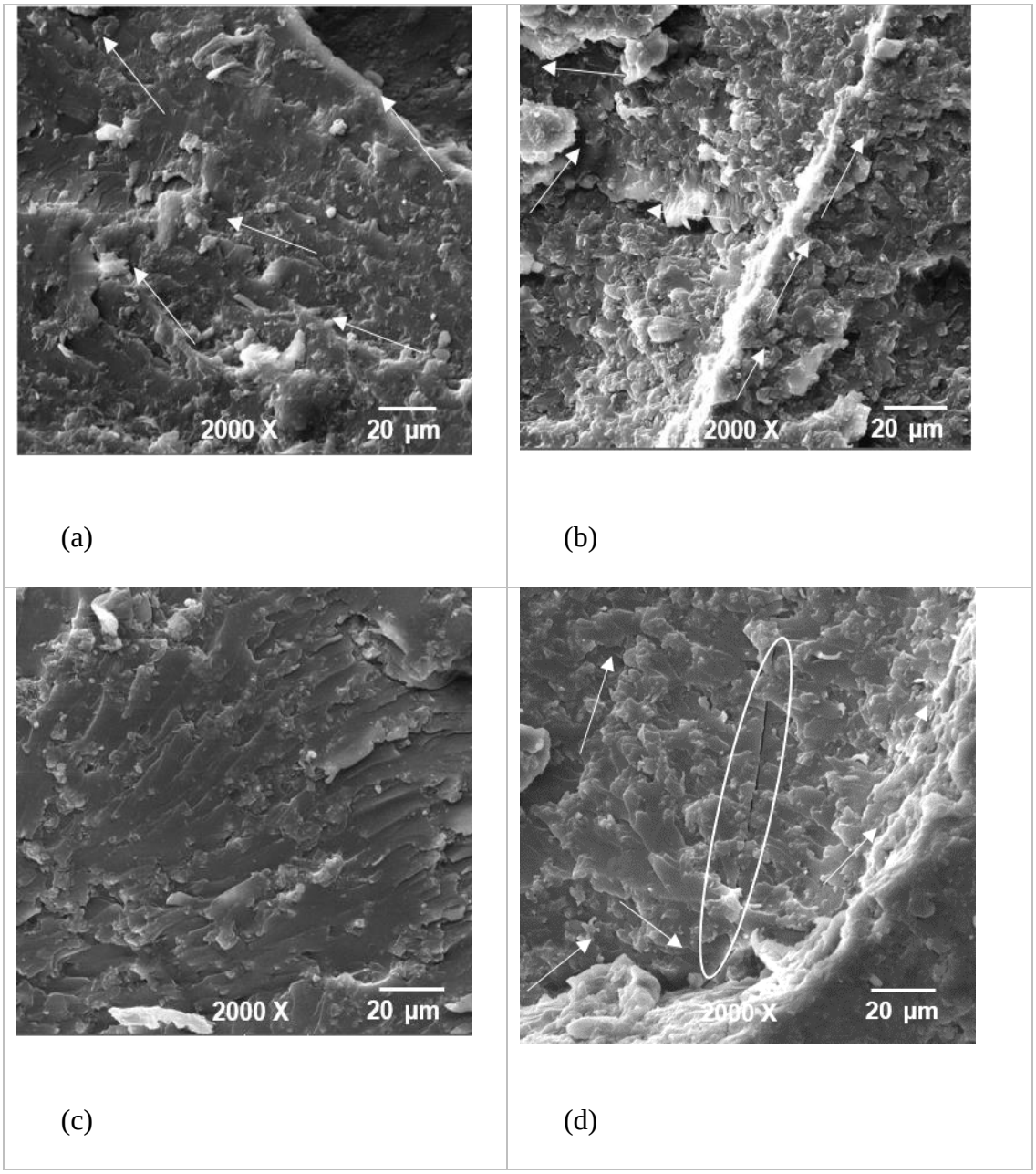

Figure 4.28 SEM fractographs at fixed magnification (2000X) of uP/c nanocomposites containing: nanoclay loading of (a) 1wt% (b) 2wt% (c) wt3% (d) 4wt%

Fig 4.28 investigates the effect of clay addition on the fractured surface morphology for the uP/c nanocomposites containing 1, 2, 3 and 4wt% of clay loading. The fractographs show that the morphology of the fractured surfaces became coarse for all nanocomposites

as a reason of brittle fracture. When the tensile load is applied, the cracks initiate at clay cluster regions because of good adhesion between the uP matrix and nanoclay particles, the applied load cracks the agglomerated nanoclay clusters, and then the cracks propagate perpendicular to the direction of the load. The brittle fracture for nanocomposites containing 1, 2 and 3wt% clay loading (Fig 4.28: a-c) is transgranular fracture. In case of 4wt% clay loading (Fig 4.28-d) the secondary cracks are observable, this could be due to stress concentration caused by the high clay loading which compromises the advantage of nanoclay's aspect ratio. The rough fractured surfaces seem to be due to the changing in cracks directions because of the presence of nc inside crack paths [68]. Secondary cracks may also be due to weak bounding between uP chains and nc, besides the presence of inclusions inside the material.

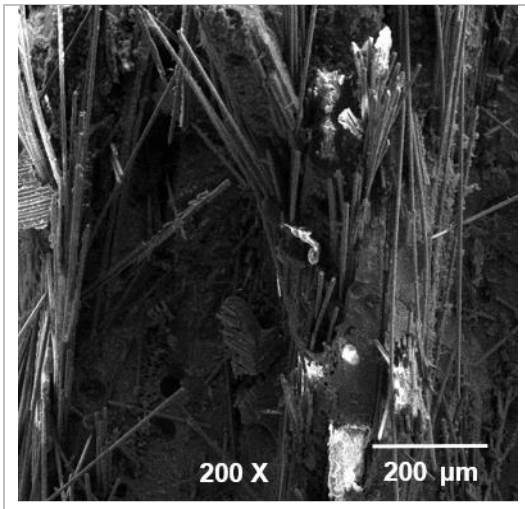

(a)

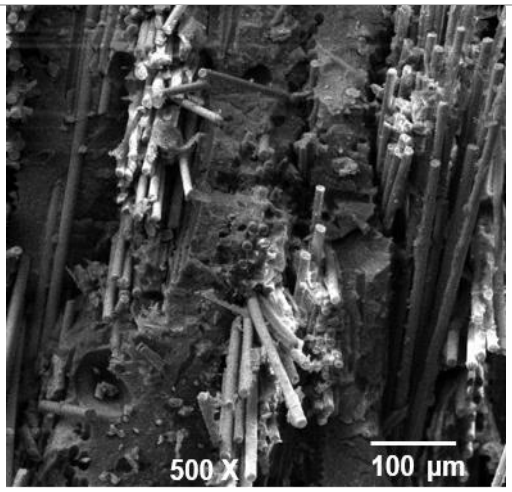

(b)

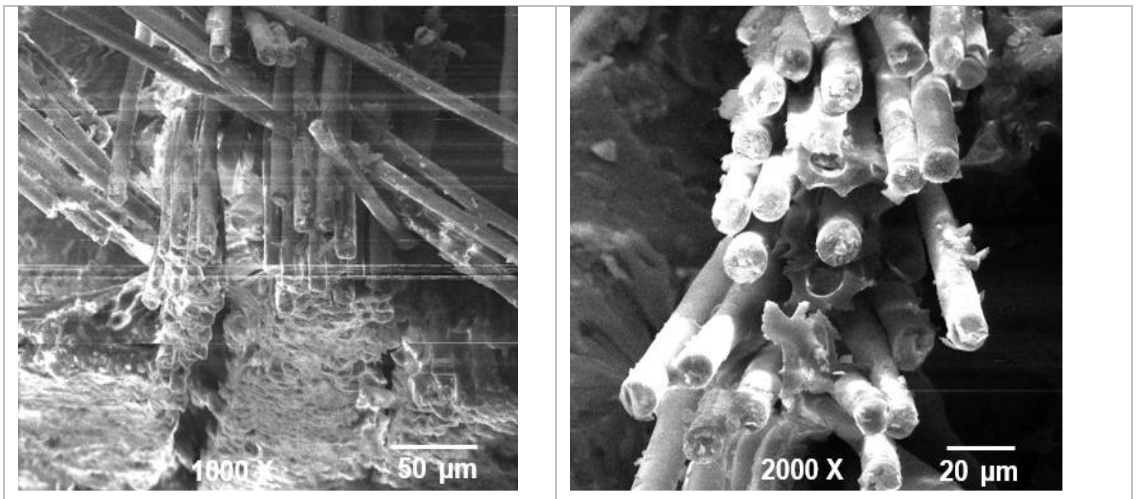

(c) (d)

Figure 4.29 SEM fractographs of GFRuP/c nanocomposite containing 3wt% clay loading at different magnifications: (a) 200 X (b) 500 X (c) 1000 X (d) 2000 X

Fig 4.29: (a-d) illustrates SEM fractographs of GFRuP/c nanocomposite contains 3wt% clay loading at different magnifications. Two types of failures could be identified: fiber pullout and delamination, the cracks take place at matrix-fiber glass interface as well as within GF.

4.8 Water Uptake of uP, uP/c and Hybrid GFRuP/c Nanocomposites

4.8.1 Weight Gain Percentage Over Time

Three specimens for each sample were cut to the standard dimensions (76.2 mm×25.4 mm×4 mm), according to D750-98 specifications [14]. All the prepared specimens were weight before their immersing them into tap water at room temperature and atmospheric pressure. Following long-term immersion procedure, all specimens were fully immersed into container full of water. After 24 hours of immersion, all specimens were removed from the container, then washed by dry cloth and weighed immediately. The same procedure repeated by the end of the first week, then by the end of every two weeks until specimens

reached or approached to the saturation. These immersion durations are recommended by D750-98 standard. The percentage weight gain was calculated for each sample by using equation 4.1, which was described in details earlier in chapter 3.

$$M_t = \frac{W_i - W_o}{W_o} \times 100 \qquad (4.1)$$

Then for each sample, the average percentage weight gain was calculated after each immersion duration up to the end of the test. Accordingly, the difference in the weight gain percentage with square root of immersion time (hours) for uP, uP/c and GFRuP/c nanocomposites were plotted as shown in Fig 4.30.

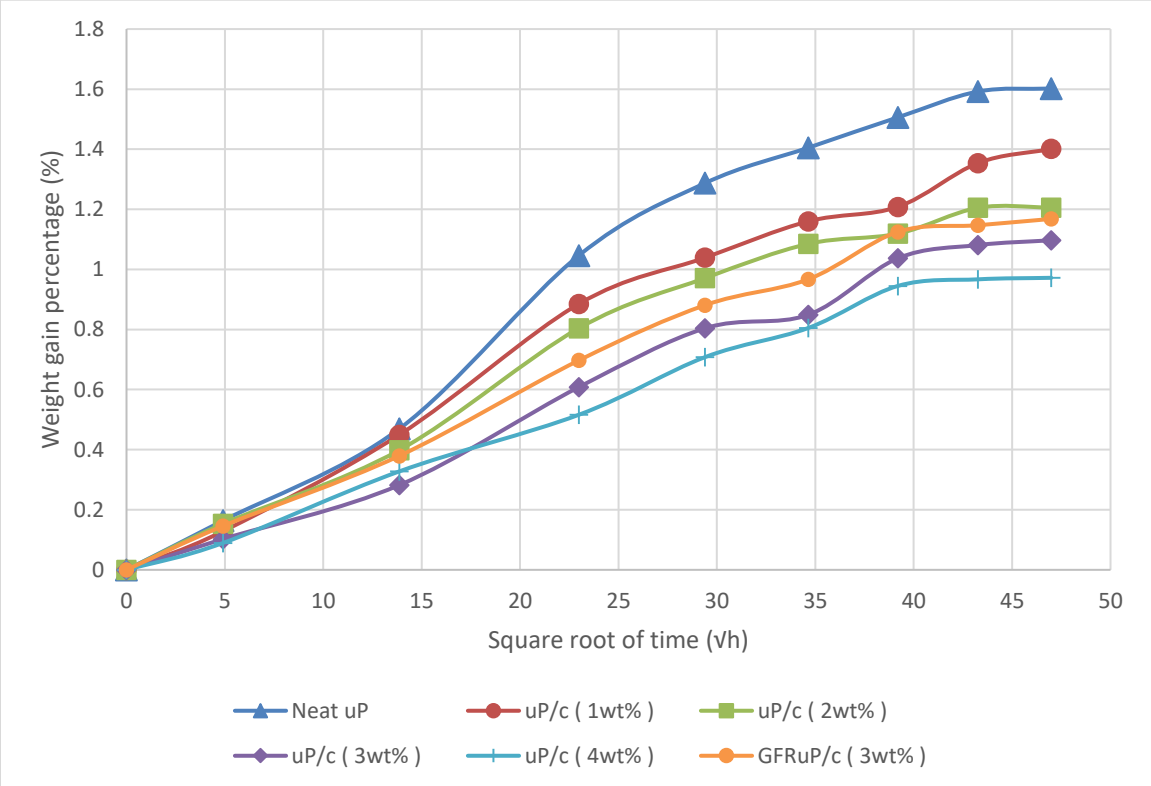

Figure 4.30 The difference in weight gain percentage with square root of immersion time ($hours^{0.5}$) for uP, uP/c and GFRuP/c (3wt%)

Fig 4.30 illustrates the water uptake behavior of uP, uP/c and GFRuP/c (3wt%). It is clear that, the water uptake behavior takes linear trend during the first 8 immersion days (square root of time was 13.85 $hours^{0.5}$), indicating that all specimens are following diffusion controlled behavior. However, after 21 days of immersion, the water gain percentage for all specimens increases over square root of time up to 78th day (square root of time was 43.26 $hours^{0.5}$). After 78 days of immersion, the increase of water uptake for all specimens is not noticeable, meaning that all specimens approached the saturation. The maximum water absorption was found to be 1.602 % in case of neat uP, for a reason that uP has some hydrophilic functional groups, such as: hydroxyl and amino-methyl. These functional groups have affinity to water [69]. Hence, some of water molecules penetrate through uP matrix and interact with it [70], resulting in the higher rate of water uptake in the neat uP. Moreover, water uptake decreased for uP/c and GFRuP/c nanocomposites, until it reached the minimum in case of 4wt% of uP/c nanocomposite with weigh gain percentage of 0.972%. The improvement in water uptake resistance mainly attributed to the presence of nanoclay. Due to the high aspect ratio of nanoclay, these nanoclay particles create tortious path for water molecules [30], [71].

The improvement in water uptake resistance for uP/c nanocomposites and GFRuP/c (3wt%) is illustrated vividly in Table 4.9.

Table 4.9 The improvement in water uptake resistance of nanocomposites compared to uP

Sample	Maximum water uptake (%)	The improvement in water uptake resistance (%)
Neat uP	1.602	-
uP/c (1wt%)	1.401	12.546
uP/c (2wt%)	1.206	24.719
uP/c (3wt.%)	1.097	31.523
uP/c (4wt%)	0.972	39.325
GFRuP/c (3wt%)	1.168	27.091

4.8.2 Diffusion Coefficient of uP, uP/c and GFRuP/c Nanocomposites

The linear trend of weight gain percentage over square root of time, which was illustrated in Fig 4.30, showing that the water uptake behavior is diffusion controlled up to 8th day of immersion. For this reason, Fick's law was used to describe the diffusivity of uP, uP/c and GFRuP/c nanocomposites. By assuming that, all of uP, uP/c and GFRuP/c nanocomposites are homogenous and the diffusion is one dimensional process through the specimen's thickness, the Fick's law could be used to describe water uptake behavior by equation 4.2 [72]

$$M_t = \frac{4M_s}{h}\sqrt{t/\pi} \times \sqrt{D} \qquad (4.2)$$

Where $M_t$is water gain percentage at time t (seconds), $M_s$is the water gain percentage at the saturation, D is diffusion coefficient (mm^2/s) and h is the specimen's thickness. By rearranging equation 4.2, the diffusion coefficient could be calculated in term of water gain percentage through equation 4.3.

$$D = \frac{\pi}{16}\left(\frac{M_t}{M_s} \times \frac{h}{\sqrt{t}}\right)^2 \qquad (4.3)$$

Therefore, the diffusion coefficient has been calculated for all samples. Table 4.10 and Fig 4.31 show the effect of nc loading on the diffusion coefficient for uP, uP/c and GFRuP/c nanocomposites. It is obvious that, the diffusion coefficient generally decreased due to the presence of nc.

Table 4.10 The effect of nc loading on the diffusion coefficient

Sample	Diffusion coefficient (mm^2/s)
Neat uP	7.13×10^{-7}
uP/c (1wt%)	7.06×10^{-7}
uP/c (2wt%)	7.35×10^{-7}
uP/c (3wt%)	5.23×10^{-7}
uP/c (4wt%)	4.70×10^{-7}
GFRuP/c (3wt%.)	6.10×10^{-7}

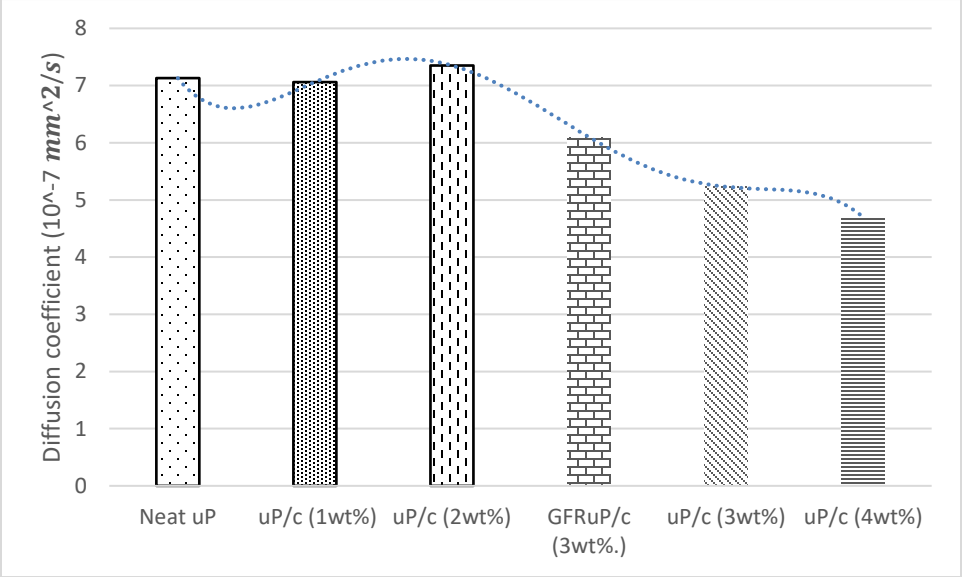

Figure 4.31 The effect of nc loading on the diffusion coefficient

4.9 The Effect of Water Uptake on The Flexural Properties uP, uP/c and Hybrid GFRuP/c Nanocomposites

After finishing water uptake test for three months immersion duration, all of water uptake specimens were cut into flexural specimens, maintaining the span length to specimen's depth ratio of 16, similar to that performed for the dry specimens before water uptake test.

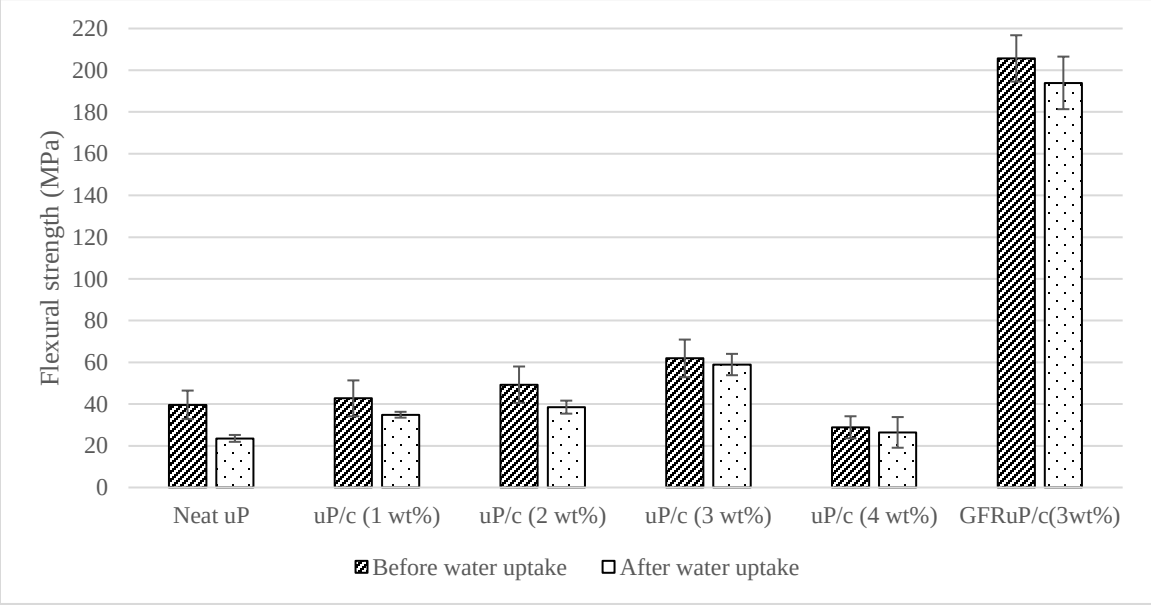

Figure 4.32 Effect of water uptake on the flexural strength of neat uP, uP/c and hybrid GFRuP/c nanocomposites

Fig 4.32 shows that water uptake is considerable in the neat uP, causing a 40% reduction in the flexural strength of neat uP. This behavior is rationalized by the presence of the water uptake due to presence of hydrophilic functional groups as mentioned previously[69]. Water uptake acts as a plasticizer for the neat uP, resulting in reduced flexural strength. However, the effect of nanoclay addition in the water uptake resistance is noticeable. Introducing only 1 and 2wt% of nc resulted in lowering the reduction of flexural strength to 18% and 21% respectively. While the reduction in the flexural strength was found to be less than 10% in case of all nanocomposites prepared with higher clay loading (3 and

4wt%), confirming that nc enhanced the barrier properties of uP/c nanocomposites and strengthened the interface between uP matrix and GF in case of GFRuP/c containing 3wt% of nc [44].

CHAPTER 5

CONCLUSIONS AND RECOMMENDATIONS

5.1 Conclusions

In this work, GFRuP/c nanocomposites were developed, showing improved mechanical properties as well as good barrier properties (minimized water uptake). HSM and ultrasonication were utilized to fabricate uP/c nanocomposites by using an optimized mixing speed. During mixing process, it was found that, increasing mixing speed minimizes agglomeration effect. However, at higher mixing speed, more bubbles form, which alters the mechanical properties due to the induced flaws and defects. Hence, 3000 rpm is considered to be the optimum mixing speed.

In the curing process, it was found that, at elevated curing temperature the shrinkage of the uP was high resulting in decomposition of the developed materials. So, in order to avoid shrinkage, initial curing was performed at ambient temperature for 24 hours, after that the materials post-cured at 120 ℃ for 6 hours. The optimized curing parameters resulted in an optimized glass transition temperature, which was found to be 177.8 ℃.

The XRD analysis showed that I.30E nanoclay exhibits the best dispersion state among the other nanoclay types (C 10A and C 20A). uP/c nanocomposites were prepared by I.30E showed the highest tensile strength when compared to uP/c prepared by C 10A and C 20A.

Tensile tests revealed that 3wt% of I.30E nanoclay loading resulted in the highest tensile strength (52.63 MPa), corresponding to 76% improvement over neat uP. Moreover, and

mainly due to clay agglomeration, going beyond 3wt% of clay loading lead to loss in the strength. Tensile test results also showed that, among the three types of nanoclays, uP/c (3wt%) which was fabricated by Nanomer I.30E has shown the highest tensile strength 52.63 MPa, while Cloisite 10A and Cloisite 20A exhibit only 33.1 MPa and 37.1 MPa respectively. The enhancement in the tensile strength could be attributed to the exfoliated structure in case of I.30E clay as seen in XRD analysis. Nanomer I.30E indicated a good compatibility between clay interlayer galleries and uP chains, so it was chosen to prepare the hybrid GFRuP/c nanocomposites. Great enhancement in the tensile strength of the hybrid GFRuP/c (3wt%) recorded a value reaching 105 MPa, yielding 165% improvement compared to the neat uP. Additionally, a simple deduction arises that nanoclay has no considerable effect on the stiffness of the nanocomposites.

Flexural test exhibited noticeable improvement of flexural strength with a maximum of 56% increase that was observed at 3wt%. However, beyond 3wt% of clay loading, the degradation of the flexural strength was observed, yielding 27% reduction in the flexural strength of uP. Integration of GF into uP resulted in great improvement of the flexural strength of GFRuP/c nanocomposites, yielding 419% enhancement when compared to the neat uP.

Fractographical analysis demonstrated brittle fracture for all nanocomposites, transgranular fracture besides secondary cracks were observed, this could be rationalized by high stress, weak bounding between polyester chains and may be also due to the presence of inclusions within the developed materials.

The maximum water uptake recorded was 1.602% in case of neat uP. Meanwhile, addition of nanoclay (nc) resulted in linear improvement of the water uptake resistance until reaching the maximum improvement of 39 % in case of 4wt% of nc loading. Flexural test revealed degradation in the flexural strength due to moisture uptake. However, the reduction was found to be minimum at higher nc loading (3 and 4wt%), meaning that nc improved water uptake resistance.

Incorporation of nc resulted in reduction of water uptake, since the maximum weight gain was found to be 1.602% for neat uP. Meanwhile, addition of nc resulted in linear improvement of the water uptake resistance until reaching the maximum improvement of 39 % in case of 4wt% of nc loading, yielding minimum weight gain of 0.972%. Flexural test revealed degradation in the flexural strength, due to moisture uptake. However, nc minimized the reduction in the flexural strength caused by water uptake. The reduction was less than 10% for all uP/c and GFRuP/c containing clay loading more than 2wt%.

5.2 Recommendations

The author would like to recommend the following points:

1. The gel time for uP resin is relatively short (15 minutes at 25 ℃), the problem is that, during mixing of curing agents with uP resin, gaseous bubbles form due to initiation of curing reaction, at this moment it is difficult to control bubble formation, also it is impractical to degas the mixture instantaneously. To solve this issue: instead of using hand lay-up method, it is recommended to use other technique which involves instantaneous vacuuming such as: VARTM, RTM and VI.

2. E-CR glass chopped strand mat was used in this work. So, it is recommended to study the effect of different glass fiber types and orientation on the mechanical properties of GFRuP/c nanocomposites.

References

[1] L. C. Sawyer, D. T. Grubb, and G. F. Meyers, *Polymer microscopy: Third edition*. Springer, 2008.

[2] William D. Callister and David G. Rethwisch, *Materials Science and Engineering*, Eighth. Wiley, 2010.

[3] Y. Fukushima, A. Okada, M. Kawasumi, T. Kurauchi, and O. Kamigaito, "Swelling Poly-6-Amide By Poly-6-Amide," *Clay Miner.*, vol. 23, pp. 27–34, 1988.

[4] A. Usuki, M. Kawasumi, A. Okada, Y. Fukushima, T. Kurauchi, and O. Kamigaito, "Synthesis of Nylon 6-clay hybrid," *J. Mater. Res.*, vol. 8, no. 5, pp. 1185–1189, 1993.

[5] D. R. Paul and L. M. Robeson, "Polymer nanotechnology: Nanocomposites," *Polymer (Guildf).*, vol. 49, no. 15, pp. 3187–3204, 2008.

[6] M. W. Dewan, M. K. Hossain, M. Hosur, and S. Jeelani, "Thermomechanical properties of alkali treated jute-polyester/nanoclay biocomposites fabricated by VARTM process," *J. Appl. Polym. Sci.*, vol. 128, no. 6, pp. 4110–4123, 2013.

[7] P. J. Schubel, M. S. Johnson, N. a. Warrior, and C. D. Rudd, "Characterisation of thermoset laminates for cosmetic automotive applications: Part III - Shrinkage control via nanoscale reinforcement," *Compos. Part A Appl. Sci. Manuf.*, vol. 37, no. 10, pp. 1757–1772, 2006.

[8] B. C. Kim, S. W. Park, and D. G. Lee, "Fracture toughness of the nano-particle reinforced epoxy composite," *Compos. Struct.*, vol. 86, no. 1–3, pp. 69–77, 2008.

[9] W. Liu, S. Hoa, and M. Pugh, "Fracture toughness and water uptake of high-performance epoxy/nanoclay nanocomposites," *Compos. Sci. Technol.*, vol. 65, no. 15–16, pp. 2364–2373, 2005.

[10] M. Al-Qadhi, N. Merah, and Z. M. Gasem, "Mechanical properties and water uptake of epoxy–clay nanocomposites containing different clay loadings," *J. Mater. Sci.*,

vol. 48, no. 10, pp. 3798–3804, 2013.

[11] A. McGown, *Science in the Real World: A simplified story of how technology using chemistry and physics is used in the real world of industry*, 2015 Editi. MoshPit Publishing, 2015.

[12] C. M. C. Pereira, M. Herrero, F. M. Labajos, A. T. Marques, and V. Rives, "Preparation and properties of new flame retardant unsaturated polyester nanocomposites based on layered double hydroxides," *Polym. Degrad. Stab.*, vol. 94, no. 6, pp. 939–946, 2009.

[13] Marketsandmarkets.com, "Unsaturated Polyester Resins Market by Type (Orthophthalic, Isophthalic & DCPD), End-Use Industry (Building & Construction, Marine, Land Transportation, Pipes & Tanks, Artificial Stone, Wind Energy, Electrical & Electronics) - Global Forecast to 2021," 2017.

[14] ASTM D570, "Standard Test Method for Water Absorption of Plastics 1," vol. 98, no. Reapproved 2005, pp. 3–6, 2015.

[15] ASTM International, "ASTM D 790 - 02 - Flexural Properties of Unreinforced and Reinforced Plastics and Electrical Insulating Materials," vol. 14, pp. 146–154, 2002.

[16] ASTM International, "Standard Test Method for Tensile Properties of Plastics," vol. 8, pp. 1–16, 2013.

[17] L. Lepluart, J. Duchet, and H. Sautereau, "Epoxy/montmorillonite nanocomposites: influence of organophilic treatment on reactivity, morphology and fracture properties," *Polymer (Guildf).*, vol. 46, no. 26, pp. 12267–12278, 2005.

[18] M. Kawasumi, "The discovery of polymer-clay hybrids," *J. Polym. Sci. Part A Polym. Chem.*, vol. 42, no. 4, pp. 819–824, 2004.

[19] K. Fu, W. Huang, Y. Lin, L. A. Riddle, D. L. Carroll, and Y.-P. Sun, "Defunctionalization of Functionalized Carbon Nanotubes," *Nano Lett.*, vol. 1, no. 8, pp. 439–441, 2001.

[20] C. Peng, H.-S. Kim, and J. Hyoung-Joon, “Preparation, Properties and Application of Polyamide/Carbon Nanotube Nanocomposites,” *Macromol. Res.*, vol. 17, no. 4, pp. 207–217, 2009.

[21] K. Saeed and S. Y. Park, “Preparation of multiwalled carbon nanotube/nylon-6 nanocomposites by in situ polymerization,” *J. Appl. Polym. Sci.*, vol. 106, no. 6, pp. 3729–3735, 2007.

[22] K. Nevalainen, J. Vuorinen, V. Villman, R. Suihkonen, P. Järvelä, J. Sundelin, and T. Lepistö, “Characterization of twin-screw-extruder-compounded polycarbonate nanoclay composites,” *Polym. Eng. Sci.*, vol. 49, no. 4, pp. 631–640, 2009.

[23] J. W. Cho and D. R. Paul, “Nylon 6 nanocomposites by melt compounding,” *Polymer (Guildf).*, vol. 42, pp. 1083–1094, 2001.

[24] M. Albdiry, B. Yousif, H. Ku, and K. Lau, “A critical review on the manufacturing processes in relation to the properties of nanoclay/polymer composites,” *J. Compos. Mater.*, vol. 47, no. 9, pp. 1093–1115, 2012.

[25] E. C. Lee, D. F. Mielewski, and R. J. Baird, “Exfoliation and dispersion enhancement in polypropylene nanocomposites by in-situ melt phase ultrasonication,” *Polym. Eng. Sci.*, vol. 44, no. 9, pp. 1773–1782, 2004.

[26] I. Mironi-Harpaz, M. Narkis, and a. Siegmann, “Nanocomposite systems based on unsaturated polyester and organo-clay,” *Polym. Eng. Sci.*, vol. 45, no. 2, pp. 174–186, 2005.

[27] D. Suh, “The property and formation mechanism of unsaturated polyester–layered silicate nanocomposite depending on the fabrication methods,” *Polymer (Guildf).*, vol. 41, no. 24, pp. 8557–8563, 2000.

[28] K. V. P. Chakradhar, K. Venkata Subbaiah, M. Ashok Kumar, and G. Ramachandra Reddy, “Epoxy/Polyester Blend Nanocomposites: Effect of Nanoclay on Mechanical, Thermal and Morphological Properties,” *Malaysian Polym. J.*, vol. 6, no. 2, pp. 109–118, 2011.

[29] P. Prabhu, P. Jawahar, M. Balasubramanian, and T. P. Mohan, “Machinability study of hybrid nanoclay-glass fibre reinforced polyester composites,” *Int. J. Polym. Sci.*, vol. 2013, 2013.

[30] M. Al-Qadhi, “Development and Characterization of Epoxy-Clay Nanocomposites,” KFUPM, 2012.

[31] M. A. Bashir, “Effect of nanoclay dispersion on the processing of polyester nanocomposites,” McGill University, 2008.

[32] M. L. and D. T. Hamid Dalir, Rouhollah D. Farahani, Vireya Nhim, Benjamin Samson, “Microstructural and Mechanical Properties of Polyester/Nanoclay Nanocomposites: Microstructure-Mixing Strategy Correlation,” in *MRS Proceedings, 13*, 2011.

[33] F. Bensadoun, N. Kchit, C. Billotte, F. Trochu, and E. Ruiz, “A Comparative Study of Dispersion Techniques for Nanocomposite Made with Nanoclays and an Unsaturated Polyester Resin,” *J. Nanomater.*, vol. 2011, pp. 1–12, 2011.

[34] H. N. Dhakal, Z. Y. Zhang, and M. O. W. Richardson, “Nanoindentation behaviour of layered silicate reinforced unsaturated polyester nanocomposites,” *Polym. Test.*, vol. 25, no. 6, pp. 846–852, 2006.

[35] J. M. Esfahani, M. Esfandeh, and A. R. Sabet, “High-velocity impact behavior of glass fiber-reinforced polyester filled with nanoclay,” *J. Appl. Polym. Sci.*, vol. 125, no. SUPPL. 1, 2012.

[36] S. Chaeichian, P. M. Wood-Adams, and S. V. Hoa, “Fracture of unsaturated polyester and the limitation of layered silicates,” *Polym. Eng. Sci.*, vol. 55, no. 6, pp. 1303–1309, Jun. 2015.

[37] N. Kchit, F. Bensadoun, T. Carrozani, C. Billotte, E. Ruiz, and F. Trochu, “A STUDY OF NANOCLAY COMPOSITES FABRICATED BY LIQUID COMPOSITE,” *10th Int. Conf. Flow Process. Compos. Mater.*, 2010.

[38] F. Bensadoun, N. Kchit, C. Billotte, S. Bickerton, F. Trochu, and E. Ruiz, “A study

of nanoclay reinforcement of biocomposites made by liquid composite molding," *Int. J. Polym. Sci.*, vol. 2011, pp. 11–13, 2011.

[39] M. Vikas., *Synthesis Techniques for Polymer Nanocomposites*. Weinheim: Wiley-VCH, 2015.

[40] S. M. Razavi, N. Dehghanpour, S. J. Ahmadi, and M. Rajabi Hamaneh, "Thermal, mechanical, and corrosion resistance properties of vinyl ester/clay nanocomposites for the matrix of carbon fiber-reinforced composites exposed to electron beam," *J. Appl. Polym. Sci.*, vol. 42393, pp. 1–8, 2015.

[41] M. Chieruzzi, A. Miliozzi, and J. M. Kenny, "Effects of the nanoparticles on the thermal expansion and mechanical properties of unsaturated polyester/clay nanocomposites," *Compos. Part A Appl. Sci. Manuf.*, vol. 45, pp. 44–48, 2013.

[42] H. M. Stephan Laske, Ivica Duretek, Andreas Witschnigg, "Influence of the Degree of Exfoliation on the Thermal Conductivity of Polypropylene Nanocomposites," *Polym. Eng. Sci.*, vol. 52, no. 8, pp. 1749–1753, 2012.

[43] A. Pandian, M. Vairavan, W. Jappes, J. Thangaiah, and M. Uthayakumar, "Effect of Moisture Absorption Behavior on Mechanical Properties of Basalt Fibre Reinforced Polymer Matrix Composites," vol. 2014, 2014.

[44] H. Yang, H. Kim, H. Park, B. Lee, and T. Hwang, "Water absorption behavior and mechanical properties of lignocellulosic filler – polyolefin bio-composites," vol. 72, pp. 429–437, 2006.

[45] S. Kajorncheappunngam, R. K. Gupta, and H. V. S. GangaRao, "Effect of Aging Environment on Degradation of Glass-Reinforced Epoxy," *J. Compos. Constr.*, vol. 6, no. 1, pp. 61–69, 2002.

[46] S. Sinha Ray and M. Okamoto, "Polymer/layered silicate nanocomposites: A review from preparation to processing," *Prog. Polym. Sci.*, vol. 28, no. 11, pp. 1539–1641, 2003.

[47] M. Biswas and S. S. Ray, "Recent progress in synthesis and evaluation of polymer-

montmorillonite nanocomposites," *Adv. Polym. Sci.*, vol. 155, pp. 167–221, 2001.

[48] L. a. Utracki, *Clay-Containing Polymeric Nanocomposites, Volumes 1-2*, First Edit., vol. 1. ismithers rapra, 2004.

[49] J. T. and M. R. K. Tanoue S., L. A. Utracki, A. Garcia-Rejon, "Preparation of Polystyrene/Organoclay Nanocomposites by Melt Compounding Using a Twin Screw Extruder," in *Japanese Society of Polymer Processing annual meeting*, 2003.

[50] S. Calorimetry, "Standard Test Method for Transition Temperatures of Polymers By Differential," *Test*, vol. 8, no. July, pp. 1–7, 2004.

[51] F. Hussain, "Review article: Polymer-matrix Nanocomposites, Processing, Manufacturing, and Application: An Overview," *J. Compos. Mater.*, vol. 40, no. 17, pp. 1511–1575, 2006.

[52] M. Yuhazri and P. Phongsakorn, "A Comparison Process Between Vacuum Infusion And Hand Lay up Method Toward Kenaf/Polyester Composites," *Int. J. Basic & Appl.*, vol. 10, no. 33, pp. 63–66, 2010.

[53] R. a. Malloy, *Plastic Part Design for Injection Molding*, 2nd Editio. Hanser, 2010.

[54] A. Rafiq, "Development and Characterization of Hybrid Glass Fiber and Epoxy Clay Nanocomposites," KFUPM, 2014.

[55] M. V. Alonso, M. Oliet, J. García, F. Rodríguez, and J. Echeverría, "Transformation of dynamic DSC results into isothermal data for the curing kinetics study of the resol resins," *J. Therm. Anal. Calorim.*, vol. 86, no. 3, pp. 797–802, 2006.

[56] J. Shawe, R. Riesen, J. Widmann, and M. Schubnell, "UserCom," *Mettler Toledo*, pp. 1–28, 2000.

[57] P. With, P. Amic, and R. J. Farris, "Thermal and Mechanical Properties of the Precursor Polymers : Comparison of Their," *Polym. Eng. Sci.*, vol. 39, no. 4, pp. 638–645, 1999.

[58] B. Qi, Q. X. Zhang, M. Bannister, and Y. W. Mai, "Investigation of the mechanical

properties of DGEBA-based epoxy resin with nanoclay additives," *Compos. Struct.*, vol. 75, no. 1–4, pp. 514–519, 2006.

[59] S. C. Zunjarrao, R. Sriraman, and R. P. Singh, "Effect of processing parameters and clay volume fraction on the mechanical properties of epoxy-clay nanocomposites," *J. Mater. Sci.*, vol. 41, no. 8, pp. 2219–2228, 2006.

[60] M. S. Farahat, "Mechanical characteristics of modified unsaturated polyester resins derived from poly(ethylene terephthalate) waste," *Polym. Int.*, vol. 51, no. 2, pp. 183–189, 2002.

[61] A. A. Farag, A. S. Ismail, and M. A. Migahed, "Inhibition of carbon steel corrosion in acidic solution using some newly polyester derivatives," *J. Mol. Liq.*, vol. 211, pp. 915–923, 2015.

[62] A. Yasmin, J. L. Abot, and I. M. Daniel, "Processing of clay / epoxy nanocomposites by shear mixing," vol. 49, pp. 81–86, 2003.

[63] S. F. Al, M. S. Chowdary, and M. S. R. N. Kumar, "Effect of Nanoclay on the Tensile properties of," vol. 3, no. 5, pp. 1977–1980, 2014.

[64] H. Alamri, I. M. Low, and Z. Alothman, "Mechanical, thermal and microstructural characteristics of cellulose fibre reinforced epoxy/organoclay nanocomposites," *Compos. Part B Eng.*, vol. 43, no. 7, pp. 2762–2771, 2012.

[65] M. S. Saharudin, R. Atif, I. Shyha, and F. Inam, "The degradation of mechanical properties in polymer nano-composites exposed to liquid media – a review.," *RSC Adv.*, vol. 6, no. 2, pp. 1076–1089, 2016.

[66] A. B. Inceoglu and U. Yilmazew, "Synthesis and Mechanical Properties Of Unsaturated Polyester Based Nanocomposites," *Polym. Eng. Sci.*, vol. 43, no. 3, pp. 661–669, 2003.

[67] X. Kornmann, L. a. Berglund, J. Sterte, and E. P. Giannelis, "Nanocomposites based on montmorillonite and unsaturated polyester," *Polym. Eng. Sci.*, vol. 38, no. 8, pp. 1351–1358, 1998.

[68] K. Wang, L. Chen, J. Wu, M. L. Toh, C. He, and A. F. Yee, “Epoxy nanocomposites with highly exfoliated clay: Mechanical properties and fracture mechanisms,” *Macromolecules*, vol. 38, no. 3, pp. 788–800, 2005.

[69] S. Ogata, N., Sanui, K., Shimozato, Y. and Munemura, “Syntheses of functional condensation polymer. I. Polyesters having pendant functional groups such as hydroxyl, formyl, aldoxime, aminomethyl and hydroxymethyl,” *J. Polym. Sci. Polym. Chem.*, vol. Ed., 14, pp. 2969–2981, 1976.

[70] W. S. Chow, “Water absorption of epoxy/glass fiber/organo-montmorillonite nanocomposites,” *Express Polym. Lett.*, vol. 1, no. 2, pp. 104–108, 2007.

[71] H. Alamri and I. M. Low, “Effect of water absorption on the mechanical properties of nanoclay filled recycled cellulose fibre reinforced epoxy hybrid nanocomposites,” *Compos. Part A Appl. Sci. Manuf.*, vol. 44, no. 1, pp. 23–31, 2013.

[72] H. N. Dhakal, Z. Y. Zhang, and M. O. W. Richardson, “Effect of water absorption on the mechanical properties of hemp fibre reinforced unsaturated polyester composites,” vol. 67, pp. 1674–1683, 2007.

Vitae

Name :Omer Mohamed Ahmed Mohamed

Nationality :Sudanese

Date of Birth :12/17/1990

Email :omer0mohamed@yahoo.com

Address :Saudi Arabia, Dhahran, KFUPM, 31261

Education

M.S., Mechanical Engineering. May 2017
King Fahd University of Petroleum and Minerals, Dhahran, Saudi Arabia
Thesis Title: Development and Characterization of Hybrid Glass Fiber Reinforced Unsaturated Polyester/Clay Nanocomposites.
CGPA 3.464 out of 4
B.S., Mechanical Engineering. September 2013
University of Khartoum, Sudan
Thesis Title: Design and selection of air conditioning system for University of Khartoum lecture halls complex.
CGPA 7.39 out of 10

Conference Paper

Omer Mohamed and Nesar Merah, "Effects of Nanoclay on Mechanical Properties of Unsaturated Polyester", Frontiers in Materials Processing Applications, Research and Technology, France, July 9-12, 2017.

Training and Courses

Trainee Mechanical Engineer: Earthmoving corporation, Madani workshop, Gezira state, Feb. 2011. Achievements: Offered major contributions to engine overhaul.

Intensive course in heating, ventilation and air conditioning (HVAC), Soft star training center, Jan. 2013

Intensive course in 3D Design(Solidworks), Soft star training center, Oct. 2012

Introduction to Abaqus workshop, Ultimate Solutions Company, Nov. 2014

Finite element modeling using COMSOL multiphysics workshop, COMSOL technical support at Mechanical engineering department-KFUPM, Nov., 2015

Development of Nanomaterials for petro-catalytic applications workshop, CENT, KFUPM, Oct. 2016

National instruments training course

Experience

Part-time job at mechanical engineering department, Introduction to Mechanical Engineering Design (ME218) course facilitator. Feb 2016 – May 2016

Part-time job at mechanical engineering department, Manufacturing and Design (ME406) course grader. Feb 2017 – May 2017

Part-time job at registrar office, registration assistant